

Revista **ALCONPAT**

Latin American Journal of Quality Control, Pathology and Construction Recovery

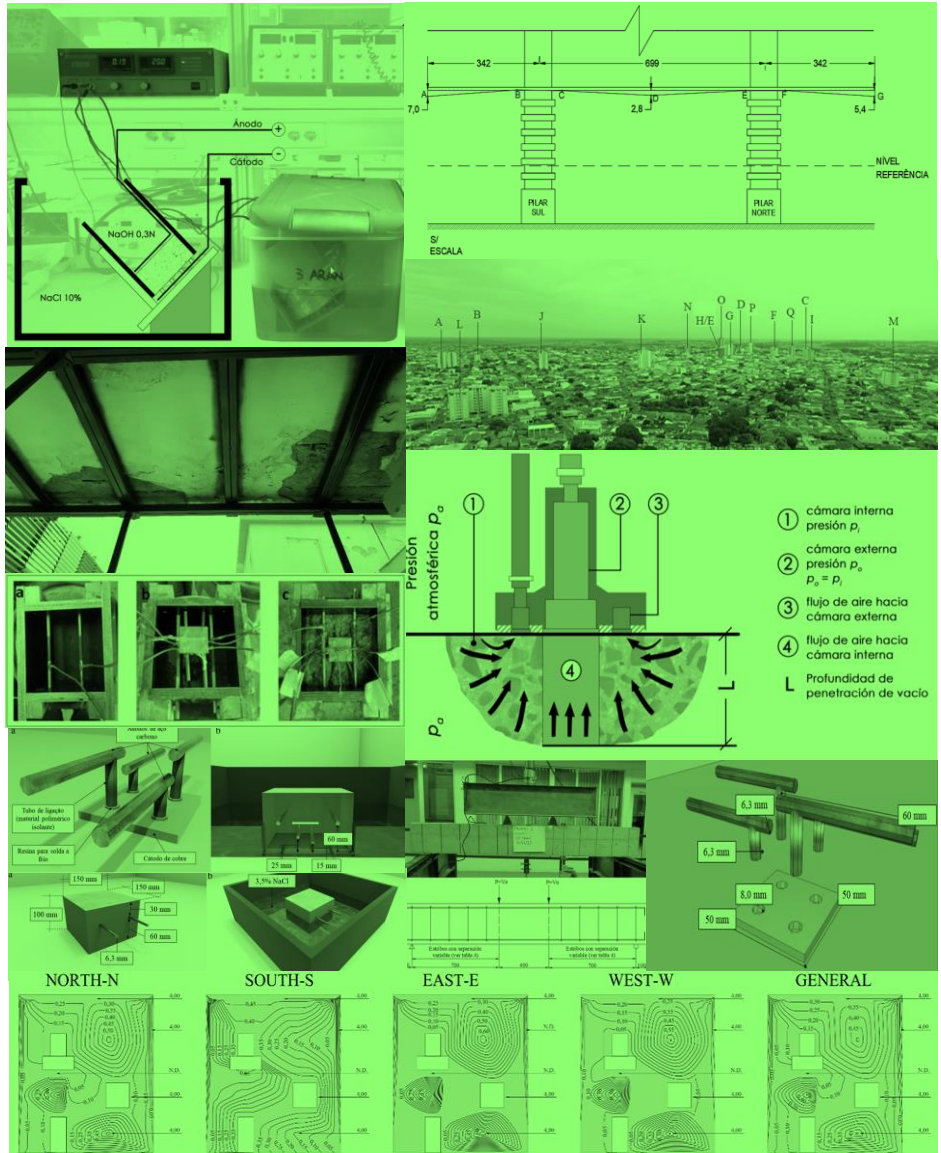
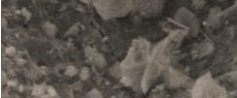
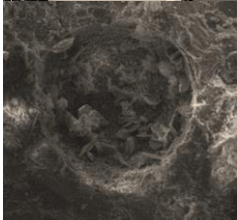
DOI: <https://doi.org/10.21041/ra.v11i3>
editorial.revista.alconpat@gmail.com

eISSN: 2007-6835

Volume 11

September – December 2021

Issue 3



Latin American Journal of Quality Control, Pathology and Construction Recovery

<http://www.revistaalconpat.org>



ALCONPAT International

Founders members:

Liana Arrieta de Bustillos – **Venezuela**
Antonio Carmona Filho - **Brazil**
Dante Domene – **Argentina**
Manuel Fernández Cánovas – **Spain**
José Calavera Ruiz – **Spain**
Paulo Helene, **Brazil**

Board of Directors International:

President of Honor

Angélica Ayala Piola, **Paraguay**

President

Carmen Andrade Perdriz, **Spain**

Managing Director

Pedro Castro Borges, **Mexico**

Executive Secretary

José Iván Escalante García, **Mexico**

Technical Vice President

Enio Pazini Figueiredo, **Brazil**

Administrative Vice President

Luis Álvarez Valencia, **Guatemala**

Manager

Paulo Helene, **Brazil**

Revista ALCONPAT

Editor in Chief:

Dr. Pedro Castro Borges
Centro de Investigación y de Estudios Avanzados del
Instituto Politécnico Nacional, Unidad Mérida
(CINVESTAV IPN – Mérida)
Merida, Yucatan, **Mexico**

Co-Editor in Chief:

Dr. Francisco Alberto Alonso Farrera
Universidad Autónoma de Chiapas
Tuxtla Gutiérrez, Chiapas, México

Executive Editor:

Dr. José Manuel Mendoza Rangel
Universidad Autónoma de Nuevo León,
Facultad de Ingeniería Civil
Monterrey, Nuevo Leon, **Mexico**

Associate Editors:

Dr. Manuel Fernandez Canovas
Universidad Politécnica de Madrid.
Madrid, **Spain**

Ing. Raúl Husni

Facultad de Ingeniería Universidad de Buenos Aires.
Buenos Aires, **Argentina**

Dr. Paulo Roberto do Lago Helene
Universidade de São Paulo.
São Paulo, **Brazil**

Dr. José Iván Escalante García
Centro de Investigación y de Estudios Avanzados del
Instituto Politécnico Nacional (Unidad Saltillo)
Saltillo, Coahuila, **Mexico**.

Dra. Oladis Troconis de Rincón
Centro de Estudios de Corrosión
Universidad de Zulia
Maracaibo, **Venezuela**

Dr. Fernando Branco Universidad
Técnica de Lisboa
Lisboa, **Portugal**

Dr. Pedro Garcés Terradillos
Universidad de Alicante
San Vicente, **Spain**

Dr. Andrés Antonio Torres Acosta
Instituto Tecnológico y de Estudios Superiores de
Monterrey, Querétaro
Querétaro, **Mexico**

Dr. Filippo Ubertini
Università degli Studi di Perugia,
Perugia, **Italy**

Dr. Ravindra Gettu
Indian Institute of Technology Madras,
Chennai, **India**

**JOURNAL OF THE LATIN-AMERICAN
ASSOCIATION OF QUALITY CONTROL,
PATHOLOGY AND RECOVERY OF
CONSTRUCTION**

<http://www.revistaalconpat.org>

With great satisfaction, we present the third issue of the tenth year of the ALCONPAT Journal.

The objective of the Journal is to publish contributions of basic and applied research directly associated with the solution of problems related with quality control, pathology and recovery of constructions being welcomed studio cases in these areas.

This V11N3 edition begins with a work from **Brazil**, where Friancieli Tiecher and colleagues evaluate different types of cement against the incidence of Late Ettringite Formation (DEF), using mortars produced in the laboratory and exposed to a high curing temperature. during a study period of 12 months. DEF represents one of the types of internal sulfate attack (ISA) related to an expansive chemical reaction that occurs in concrete that involves cement sulfates. The experiments included the evaluation of tensile, compressive and expansion strengths, and microstructural characteristics over time. It was observed that the mortar tests required a prolonged evaluation period to distinguish the behaviors between the cements. In addition, the initial high-strength cement had the worst performance in relation to DEF.

In the second work, from **Spain**, Flora Hebe Gurdían Currán and colleagues evaluate the mechanical and durability properties of concretes with low environmental impact with substitutions of cement by industrial by-products (35% fly ash and 15% catalytic cracking catalyst) and aggregates. coarse from recycled aggregates (20% and 100%). The concretes studied have been subjected to tests for mechanical characterization, porosity, air permeability and chloride ion penetration level. The results obtained show that the mechanical properties are reduced with the increase in the proportions of recycled aggregate and of the residues used as substitution in the cementitious matrix, while the durability properties are only affected by the increase in the percentage of aggregates. recycled. All the concretes studied are suitable to be used as structural concrete.

The third work in this issue is from **Mexico**, where César Antonio Juárez Alvarado and colleagues propose partially replacing stirrups with steel fibers to improve the shear strength of beams. As variables they used the water / cement ratio (a / c), 0.55 and 0.35, the fiber volume (V_f), 0, 0.3, 0.5, 0.7% and 0, 0.2, 0.4, 0.6% respectively, and the stirrup separation. The results showed that the shear resistance with stirrups and fibers was greater than the resistance of the reinforced beams with only stirrups. The comparison between the experimental data and analytical models for the prediction of resistance, showed that the effect

of the relationship (a / c), (V_f), and the contribution of longitudinal and transverse steel is adequately predicted. In addition, the studied models predicted mostly conservative values for the ultimate experimental shear strength.

In the fourth article from **Venezuela**, Oladis Troconis de Rincón and colleagues evaluate the effect of waste clay from a polyol production process, as a partial substitute for cement in reinforced concrete, in concentrations of 0%, 5% and 10%. The physical-mechanical characteristics of the concrete and the electrochemical characteristics of the steel were determined during a period of 356 days (ISO 11474), in 15x10x5 cm specimens, with two steel bars embedded in the concrete. The results indicate that the compressive strength decreased proportionally according to the clay content, increasing for the 90 days of curing. However, the capillary sorption of the concrete decreased, which allowed the steel in a marine environment to maintain its passive state for longer than its targets, for the evaluated a / c ratios (0.45 and 0.60).

The fifth article, by Analiet Calvo Valdés and colleagues, comes from **Brazil** and aims to evaluate the effectiveness of a multi-electrode galvanic sensor in detecting the probability of corrosion in reinforced concrete prisms subjected to wet and dry cycles in a solution. NaCl. Corrosion potential readings (E_{corr}) obtained using a copper sulfate copper electrode (Cu / CuSO₄), galvanic current (I_{gal}) and galvanic potential (E_{par}) readings were analyzed. The developed sensor showed sensitivity to detect the chloride front and predict the possibility of armor corrosion. The variables E_{corr} , E_{par} and I_{gal} presented different behaviors as parameters to monitor corrosion.

The sixth work of this issue is written by Renan Dias and colleagues from **Brazil**. This work aimed to identify, map and quantify the pathological manifestations (BD) in mortar façade coatings (EMR) of 22 residential buildings in Fernandópolis-SP, Brazil. To quantify the BDs, the incidence (M-INC) and intensity (M-INT) methods were used, considering five typified regions of the façade: continuous walls (1-OCW), around gaps (2-OOP), upper part of parapets and eaves (3-TOP), under balconies / balconies / cantilevers (4-BCP) and corners / edges (5-OCE). 4351 and 481 BDs were observed by M-INT and M-INC, respectively, performing standard degradation maps. The most frequent BD were stains and cracks. The regions most affected by M-INT were 2-OOP (34.5%), 1-OCW (23.3%) and 4-BCP (21.60%), and for M-INC they were 1- OCW (39, 9%), 3 -TOP (29.3%) and 2-OOP (16.6%).

The article that closes the edition is by Taís Lara Pio Santos and Paulo Francinete Silva Júnior from **Brazil**, they present the methodology for the inspection and mapping of the pathological manifestations in the monument of the Pórtico del Bautismo Cultural de Goiânia. It is a monument from the early 40s of the 20th century, representative of the art deco architectural style. In 2003 this monument was listed by the National Institute of Historical and Artistic Heritage, but despite its invaluable historical value, the

structure has several pathological manifestations. To achieve this objective, the following procedures were performed: (1) visual inspection; (2) photographic record; (3) anamnesis and (4) trials. The tests carried out were sclerometry, pacometry and deformation measurement. The main pathological manifestations identified were cracking, mortar detachment, reinforcement corrosion and excessive deformation.

This issue includes for the first time a Technical Editorial, prepared by members of the expanded JDI, which illustrates the lessons to take into account when structural failures occur. In this case, the collapse of Miami, was the issue addressed.

We are confident that the articles in this issue will constitute an important reference for those readers involved with questions of evaluations and characterizations of materials, elements and structures. We thank the authors participating in this issue for their willingness and effort to present quality articles and meet the established deadlines.

On behalf of the Editorial Board

A handwritten signature in black ink, appearing to read 'Pedro Castro Borges', written over a circular stamp or mark.

Pedro Castro Borges
Editor in Chief

TECHNICAL EDITORIAL

Need for periodic inspections in buildings.

Creation of the Directorate of structural failures of Alconpat Internacional

This technical editorial was timely released as an institutional statement on the occasion of the Miami landslides and the immediate actions that Alconpat International took. That statement is reproduced verbatim here, strictly respecting its content. In addition, the names of those who make up the new Directorate of structural failures of Alconpat International are provided.

As specialists in concrete pathology, the images of the collapse of the building near Miami seemed overwhelming, both because of the number of victims that occurred at night, and because of the sequence of how it occurred. This feeling of anguish occurs because the main objective of structural engineering is the safety of the lives of the people who use structures and buildings, in addition to their functionality and aesthetics. Safety in which the building does not collapse is the essence of structural engineering. In our case, the specialty that we develop is added to this original objective. Like doctors to the human body, we are dedicated to detecting possible injuries and deterioration that the action of the environment, the loads on the building or the use itself may have caused over the years.

Absolute security does not exist and the more security the more expensive the structure is. Therefore, during the design phase of a new structure, calculations are commonly optimized so that the probability of collapse of residential buildings is 1 in a million. That is, safety is cost-optimized so that the probability of collapse is reasonably small. This theoretical probability was first proposed by the CEB (Euro International Concrete Committee) and then implicitly or explicitly adopted worldwide as the basis for all structural codes. Currently, there is an International Committee on Structural Safety (JCSS) that is responsible for maintaining and disseminating knowledge in this area. The result of decades of application of the principles of what we technically call “limit states” has been highly satisfactory, since it is a general perception that, if the rules based on these concepts are followed in each country, accidents are really very rare.

In the case of the building near Miami, the construction was 40 years old, so the safety level of the project should not have been affected, which must be maintained throughout the useful life of the structure. Without going into technical details, security cannot be less than that established by law and must be maintained over time and for that. If necessary, the buildings are reinforced and repaired. Therefore, the periodic inspections must contain a priority section so that it is reviewed and verified that the structural safety continues to maintain the levels foreseen in the project. It is not only a matter of detecting dampness or functional failures or of enclosures and roofs, which are also important since they affect comfort, but comparatively they are secondary when human life is at stake. The fundamental objective should be to review the structural components and confirm that their good performance is maintained.

Therefore, the inspector should not only have knowledge of structural engineering but also of pathology and durability of the materials, that is to say, know which injuries and deterioration are possible due to the particular location of each structure, in detecting its degree of risk and its impact on the required structural safety levels.

There are already guides and recommendations on how to carry out the inspection and what tests to carry out in existing structures, to detect hidden injuries despite the good external appearance, such as unexpected decreases in the mechanical resistance of concrete due to chemical attacks, due to high

salinities in water tables or by the corrosion of reinforcing steel in marine environments, such as that at the site of the collapse.

In the case of the collapsed building, we do not dare to venture an opinion on the causes of the collapse as we do not have the necessary data for its analysis, but if we want to state that it is necessary to "learn lessons" that allow us to avoid other accidents in similar circumstances. Only a rigorous forensic analysis, developed by specialists, will be able to confirm the true cause from all the hypotheses that are raised.

We want to manifest that some issues seemed essential to us in the stage in which the debris removal works were carried out, fully respecting the need for them to have been as fast as possible, always considering that the highest priority is to find life or at least human remains and personal belongings. Reputable specialists in the pathology and durability of concrete and materials, and there are, for example, in Florida universities themselves, who advise and collaborate with rescuers to take samples and identify clues about the possible causes of the collapse. If those tests are not acquired now, crucial evidence to elucidate the validity of the hypotheses that need to be developed to explain the collapse may be lost. For example, it is essential to have expertly selected samples of the concretes and trusses of the pillars on the ground floor and the slabs of the basement.

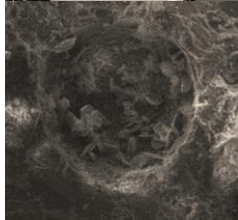
As the demolition of the remaining part of the building has been determined for safety reasons, there must be a separation of remains between one and the other collapse so that an immediate inspection of the part of the building that was still standing is undertaken, in order to verify the degree of injuries or the integrity of its materials, especially of the base of the pillars and the areas of connection with the foundations and the slabs of the mezzanines. This will allow a comparison between both collapses, which only an inspection by specialists in pathology can help to elucidate.

In addition, since there is a twin building that has collapsed, it would be necessary to carry out an inspection by the aforementioned specialists in concrete durability to expand the possibility of confirming the hypotheses that may be raised.

As specialists in construction pathology of ALCONPAT (Latin American Association for Quality Control, Pathology and Construction Recovery) we want to declare that we have immediately constituted within our organization, a commission of independent experts comparable to the way it is done with the aeronautical accidents. In particular accidents, defects can be detected that should not be repeated in other constructions, including the improvement of the diagnoses to be carried out on the structures in service. It is essential that these types of accidents are explained by structural engineering in a transparent and usable way according to the codes and recommendations of the world. Only transparency and publicity of the conclusions will restore to society the confidence that the knowledge and professionals capable of detecting defects and injuries in structures really exist and thus anticipating and avoiding other similar accidents with the most regrettable consequences, losses. of human lives.

The Directorate of Structural Failures of Alconpat International was made up of Raúl Husni (President, Argentina), Jesús Rodríguez (Member, Spain), Andrés Torres (Member, Mexico), Paulo Helene (Member, Brazil), and Alberto Sagüés (Member, Argentina / USES).

Signed by:
International Board of Directors (expanded)



CONTENT

Page

BASIC RESEARCH

Tiecher, F., Langoski, M., Hasparyk, N.: Behavior of mortars with different types of cement when induced to Delayed Ettringite Formation (DEF) 1 - 16

Gurdián, H., Garcés, P., Zornoza, E., García Alcocel, E.: Durability of concrete with pozzolanic admixtures and recycled aggregates. 17 – 30

Juárez-Alvarado, C. A., Mendoza-Rangel, J. M., Terán-Torres, B. T., Valdez-Tamez, P. L., Castruita-Velázquez, G.: Theoretical-experimental behavior of steel fibers as a partial replacement for shear reinforcement in reinforced concrete beams. 31 – 49

Troconis de Rincón, O., Millano, V., Suarez, W., Navarro, L., De Turrís, A., Amesty, R.: Evaluation of the effect of waste clay from a polyol production process as a partial substitute for cement in reinforced concrete 50 - 63

APPLIED RESEARCH

Calvo Valdés, A., Medeiros, M. H. F., Macioski, G.: Corrosion sensor for monitoring reinforced concrete structures: Tests on reinforced concrete specimens. 64 - 87




CASE STUDY

Dias, R., Pagoto, L., Tsutsumoto, N., Fioriti, C.: Mapping External Mortar Render (RAF) defects: case study in multi-storey residential buildings. 88 - 107

DOCUMENTARY RESEARCH

Pio Santos, T. L., Silva Júnior, P. F.: Documentation of the pathological manifestations of the Portico of the Cultural Baptism of Goiânia - Art Déco historical monument. 108 - 122

Behavior of mortars with different types of cement when induced to Delayed Ettringite Formation (DEF)

F. Tiecher^{1*}, M. Langoski², N. Hasparyk³

*Contact author: francieli.bonsebiante@imed.edu.br

DOI: <https://doi.org/10.21041/ra.v11i3.537>

Reception: 16/05/2021 | Acceptance: 03/08/2021 | Publication: 01/09/2021

ABSTRACT

The purpose of this paper is to present an evaluation of different types of cement and the incidence of Delayed Ettringite Formation (DEF) through mortar composites cast in the laboratory and exposed to a high curing temperature over a 12-month study period. DEF represents one of the types of Internal Sulfate Attacks (ISA) related to an expansive chemical reaction that occurs inside of concrete involving the sulfates from cement. Experiments involved the assessment of expansions, compressive and tensile strengths as well as microstructural characteristics over time. It was observed that tests performed on mortars and with a specific mix required an extended evaluation period to distinguish the behaviors. Furthermore, high early-strength cement featured the worst binder when faced with DEF.

Keywords: ettringite; DEF; expansions; mechanical properties; mortar; microstructure.

Cite as: Tiecher, F., Langoski, M., Hasparyk, N. (2021), “*Behavior of mortars with different types of cement when induced to Delayed Ettringite Formation (DEF)*”, Revista ALCONPAT, 11 (3), pp. 1 – 16, DOI: <https://doi.org/10.21041/ra.v11i3.537>

¹ Escola Politécnica, Mestrado em Engenharia Civil, IMED, Passo Fundo, Brazil

² Mestrado em Engenharia Civil, IMED, Passo Fundo, Brazil

³ Departamento de Durabilidade, Eletrobrás Furnas S.A., Aparecida de Goiânia, Brazil

Contribution of each author

In this work, the author F. Tiecher was in charge of analyzing and discussing the results and writing the article. The author N. Hasparyk was responsible for the scanning electron microscope analysis, the analysis and discussion of the results, as well as the writing of the article. The author M. Langoski was in charge of carrying out the laboratory tests.

Creative Commons License

Copyright 2021 by the authors. This work is an Open-Access article published under the terms and conditions of an International Creative Commons Attribution 4.0 International License ([CC BY 4.0](https://creativecommons.org/licenses/by/4.0/)).

Discussions and subsequent corrections to the publication

Any dispute, including the replies of the authors, will be published in the second issue of 2022 provided that the information is received before the closing of the first issue of 2022.

Comportamento de argamassas com diferentes tipos de cimento quando induzidas à Formação de Etringita Tardia (DEF)

RESUMO

Este trabalho objetiva a avaliação de diferentes tipos de cimento frente à incidência de Formação de Etringita Tardia (DEF), através de argamassas produzidas em laboratório e expostas a alta temperatura de cura durante um período de estudo de 12 meses. A DEF representa um dos tipos de Ataque Interno de Sulfato (ISA) relacionado a uma reação química expansiva que ocorre no concreto envolvendo sulfatos do cimento. Os experimentos envolveram avaliação de expansões, resistências à compressão e à tração, e características microestruturais ao longo do tempo. Observou-se que os ensaios em argamassas exigiram um período de avaliação prolongado para distinguir os comportamentos entre os cimentos. Além disso, o cimento de alta resistência inicial apresentou o pior comportamento em relação à DEF.

Palavras-chave: etringita; DEF; expansões; propriedades mecânicas; argamassa; microestrutura.

Comportamiento de los morteros con diferentes tipos de cemento cuando son inducidos a la Formación de Etringita Tardía (DEF)

RESUMEN

Este trabajo tiene como objetivo evaluar diferentes tipos de cemento frente a la incidencia de la Formación de Etringita Tardía (DEF), utilizando morteros producidos en laboratorio y expuestos a una alta temperatura de curado durante un período de estudio de 12 meses. DEF representa uno de los tipos de ataque interno de sulfato (ISA) relacionado con una reacción química expansiva que ocurre en el concreto que involucra sulfatos de cemento. Los experimentos incluyeron la evaluación de las resistencias a la expansión, a la compresión y a la tracción, y las características microestructurales a lo largo del tiempo. Se observó que las pruebas en morteros requirieron un período de evaluación prolongado para distinguir los comportamientos entre los cementos. Además, el cemento de alta resistencia inicial tuvo el peor comportamiento en relación con el DEF.

Palabras clave: etringite; DEF; expansiones; propiedades mecánicas; argamasa; microestructura.

Legal Information

Revista ALCONPAT is a quarterly publication by the Asociación Latinoamericana de Control de Calidad, Patología y Recuperación de la Construcción, Internacional, A.C., Km. 6 antigua carretera a Progreso, Mérida, Yucatán, 97310, Tel.5219997385893, alconpat.int@gmail.com, Website: www.alconpat.org

Reservation of rights for exclusive use No.04-2013-011717330300-203, and ISSN 2007-6835, both granted by the Instituto Nacional de Derecho de Autor. Responsible editor: Pedro Castro Borges, Ph.D. Responsible for the last update of this issue, Informatics Unit ALCONPAT, Elizabeth Sabido Maldonado.

The views of the authors do not necessarily reflect the position of the editor.

The total or partial reproduction of the contents and images of the publication is carried out in accordance with the COPE code and the CC BY 4.0 license of the Revista ALCONPAT.

1. INTRODUCTION

Primary ettringite is produced from the reaction of aluminates and sulfate ions from clinker (C_3A ; C_4AF ; SO_3) during the hydration process. However, this compound becomes unstable when concrete temperatures exceed 60-65°C during the first hours after casting. This situation can occur due to excessive hydration heat generated by cement hydration or even by thermal curing processes that are usually adopted for pre-cast elements in the industry. Thus, after cooling, DEF can occur (Taylor, 1997; Bauer, 2006; Ifsttar, 2018).

Several laboratory studies are presented in the literature, although different parameters impair accurate comparisons. Aside from sulfate ions and temperature, the main conditional factors are the presence of aluminates and high moisture (Mehta; Monteiro, 2014; Neville, 2016; Kchakech et.al., 2016; Thiebaut et.al., 2018; Ramu et.al., 2021).

Other influential factors can activate DEF more quickly. Among them are the types of materials used for concrete and exposure conditions (Fu et.al., 1997; Leklou et.al., 2013). In relation to concrete expositions, moisture is necessary to promote DEF, besides temperature rise at the first hydration stages of cement (Godart, 2017). In addition to the level of temperature, the dwell time of the peak of temperature also influences the rate of ettringite crystallization (Kchakech et al., 2016; Giannini et al., 2018). Some researchers evaluated the effect of pozzolanic admixtures (Al Shamaa et.al., 2016; Dayarathne et.al., 2013; Ramlochan et.al., 2013; Amine et.al., 2017; Asamoto et.al., 2017; Leklou et.al., 2016; Rashidi et.al., 2017), even though there has been no clear agreement on these incorporations to date. Some researches point to pozzolan admixtures as a mitigative measure to reduce temperature rise of concrete during the cement hydration (Ramlochan et al. 2003; Mehta; Monteiro, 2014; Amine et al., 2017). Mineral admixtures have been studied in relation to their interaction along cement hydration (Dayarathne et.al., 2013; Amine et.al., 2017). Some researchers indicate a beneficial effect of fly-ash (Ramlochan et.al., 2003; Dayarathne et.al., 2013; Amine et.al., 2017; Asamoto et.al., 2017; Leklou et.al., 2017), but others suggest this admixture just delays the neoformations and the expansive process of DEF (Schovanz, 2019; Bronholo, 2020; Schovanz et.al., 2021).

The content of pozzolans varies between studies aimed at mitigating DEF occurrence. Some researchers tested a range of 15% as suitable for prevention (Amine et.al., 2017), whereas others indicate that 30% of fly-ash is required (Leklou et.al., 2017). These differences are usually related to the type and composition of the mineral admixtures (Ramlochan et.al., 2003).

The concentrations of some components can interfere with the chemical process. Taylor et al. (2001) points out the relation of SO_3/Al_2O_3 in DEF occurrence. In the case of cement replacement by fly-ash, this relation tends to reduce and minimize DEF expansions (Ramlochan et.al., 2013; Leklou et.al., 2016).

The manufacture of cement involves incorporating different mineral admixtures and contents, depending on the local availability of supplies. This is a global practice; aside from reducing energetic consumption in the clinker production, there exists an optimal usage of residues to offset one's carbon footprint. Furthermore, this practice can also improve concrete performance and resistance to chemical attacks. However, little is known about blended cements. The performance of high early-strength cement is known to bring severe damages to concrete (Schovanz et.al., 2021) and is responsible for several cases of DEF diagnosed in some elements and structures in Brazil (Hasparyk et.al., 2016; Godart, 2017; Hasparyk and Kuperman, 2019). High contents of cement and specific physical-chemical characteristics can interfere in heat liberation during hydration heat (Melo et.al., 2011; Godart, 2017).

Some studies at laboratories with mortars can be observed in the literature to favor DEF (Adamopoulou et.al., 2011; Dayarathne et.al., 2013; Leklou et.al., 2016). The same practice was previously used for other types of pathologies (like alkali-aggregate reactions) in order to simplify

test methods and include them in the standards.

Evidence of the relation between C3A and the intensity of formed ettringite can be observed in the studies involving mortars by Katsioti et al. (2011). Furthermore, researchers like Asamoto et al. (2017) had determined at the laboratory that DEF will occur just in the presence of contents of SO₃ above 3%. In addition, Adamopoulou et al. (2011) identified DEF prematurely (3 months) in mortars that were thermally cured at 50°C, even though the majority of studies state that maximum limit temperatures should not exceed 65°C (Al Shamaa et al., 2016; Godart, 2017). Bronholo (2020) did not detect expansive expansions in mortars with fly-ash cement when mortars were exposed to coupled attacks of DEF and ASR over one year. However, DEF was discovered to be present in the cement matrixes of the mortars through microstructural analyses.

This study aimed to evaluate the influence of different types of cement on DEF occurrence using laboratory tests and analyses performed in cement composites.

2. EXPERIMENTAL PROGRAM

2.1 Materials

The experimental program included four different types of Portland cement as follows: High Early Strength Cement (CP V); Blended Cement with Fly-Ash (about 9% of pozzolan - CP II-Z); Blended Cement with Limestone Filler (about 6% of filler - CP II-F); Pozzolanic Cement with Fly-Ash (about 24% - CP IV). Table 1 presents chemical characteristics of cements obtained by X ray fluorescence and also their fineness by Blaine.

Table 1. Main characteristics of cements

Parameter (in %)	CP V	CP II-F	CP II-Z	CP IV
<i>CaO</i>	0.93	0.74	1.02	0.85
<i>SiO₂</i>	19.56	20.41	22.69	30.73
<i>Al₂O₃</i>	5.26	4.55	5.82	8.60
<i>Fe₂O₃</i>	2.87	2.12	3.07	3.83
<i>Na₂O_{eq}</i>	0.54	0.47	0.41	1.02
<i>MgO</i>	1.03	1.35	1.10	1.57
<i>SO₃</i>	2.93	2.52	1.85	0.05
<i>SO₃/Al₂O₃</i>	0.56	0.55	0.32	0.01
<i>Insoluble residue</i>	0.55	5.74	8.72	24.48
<i>Loss on ignition</i>	4.28	8.71	6.08	5.13
<i>Blaine Fineness</i>				
<i>(in cm²/g)</i>	4,250	4,450	5,110	4,050

*Na₂O_{eq} = 0.658 K₂O + Na₂O.

The fine aggregate used in the experiments has 4.8 mm of maximum size and is alkali silica reaction (ASR) innocuous, according to the previous accelerated mortar bar test (Brazilian Standard NBR 15577, 2018).

2.2 Procedures of casting and curing

The mix of mortars presented a proportion of 1:2.275 of cement: fine aggregate and the water-cement ratio was equal to 0,485, according to ASTM C 1012 (2018).

The procedure and thermal cycle adopted to induce DEF was previously proposed by Schovanz (2019) and Hasparyk et al. (2020). Specimens were cast and maintained for 6 hours in a moist room until the beginning of the thermal cycle (pre-curing period). In the sequence, specimens were submerged in water with a gradual increase of temperature from 25°C up to 85°C, remaining in this condition for 12 hours, followed by cooling up to 38°C. Both the heating and cooling rate was 10°C per hour over time and up to one year (Figure 1).

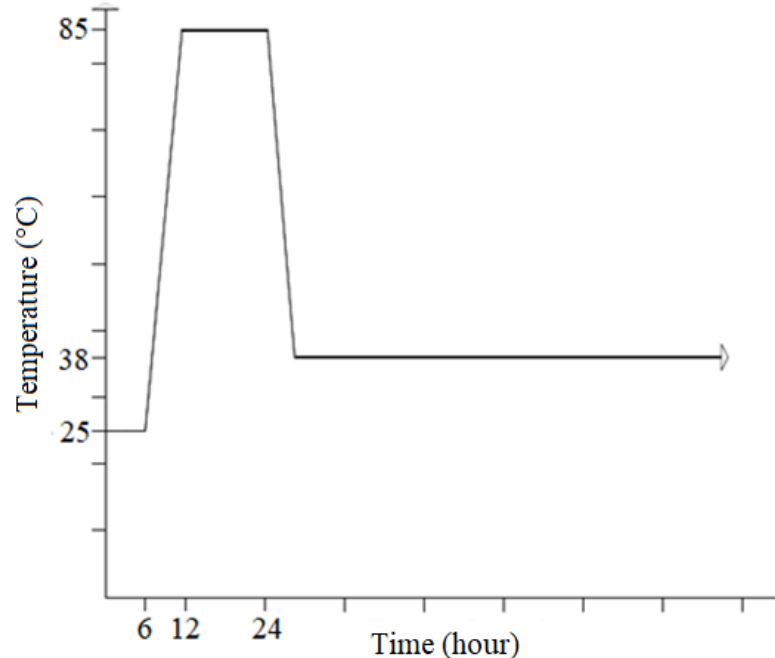


Figure 1. Thermal cycle and exposure environment

2.3 Laboratory investigations

Physical, mechanical and microstructural analyses were performed to evaluate DEF. Expansions and mass variations were monitored periodically with 3 mortar prisms for each cement (25x25x285 mm) over 365 days. Mechanical properties such as compressive strength and diametral tensile strength were also determined in 4 cylindrical specimens for each age and cement (50x100 mm) over time by NBR 7215 (ABNT, 2019) and NBR 7222 (ABNT, 2011), respectively. The microstructural analyses were performed through a scanning electron microscope with EDS. Fracture samples collected from the internal part of the specimens after mechanical tests were investigated by a secondary electron detector (SE).

3. RESULTS AND DISCUSSIONS

According to Figure 2, values of expansion for mortars containing cement with no admixture were much higher than those in the presence of some admixture. The first major increase began after 150 days and lasted up to 200 days; after that, a dormancy period was observed for up to 260 days, followed by another increase in expansion for up to about 300 days. Then, the growing rate of expansion was intensified up to 365 days (the maximum expansion was 1.8%). Although the fly-ash cements (both, CP II-Z and CP IV) produced reduced expansions (below 0.10% at 365 days), a higher dispersion for expansions was observed over time. Cement with limestone filler (CP II-F type) performed entirely differently from the others. Over time and up to about 300 days, there were minor expansions below 0.06%. After this period, a significant growth rate was perceived for up to 365 days, when mortar achieved an average expansion of 0.45%.

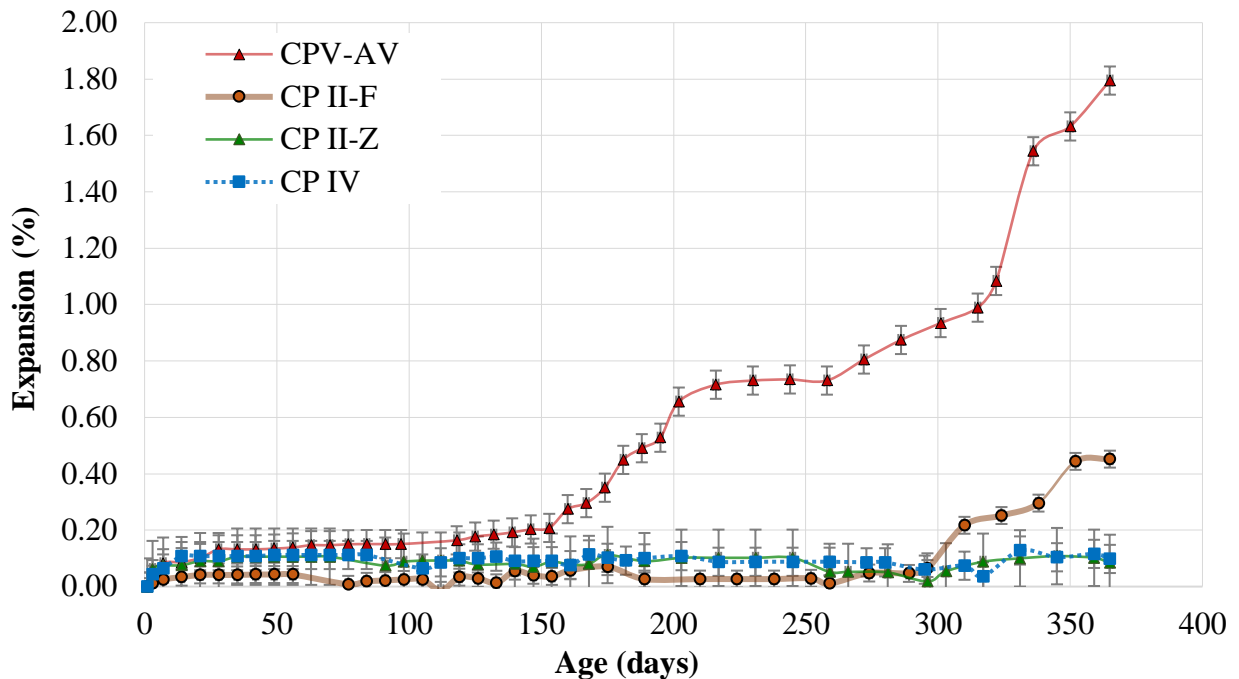


Figure 2. Evolution of DEF expansions over time

It can be mentioned that fly-ash influences the contents of Al_2O_3 and SO_3 (Table 1) of cement, with a significant reduction in the $\text{SO}_3/\text{Al}_2\text{O}_3$ relation followed by reduced DEF expansions.

According to the literature (Ramlochan et.al., 2013; Leklou et.al., 2016), those parameters can support a better understanding of the performance of cement with fly-ash (CP II-Z and CP IV) in relation to the other. CP V and CP II-F do not contain pozzolans, and the main difference is related to the fineness (CP V - $4.250 \text{ cm}^2/\text{g}$; CP II-F - $4.450 \text{ cm}^2/\text{g}$) and the presence of limestone filler (5.74%). Cement fineness accelerates hydration reactions and, thus, the heat of hydration. Shamaa et al. (2016) had previously presented the effect of filler in the kinetic of DEF reaction; however, it is not capable of mitigating DEF. According to the authors, expansions can increase and the latency period can be reduced with the increase of particles of limestone filler in the mixes. The reaction of dissolved carbonate ions from the limestone filler with the aluminate phases of Portland cement leads to the formation of carboaluminates as opposed to sulfoaluminates, and stabilizes the ettringite that is produced at early ages.

Mechanical properties were coherent among tested cements and were determined by comparing expansions. The compressive strength of mortars increased from one month to six months for all tested cements (Figure 3). On the other hand, at 12 months there was a decrease. The drop of this property in comparison to 1 month was much more critical for the cement with no admixture (CP V) and the one with limestone filler (CP II-F), 63% and 54%, for expansion levels of 1.79 and 0.45, respectively. Even though the level of expansions for CP V was higher than the one for CP II-F, since CP V is a high early strength cement, mortar achieved higher strengths at the first ages compared to the CP II-F concrete. Furthermore, expansion stages above 0.40% are too high to impact strengths and damage cement composites, as expected (Schovanz, 2019; Bronholo, 2020).

In the presence of fly-ash, and especially for the CP II-Z, a decrease was not observed at one year, considering low expansions (less than 0.10%), but in relation to 6 months, there was a reduction of just about 2% in the presence of this cement, meanwhile pozzolanic cement (CP IV) suffered a decrease of about 25% for the same period (Figure 3 and Table 2).

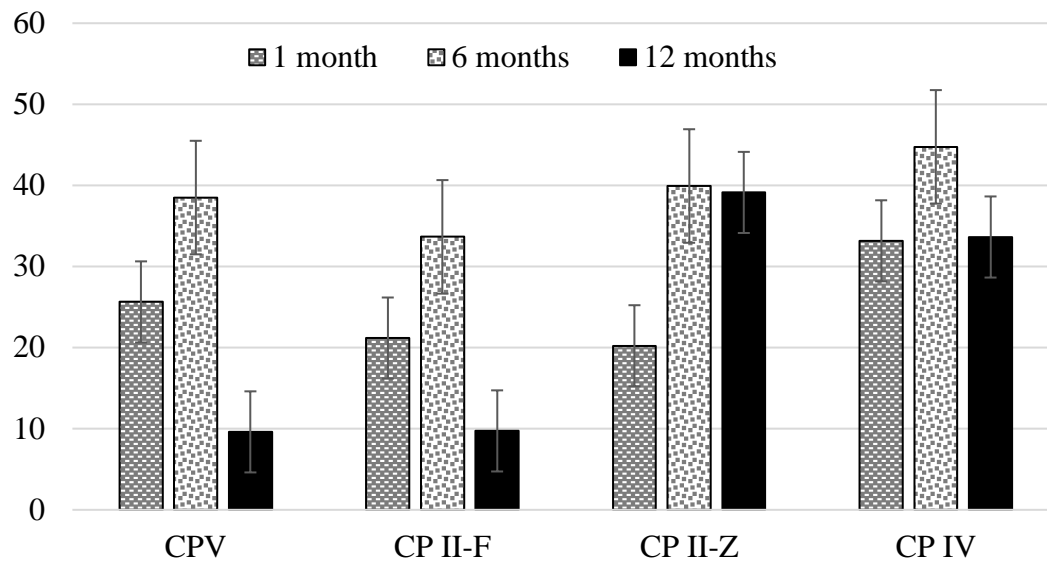


Figure 3. Compressive strength over time

Even though compressive strength is not the main property influenced by the most expansive reactions, it is not valid in the case of DEF. Microcracking generated by DEF starts in the interfacial transition zone (TZ) between cement and aggregate, leading to negative influence in this property, and especially in mixes with cement pozzolanic admixtures (Taylor et al., 2001). Self-healing of cracking in cement composites can be achieved through the use of pozzolan admixtures (Van Tittelboom and De Belie, 2013). This phenomenon can explain the better performance of composites with fly-ash in relation to the compressive strength (Termkhajornkit et al., 2009).

Tensile strength featured a slightly higher sensitivity due to the higher expansions of CP V (1,79%) and CP II-F (above 0.45%). Soon, at six months there was already a drop of this property followed by a new drop at 12 months. At six months, tensile strength had a reduction of about 9% for both types of cement. At the last age, mortars with CP V and CP II-F suffered a decrease of 68% and 57%, respectively (Table 2 and Figure 4). Some researchers have shown that expansions of the order of 0.2-0.3% are able to affect tensile strength meanwhile compressive strengths are influenced at higher levels of expansions (Giannini et al., 2018; Leklou et al., 2016).

Mortars with fly-ash performed differently due to an increase of tensile strength up to the first six months, somewhat following the behavior of compressive strength, but over time and at 12 months, there was a drop of 19% and 12% for CP II-Z and CP IV, respectively (Figure 4). The initial gain in the tensile strength occurs due to the pozzolanic reactions involving the mineral admixtures that are present in these cements.

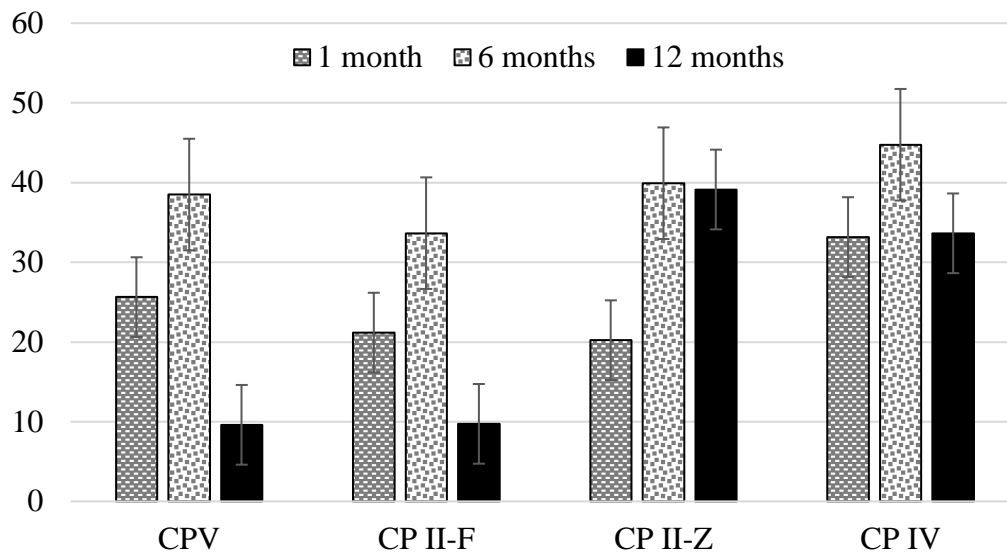


Figure 4. Tensile strength over time

Table 2. Behavior of mortar properties in relation to expansions at one year

<i>Cement Type</i>	<i>% Reduction in Compressive Strength</i>	<i>% Reduction in Tensile Strength</i>	<i>Expansion (%)</i>
CP V	-63	-68	1.79
CP II-F	-54	-57	0.45
CP II-Z	93	9	0.08
CP IV	1	-9	0.10

According to Table 2, it is evident that for expansions above 0.45%, the damage to mechanical properties is very expressive, with reductions above the order of 50%. Furthermore, for expansions measured in mortars of about 0.10%, there are already clear signs of a beginning of DEF deterioration since tensile strength appears with a significant reduction of about 10% at one year. This negative reflex raises concern about the performance of concretes cast with this type of pozzolanic cement in relation to DEF. The level of expansion does not seem as high as expected, but mechanical consequences are detected, and DEF was observed through microstructural analyses. Thus, for DEF studies in mortars, a threshold at one year should be less than this value. Further research is necessary to define a completely reliable test method and limit of expansions. A correlation between both the strength and the level of expansions is presented in the Figure 5 and Figure 6. As expansions increase, the strengths reduce for the cement types CP V and CP II-F; on the other hand, it is not possible to establish a correlation in the presence of those cements with fly-ash (CP II-Z and CP IV). In order to corroborate this statement, microstructural analyses were performed and clearly indicate formations of ettringite crystals in the mortars containing fly-ash. Mortar samples from the other cements were also analyzed and DEF detected. In Figures 7 - 10, DEF occurrence can be confirmed, and some EDS spectra are presented confirming the chemical feature of ettringite formations.

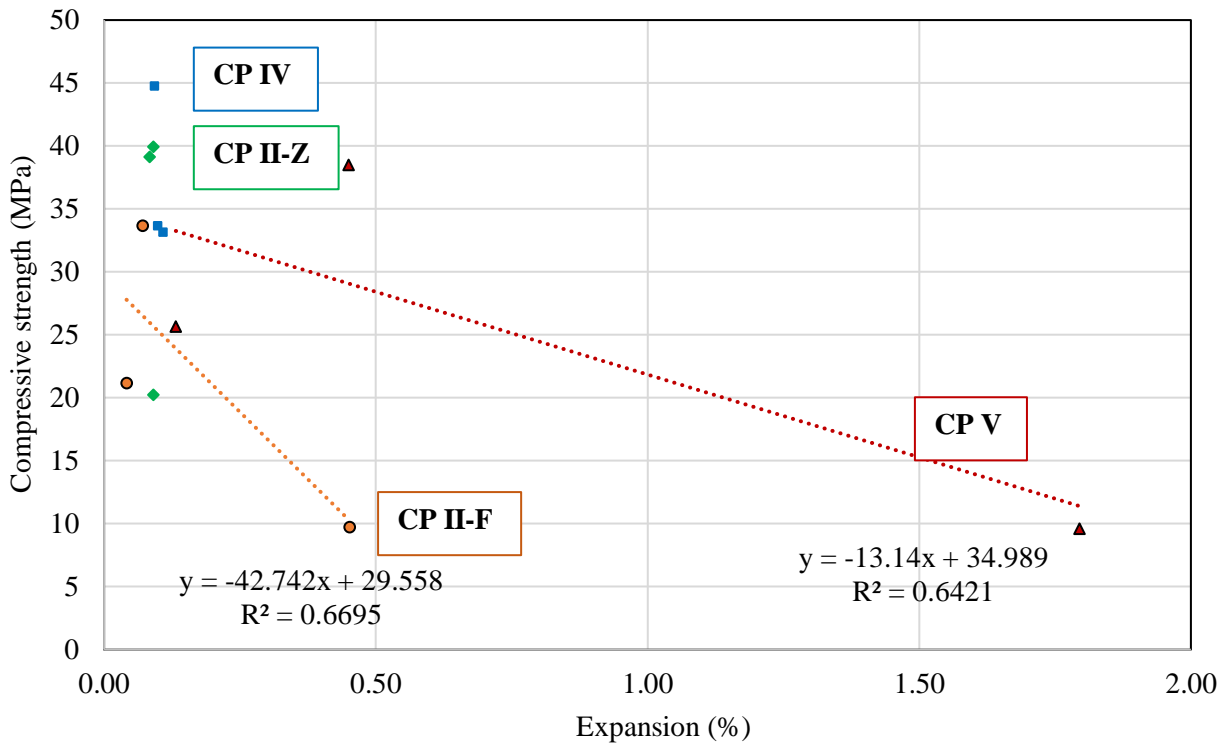


Figure 5. Correlation between compressive strength and expansion

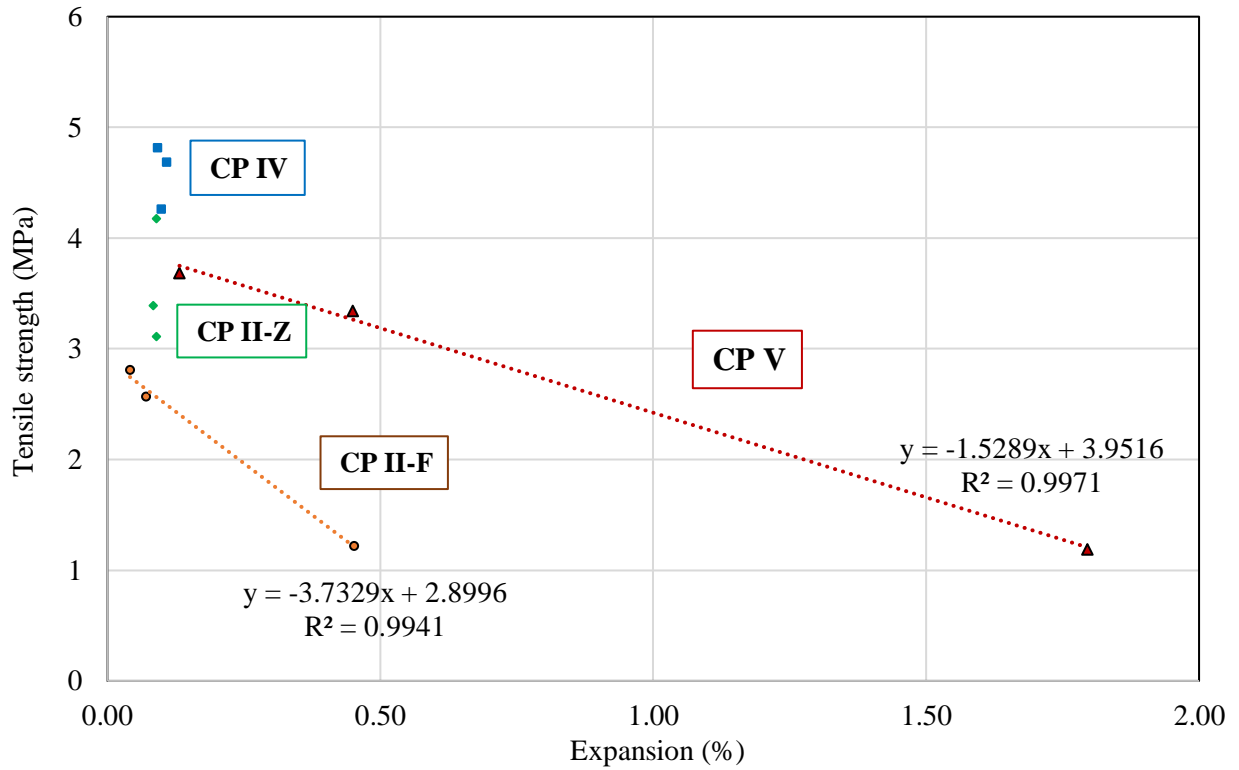


Figure 6. Correlation between tensile strength and expansion

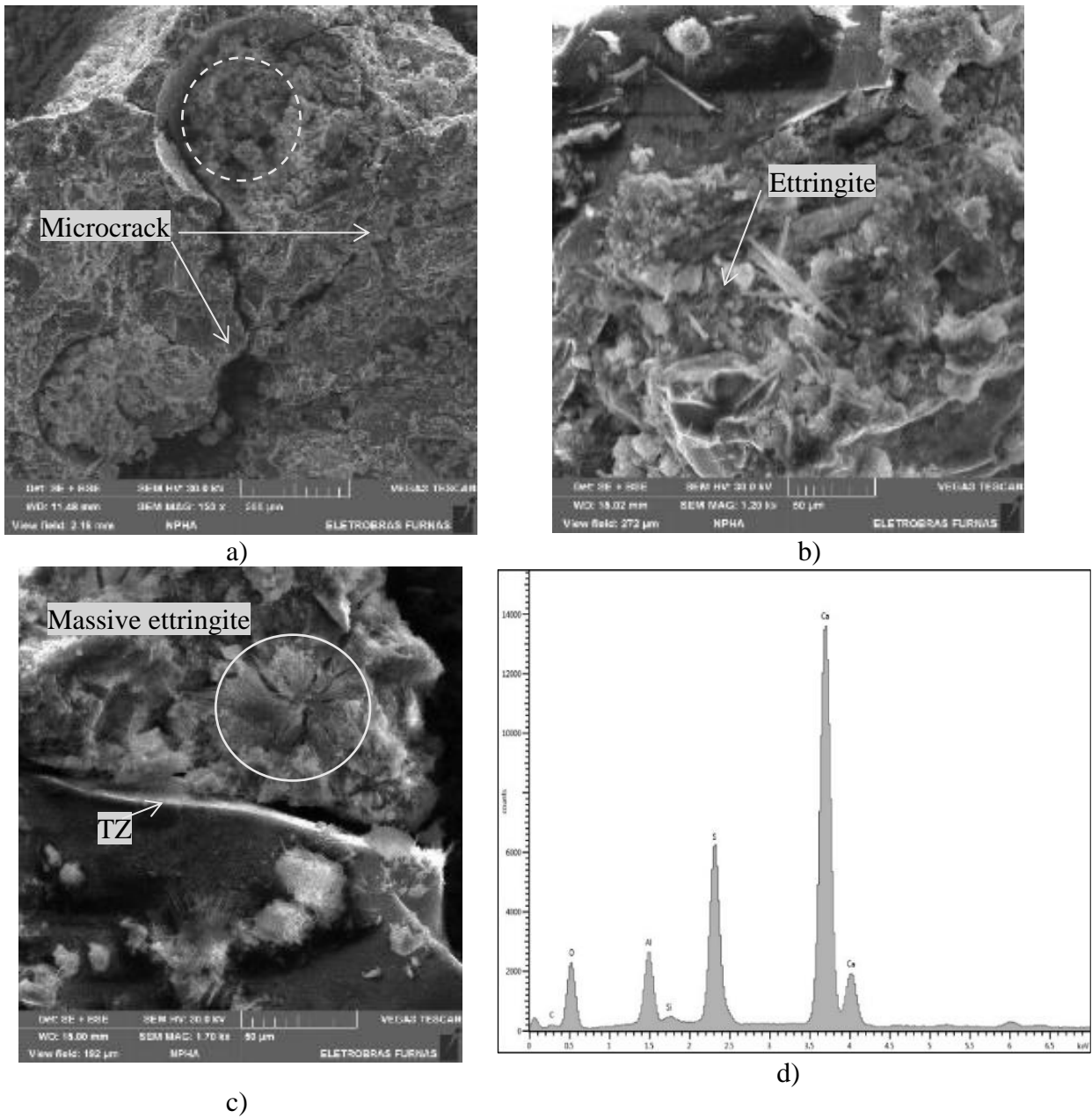


Figure 7. Micrographs of mortars with CP V at one year: a) Voids filled and intense microcracking; b) Fragile paste; with ettringite formation; c) TZ weakened and massive ettringite in the cement paste; d) EDS spectrum of ettringite crystals indicated in the Fig. 7a.

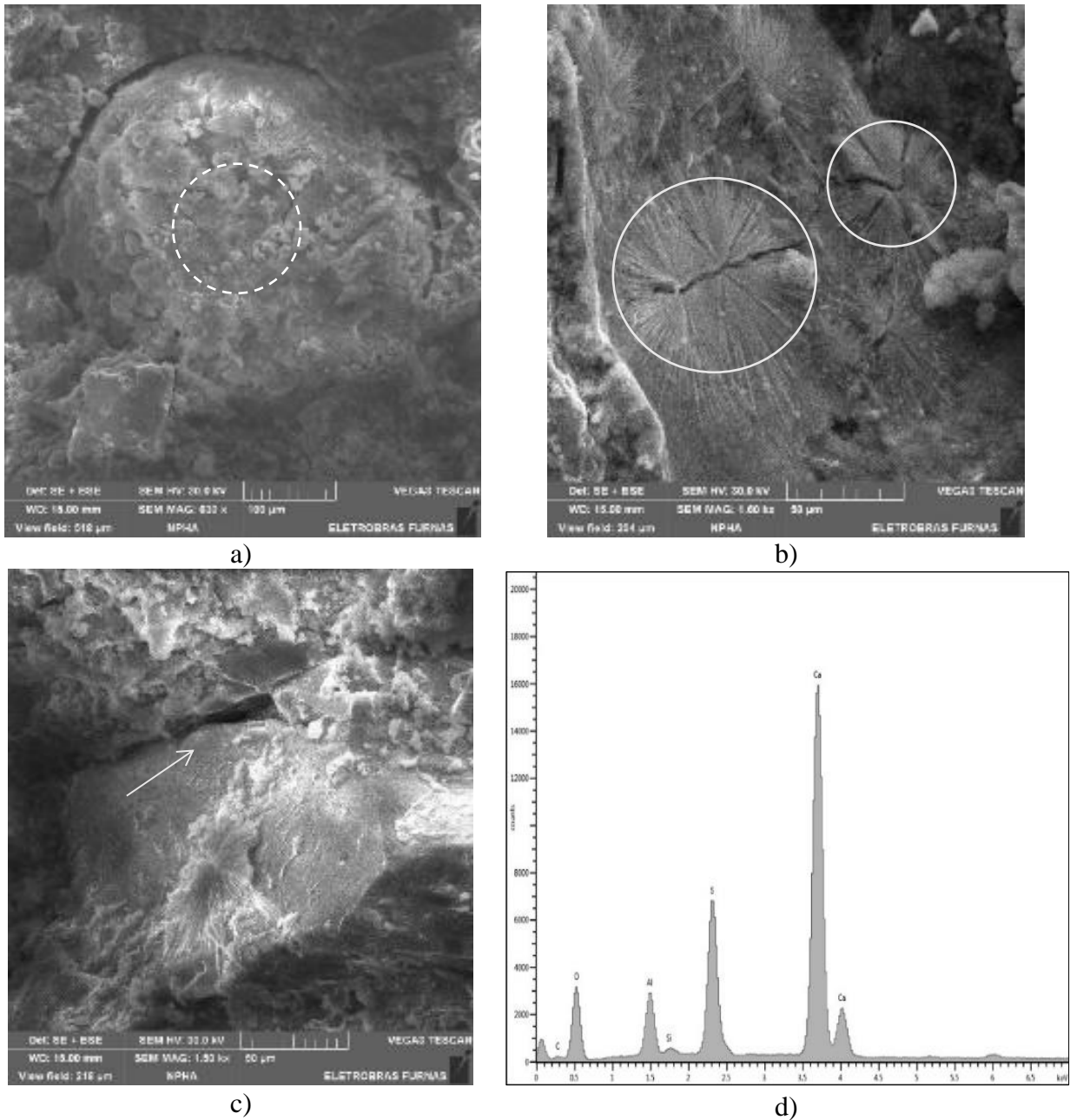


Figure 8. Micrographs of mortars with CP II-F at one year: a) DEF filling a void; b) Compressed Ettringite crystals in the cement paste; c) Loss of adherence between cement paste and aggregate and neoformations in the surface of aggregate; d) EDS spectrum of massive ettringite indicated in Fig. 8a.

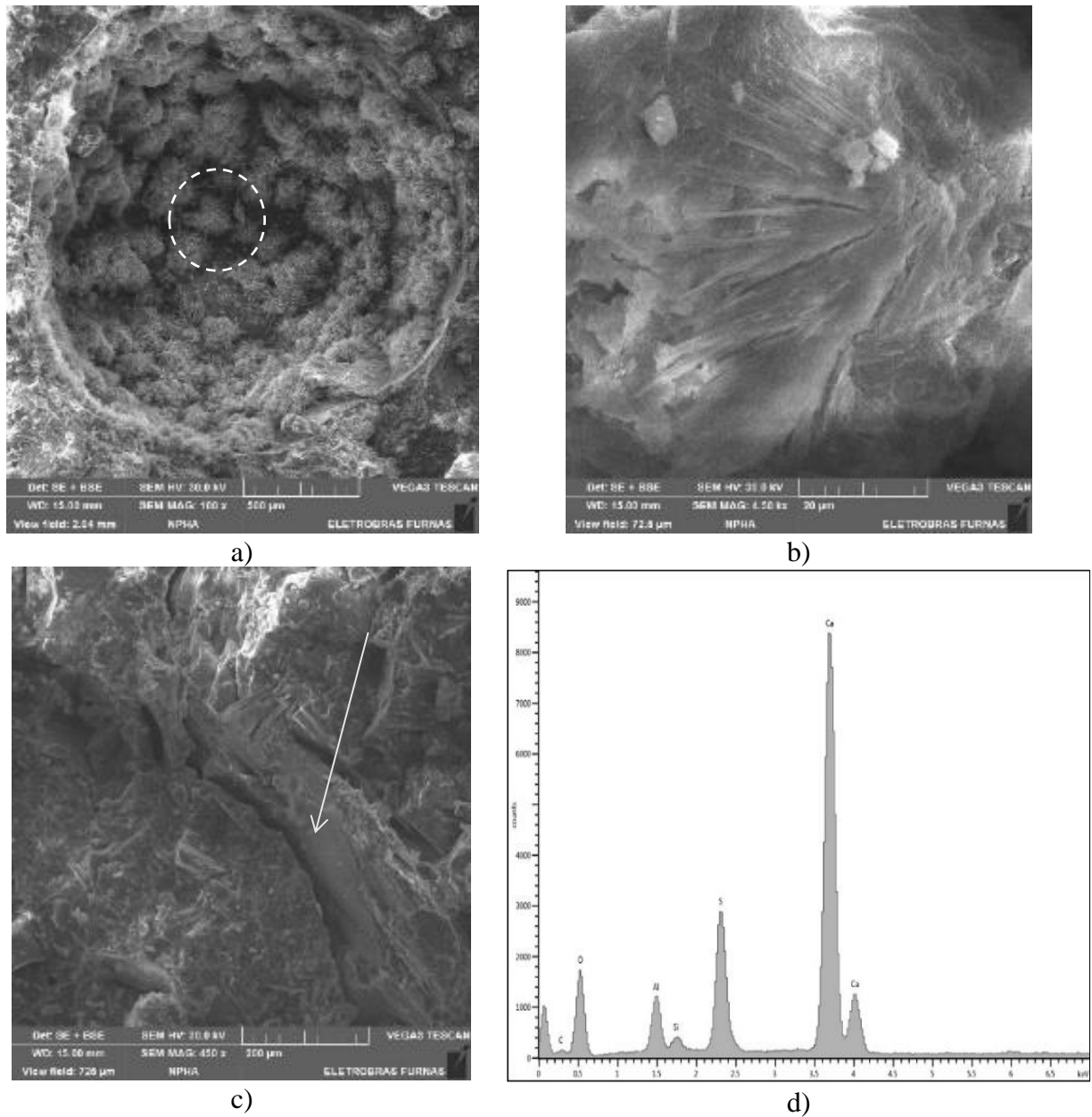


Figure 9. Micrographs of mortars with CP II-Z at one year:

- a) Agglomeration of ettringite in a void; b) Massive formations in the cement paste; c) Detachment between paste and aggregate; d) EDS spectrum of ettringite agglomerations indicated in Fig. 9a.

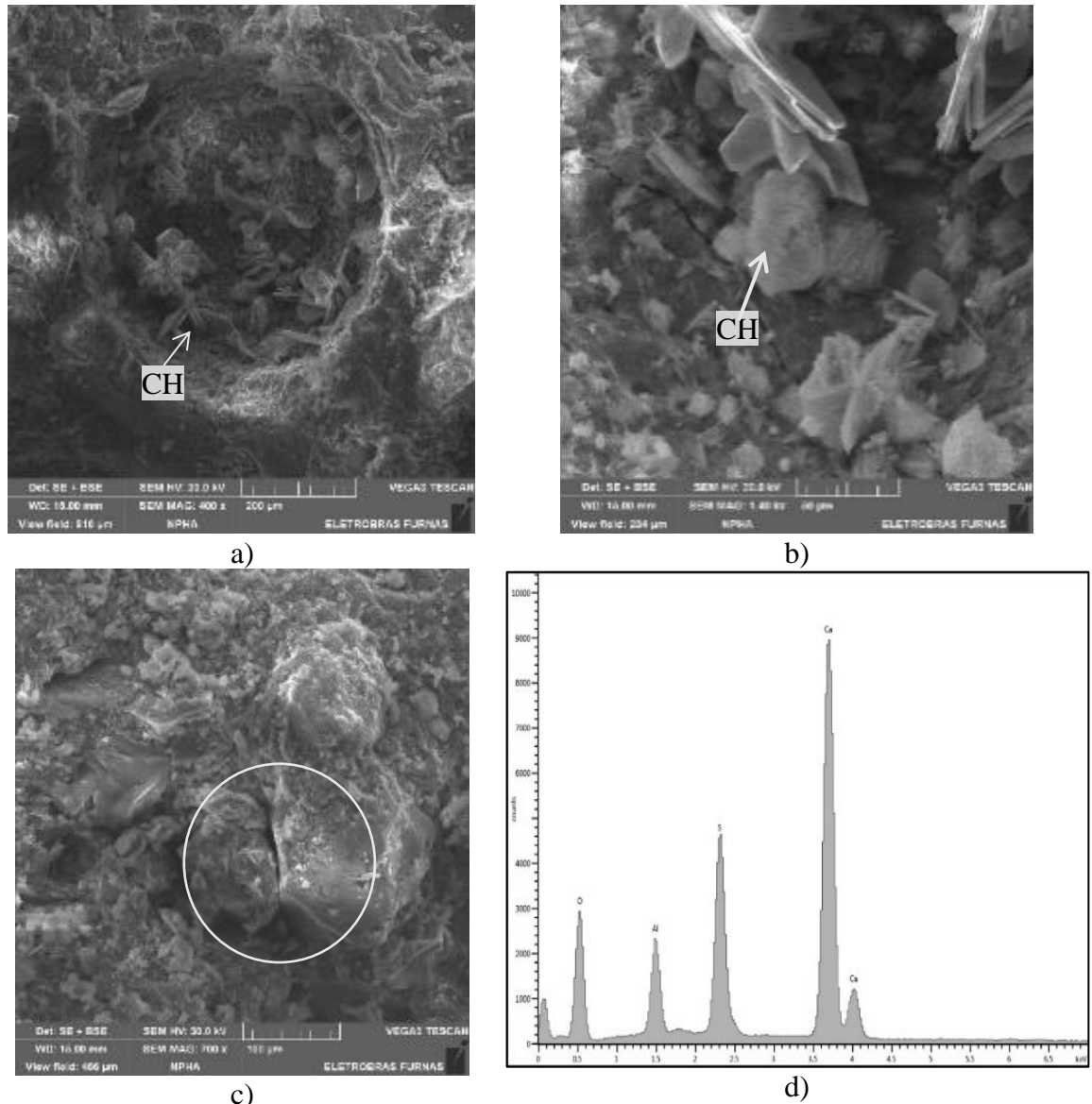


Figure 10. Micrographs of mortars with CP IV at one year:

- a) CH crystals inside a void with a few Ettringite formations;
- b) Detail of a few ettringite crystals and CH;
- c) Some grains of aggregate disconnected in the mortar;
- d) EDS spectrum of crystals indicated in Fig. 10b.

Analyses performed at one year by SEM and EDS had evidenced the presence of delayed ettringite in some conditions. It is possible to compare differences from each cement used and also the magnitude of neoformations. Expansions, as well as mechanical behavior, can be explained by microstructure. DEF damages for tensile strength followed this descending order: CP V; CP II-F; CP II-Z; CP IV. From a microstructural point of view, ettringite neoformation incidences in the voids and cement paste and fragility of paste were observed in the same order. However, some loss of adherence between paste and aggregate was detected in all the samples, independent of the cement type. Furthermore, for mortars cast without fly-ash pozzolan (CP V e CP II-F), the presence of ettringite neoformations was more significant. Compressive strength behavior was similar to tensile strength, even though cement CP II-Z did not promote an abrupt decrease when compared

to cement CP IV at one year. In relation to DEF expansion levels, major values were achieved for cement with no admixture (CP V), followed by the CP II-F cement. In addition, major damages for cement pastes and TZ were demonstrated by SEM in the presence of DEF.

4. CONCLUSIONS

The present study evaluated DEF in mortars with different cement types. The results from the experimental program led to the following conclusions:

- Cements without fly-ash are more prone to DEF, with major expansions and negative influences in mechanical properties;
- The presence of limestone filler promotes a modification in the kinetics of the reaction, delaying the expansive process from DEF, but with no mitigation;
- Mixes cast with fly-ash cements had performed better, with minor negative consequences in the mechanical properties as well as fewer levels of expansion due to the self-healing properties of fly-ash in the presence of water;
- The procedure at the laboratory was able to induce DEF and promoted influences in cement paste integrity, including the fragility of the paste and transition zones and the mechanical properties. Anyway, lab procedures must be carefully adopted for mortars as different expansive behaviors are observed between tested cement. Cement with no admixture of high early strength could be evaluated at five months, but the same did not occur for the other types, appointing the necessity of later ages of evaluation, including after one year;
- Damages from induced DEF to mechanical properties of mortars were very expressive. For expansions above 0.45%, reductions of the order of 50% occurred. Furthermore, for expansions of about 0.10%, clear signs of DEF deterioration were observed in the mortar's microstructure and tensile strength at one year, even in the presence of fly-ash, flagging the risk of damage evolution.

5. ACKNOWLEDGEMENTS

The authors would also like to acknowledge Meridional Faculty (IMED) - Passo Fundo/RS Campus and Fundação Meridional. This research was supported in part by FURNAS CENTRAIS ELÉTRICAS S.A. The authors would also like to express their gratitude for the opportunity to participate in the R&D Project from ANEEL (Brazilian Agency of Electrical Energy).

6. REFERENCES

- Adamopoulou, E., Pipilikaki, P., Katsiotis, M. S, Chaniotakis, M., Katsioti, M. (2011). "How sulfates and increased temperature affect delayed ettringite formation (DEF) in white cement mortars." *Construction and Building Materials*, Vol. 25, pp. 3583-3590. <https://doi.org/10.1016/j.conbuildmat.2011.03.051>
- Al Shamaa, M., Lavaud, S., Divet, L., Colliat, J.B, Nahas, G., Torrenti, J. M. (2016). "Influence of limestone filler and of the size of the aggregates on DEF." *Cement Concrete Composites*, Vol. 71, pp. 175-180. <https://doi.org/10.1016/j.cemconcomp.2016.05.007>
- Amine, Y., Leklou, N., Amiri, O. (2017). "Effect of supplementary cementitious materials (SCM) on delayed ettringite formation in heat cured concretes." *Energy Procedia*, Vol. 139, pp. 565-570. <https://doi.org/10.1016/j.egypro.2017.11.254>
- Asamoto, S., Murano, K., Kurashige, I., Nanayakkara, A. (2017). "Effect of carbonate ions on delayed ettringite formation." *Construction and Building Materials*, Vol. 147, pp. 221-226. <https://doi.org/10.1016/j.conbuildmat.2017.04.107>

- Bronholo, J. L. (2020). *Estudo do ataque individual e misto de DEF e RAA e de seus efeitos deletérios nas propriedades físico-químicas e mecânicas de concretos e argamassas de cimento Portland pozolânico e de alta resistência*. Dissertação de Mestrado em Engenharia Civil – LACTEC, Curitiba, Brasil.
- Colleparidi, M. A. (2003). “*State-of-the-art review on delayed ettringite attack on concrete.*” *Cement and Concrete Composites*, Vol. 25, pp. 401-407. [https://doi.org/10.1016/S0958-9465\(02\)00080-X](https://doi.org/10.1016/S0958-9465(02)00080-X)
- Divet, L., Randriambololona, R. (1998). “*Delayed ettringite formation: the effect of temperature and basicity on the interaction of sulphate and C-S-H phase.*” *Cement and Concrete Research*, Vol. 28, pp. 357-363. [https://doi.org/10.1016/S0008-8846\(98\)00006-4](https://doi.org/10.1016/S0008-8846(98)00006-4)
- Dayarathne, W. (2013). “*Evaluation of the potential for delayed ettringite formation in concrete.*” National Engineering Conference, Sri Lanka.
- Fu, Y., Ding, J., Beaudoin, J. J. (1997). “*Expansion of Portland cement mortar due to internal sulfate attack.*” *Cement and Concrete Research*, Vol. 27, pp. 1299-1306. [https://doi.org/10.1016/S0008-8846\(97\)00133-6](https://doi.org/10.1016/S0008-8846(97)00133-6)
- Godart, B. (2017). “*Pathology, Assessment and Treatment Structures Affected by Delayed Ettringite Formation.*” *Structural Engineering International*, Vol. 27, pp. 362-369. <https://doi.org/10.2749/101686617X14881932436771>
- Hasparyk, N. P., Kuperman, S. C., Torres, J. R. (2016). “*Combined attack from ARS and DEF in the foundation.*” In: *Proceeding of 15^o International Conference on Alkali Aggregate Reaction in Concrete – 15th ICAAR*, Ed. Bernardes, H.; Hasparyk, N.P. São Paulo, 2016.
- Ifsttar (2018). “*Recommendations for preventing disorders due to Delayed Ettringite Formation*”. Merne-la-Vallée. *Technics and methods, GTI5-A*, 70 pp ISBN 978-2-85782-745-0.
- Leklou, N., Aubert, J. E., Escadeillas, G. (2013). “*Influence of various parameters on heat induced internal sulfate attack.*” *European Journal of Environmental and Civil Engineering*, Vo. 17, pp. 141-153. <https://doi.org/10.1080/19648189.2012.755338>
- Leklou, N., Nguyen, V-H., Mounanga, P. (2017) “*The effect of the Partial Cement Substitution with Fly Ash on Delayed Ettringite Formation in Heat-cured Mortars*”. *Journal of Civil Engineering*, Vol. 21, pp. 1359-1366. <https://doi.org/10.1007/s12205-016-0778-9>
- Martin, R.-P., Sanchez, L., Founier, B., Toutlemonde, F. (2016). “*Diagnosis of AAR and DEF: Comparison of residual expansion, stiffness test and damage rating index*”. *International Conference on Alkali Aggregate Reaction in Concrete - ICAAR*.
- Melo, et al. (2011) “*Influência do calor de hidratação na formação da etringita tardia (DEF) em concreto com cimento Portland pozolânico*”. 53^o Congresso Brasileiro do Concreto – IBRACON, Brasil.
- Pavoine, A., Brunetaud, X., Divet, L. (2012). “*The impact of cement parameters on Delayed Ettringite Formation.*” *Cement and Concrete Composites*, Vol. 34, pp. 521-528. <https://doi.org/10.1016/j.cemconcomp.2011.11.012>
- Ramlochan, T., Zacarias, P., Thomas, M. D. A., Hooton, R. D. (2003) “*The effect of pozzolans and slag on the expansion of mortars cured at elevated temperature Part I: Expansive Behavior*”. *Cement and Concrete Research*, Vol. 33, pp. 807-814. <https://doi.org/10.1016/j.conbuildmat.2013.07.016>
- Rashidi, M., Paul, A., Kim, J. Y., Jacobs, L. J., Kurtis, K. E. (2017) “*Insights into delayed ettringite formation damage through acoustic nonlinearity.*” *Cement and Concrete Research*, Vol. 95, pp. 1-8. <https://doi.org/10.1016/j.cemconres.2017.02.004>
- Schovanz, D. (2019). “*Estudo da formação da etringita tardia (DEF) em concretos com cimento Portland pozolânico e de alta resistência*”. Dissertação de Mestrado em engenharia civil – Faculdade IMED, Passo Fundo, Brasil.

- Schovanz, D., Tiecher, F., Hasparyk, N. P., Kuperman, S., Lermen, R. T. (2021). *Evaluation of Delayed Ettringite Formation through Physical, Mechanical, and Microstructural Assays*. ACI Materials Journal, Vol. 119, pp. 101-109. <https://doi.org/10.14359/51728282>
- Taylor, H. F., Famy, C., Scrivener, K. L. (2001). “*Delayed ettringite formation.*” Cement Concrete Composites, Vol. 31, pp. 683-693. [https://doi.org/10.1016/S0008-8846\(01\)00466-5](https://doi.org/10.1016/S0008-8846(01)00466-5)
- Termkhajornkit, P., Nawa, T., Yamashiro, Y., Saito, T. “*Self-healing ability of fly ash–cement systems*”. Cement and Concrete Research, Vol. 31, pp. 195-203. <https://doi.org/10.1016/j.cemconcomp.2008.12.009>
- Van Tittelboom, K., De Belie, N. (2013). “*Self-healing in cementitious materials – A review.*” Materials, Vol. 6, n° 6, pp. 2182-2217. <https://doi.org/10.3390/ma6062182>

Durability of concrete with pozzolanic admixtures and recycled aggregates

H. Gurdían¹, P. Garcés¹ , E. Zornoza¹ , E. García Alcoce¹ 

*Contact author: pedro.garces@ua.es

DOI: <https://doi.org/10.21041/ra.v11i3.542>

Reception: 18/06/2021 | Acceptance: 04/08/2021 | Publication: 01/09/2021

ABSTRACT

Mechanical and durability properties of concrete with a reduced environmental impact have been evaluated. This approach consist of replacing 50% of Portland cement by fly ash (35%) and spent catalytic cracking catalyst (15%), and also substituting a 20% and 100% of natural coarse aggregates by recycled aggregates. The performance of the prepared concrete consisted of mechanical tests, porosity, air permeability and chloride penetration. The obtained results show that the mechanical performance is significantly reduced in concretes with recycled aggregates and pozzolanic binder, but durability-related properties are only affected by the use of recycled aggregates. Nevertheless, all the tested formulations are suitable for their use as structural concretes.

Keywords: recycled aggregate; spent catalytic cracking catalyst; fly ash; concrete; mechanical properties; durability.

Cite as: Gurdían, H., Garcés, P., Zornoza, E., García Alcoce, E. (2021), “*Durability of concrete with pozzolanic admixtures and recycled aggregates*”, Revista ALCONPAT, 11 (3), pp. 17 – 30, DOI: <https://doi.org/10.21041/ra.v11i3.542>

¹ Dpto. de Ingeniería Civil, Universidad de Alicante, Alicante, España.

² Dpto. de Construcciones Arquitectónicas, Universidad de Alicante, Alicante, España.

Contribution of each author

In this work the author H. Gurdían contributed with the execution of most of the experimental work, as well as with the writing and revision of this work. The author P. Garcés contributed with the supervision, direction and writing of this work (33%). The author E. Zornoza contributed with the supervision, direction and writing of this work (33%). The author E. García Alcoce contributed with the supervision, direction and writing of this work (33%).

Creative Commons License

Copyright 2021 by the authors. This work is an Open-Access article published under the terms and conditions of an International Creative Commons Attribution 4.0 International License ([CC BY 4.0](https://creativecommons.org/licenses/by/4.0/)).

Discussions and subsequent corrections to the publication

Any dispute, including the replies of the authors, will be published in the second issue of 2022 provided that the information is received before the closing of the first issue of 2021.

Comportamiento de hormigones con adiciones puzolánicas y árido reciclado

RESUMEN

Se evalúan las propiedades mecánicas y de durabilidad de hormigones de bajo impacto ambiental con sustituciones de cemento por subproductos industriales (35% cenizas volantes y 15% de catalizador de craqueo catalítico) y de áridos gruesos por áridos reciclados (20% y 100%). Los hormigones estudiados se han sometido a ensayos de caracterización mecánica, porosidad, permeabilidad al aire y nivel de penetración del ion cloruro. Los resultados obtenidos muestran que las propiedades mecánicas se ven reducidas con el incremento en las proporciones de árido reciclado y de los residuos utilizados como sustitución en la matriz cementante, mientras que las propiedades de durabilidad se ven únicamente afectadas por el aumento en el porcentaje de áridos reciclados. Todos los hormigones estudiados son aptos para ser utilizados como hormigón estructural.

Palabras clave: árido reciclado; residuo de catalizador del craqueo del petróleo; ceniza volante; hormigón; propiedades mecánicas; durabilidad.

Desempenho do concreto com adições pozolánicas e agregado reciclado

RESUMO

As propriedades mecânicas e de durabilidade de concreto com baixo impacto ambiental são avaliadas com substituições de cimento por subprodutos industriais (35% cinzas volantes e 15% catalisador de craqueamento catalítico) e de agregados graúdos por agregados reciclados (20% e 100%). Os concretos estudados foram submetidos a ensaios de caracterização mecânica, porosidade, permeabilidade ao ar e nível de penetração do íon cloreto. Os resultados obtidos mostram que as propriedades mecânicas são reduzidas com o aumento das proporções de agregado reciclado e de resíduos usados como substituição na matriz cimentícia, enquanto as propriedades de durabilidade são afetadas apenas pelo aumento na porcentagem de agregados reciclados. Todos os concretos estudados são adequados para uso como concreto estrutural.

Palavras-chave: agregado reciclado; resíduo de catalisador do craqueamento de petróleo; cinzas volantes; concreto; propriedades mecânicas; durabilidade.

Legal Information

Revista ALCONPAT is a quarterly publication by the Asociación Latinoamericana de Control de Calidad, Patología y Recuperación de la Construcción, Internacional, A.C., Km. 6 antigua carretera a Progreso, Mérida, Yucatán, 97310, Tel.5219997385893, alconpat.int@gmail.com, Website: www.alconpat.org

Reservation of rights for exclusive use No.04-2013-011717330300-203, and ISSN 2007-6835, both granted by the Instituto Nacional de Derecho de Autor. Responsible editor: Pedro Castro Borges, Ph.D. Responsible for the last update of this issue, Informatics Unit ALCONPAT, Elizabeth Sabido Maldonado.

The views of the authors do not necessarily reflect the position of the editor.

The total or partial reproduction of the contents and images of the publication is carried out in accordance with the COPE code and the CC BY 4.0 license of the Revista ALCONPAT.

1. INTRODUCTION

The growing demand of materials for use in construction has led the industry to direct its efforts towards recycling and reusing stone materials and other waste derived from the industry itself. In this sense, the main focus of this research has been the replacement of natural aggregate by recycled aggregate, and Portland cement by industrial by-products in different concretes. This has been to demonstrate their viability to be used in the manufacture of structural concrete. This would make it possible to minimize the impacts of quarries and waste dumps. To this end, numerous authors have investigated the influence of pozzolanic materials on the mechanical properties and durability of concrete, showing that these materials can offer important improvements in their properties (Hooton, 2015, Paris et al., 2016, Yin et al., 2018). One of the supplementary materials that has generated more research in its characterization as pozzolanic material is fly ash. In general, the use of fly ash is considered viable due to its high pozzolanic properties, with its notable advantages over the long-term mechanical properties and durability of concrete (Bijen, 1996, Herath et al., 2020). Another supplemental material that has generated great interest is petroleum cracking catalyst (FCC) residue. Different studies have shown that this residue can lead to improvements in compressive strength of 20-30% in the short term, and its significantly positive influence on the durability of concrete, which places it as an effective substitute for cement, at a level equivalent to other more commonly used pozzolans such as metakaolin or silica fume (García de Lomas et al., 2016, Garcés et al., 2011, Borrachero et al., 2021).

On the other hand, numerous research works have been carried out with the aim of characterizing the effect of the use of recycled concrete aggregates on the resistant characteristics and durability of concrete (Chaofeng et al., 2021, Hoai-Bao et al. 2020).

In recent years, various investigations have been developed where supplementary materials have been used with a partial or total replacement of aggregates with recycled aggregates (Corinaldesi and Moriconi, 2009, Sim and Park, 2011, Kou, 2011). Thus, Corinaldesi and Moriconi experimented with concretes made entirely with coarse and fine recycled aggregate and substitutions of Portland cement by fly ash and silica fume, and found that optimal properties can be developed in concretes if the substitution percentages are studied and planned correctly.

However, it is hardly possible to find studies that combine fly ash and FCC residue as substituent pozzolanic materials for Portland cement in the cementitious matrix of recycled concretes (Payá et al., 2016, Zornoza et al., 2008).

The objective of this research is to evaluate the mechanical and durability properties of concretes with low environmental impact that combine substitutions of 20% and 100% of natural aggregate by recycled aggregate, and 50% of Portland cement by pozzolanic materials (35% fly ash and 15% % catalytic cracking catalyst).

2. MATERIALS AND EXPERIMENTAL PROCEDURE

2.1 Materials

Two types of cementitious arrays have been used for the preparation of the specimens: one composed entirely of Portland cement (CP); and an alternative one (MA) composed of 50% CP, 35% fly ash (CV) and 15% of catalytic cracking catalyst (FCC).

The cement used has been Portland type CEM I 52.5 R designated according to the European Standard UNE-EN 197-1: 2000. The CVs used to replace cement in concrete come from Holcim Spain and have been used as supplied, without applying any treatment before use. The FCC was supplied by BP Oil España (Castellón). The chemical composition of the cement and the pozzolans used, obtained by X-ray fluorescence, are shown in Table 1.

Two types of coarse aggregate have been used in the manufacture of concrete: limestone aggregate

(AN), from crushing, and recycled aggregate (AR), from the demolition and crushing of mass concrete waste, both supplied by Holcim Morteros S. A. The supplier certifies the following percentages of impurities present in recycled aggregates: Clays <5%, light particles <1%, asphalt <1%, other impurities <1%; thus complying with the limits established in the Spanish Structural Concrete Instruction (EHE-08) on the properties of recycled aggregates for concrete. The sand used to make the test tubes is limestone crushing sand from the Fontcalent quarry (Alicante), supplied by the company Holcim Morteros S. A. The properties of the aggregates and sand used in the mixes and their granulometric curves are shown in Table 2 and Figure 1 respectively. As additive, a Sikament 200R superplasticizer was used, free of chlorides and which allows to obtain very fluid concretes, even in hot weather.

Table 1. Chemical composition of cement and pozzolans.

%	CaO	SiO ₂	Al ₂ O ₃	MgO	Fe ₂ O ₃	SO ₃	Na ₂ O	K ₂ O	P.F.*	S.D.*	Density (g/cm ³)
CP	62,87	20,21	4,94	1,05	2,85	3,37	0,10	0,95	2,34	1,32	3,1
FCC	0,11	46,04	47,47	0,17	0,58	0,02	0,30	0,02	1,50	3,79	2,7
CV	9,83	40,94	24,65	1,59	13,59	1,60	0,34	1,40	2,44	3,62	2,8

* P.F.: Loss to fire. S.D.: Not determined.

Table 2. General properties of aggregates.

Property	Normative	AN	AR	Sand
Granulometric modulus	UNE-EN 933-1	8,3	8,0	3,1
Apparent density	UNE-EN 1097-6	2700	2490	2690
Water absorption	UNE-EN 1097-6	0,6	4,5	0,6
Los Angeles coefficient	UNE-EN 1097-2	21,1	30,3	-

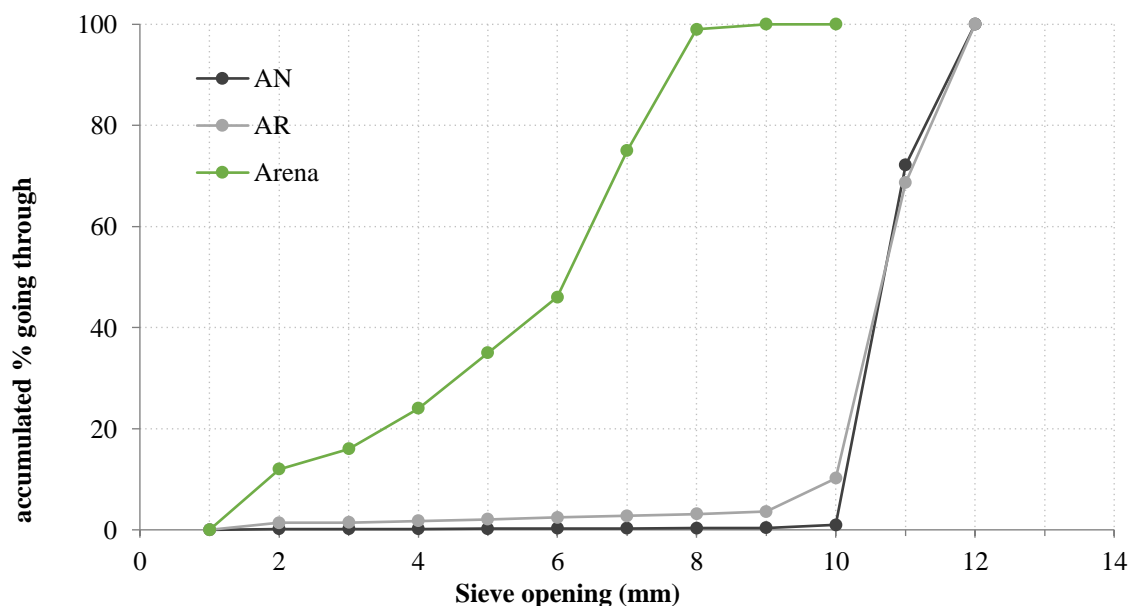


Figure 1. Granulometry of the aggregates used.

2.2 Experimental procedure

Six different compositions were elaborated (Table 3) in order to evaluate the influence that recycled aggregates and complementary cementitious materials (CV and FCC) have on the durability

properties of concrete:

- **0% AR-CP**, as reference concrete, composed entirely of natural aggregate and **CEM I 52.5 R**
- **0% AR-MA**, composed of natural aggregate and the alternative cementing matrix
- **20% AR-CP**, with substitutions of 20% of natural aggregate by recycled aggregate and **CEM I 52.5 R**
- **20% AR-MA**, with substitutions of 20% natural aggregate by recycled aggregate and the alternative cementing matrix
- **100% AR-CP**, composed entirely of recycled aggregate and **CEM I 52.5 R**
- **100% AR-MA**, also called green concrete, made with recycled aggregate and the alternative cementitious matrix

In order to be able to compare the different concretes with each other, the substitutions of natural aggregate by recycled aggregate are carried out by volume. The effective water / cementitious material ratio of 0.50 remains constant. This is achieved by adding the aggregate absorption water to the total mixing water for 10 minutes, the time that the mixing process lasts. The settlement value, obtained by the Abrams cone method (UNE-EN 12350-2: 2009), remains constant in all cases with the use of additive, which allows starting from the same workability in all concretes.

A total of 60 cylindrical specimens of Ø150x300 mm were kneaded to carry out the compression failure and air permeability tests at 28 and 365 days, and 6 cylindrical specimens of Ø100x250 mm for the tests of resistance to the penetration of chlorides at 28 days. The specimens were made according to the procedure described in the ASTM C192/C192M-07 standard. The mixing water is added in two stages; 1/3 is added with the coarse aggregates and the rest after introducing the sand and cement, reserving a little to add the additive at the end. The mixing time is 10 minutes. Once kneaded, the specimens were cured in a humid chamber (95% **HR**, 23 °C) until they were tested.

Table 3. Dosages used in this work.

	0%AR-CP	0%AR-MP	20%AR-CP	20%AR-MA	100%AR-CP	100%AR-MA
CP (kg/m³)	380	190	380	190	380	190
CV (kg/m³)	0	133	0	133	0	133
FCC (kg/m³)	0	57	0	57	0	57
a_{total} (kg/m³)	195	195	200	200	216	216
a_{ef} (kg/m³)	187	187	187	187	187	187
Arena (kg/m³)	934	934	934	934	934	934
AN (kg/m³)	981	981	785	785	0	0
AR (kg/m³)	0	0	173	173	865	865
Aditivo* (%)	1,6	1,8	1,6	1,8	1,6	1,6
Consistency (mm)	100	100	90	90	95	100

* The amount of additive is taken as a percentage of the amount of cementitious material. a_{total} is the total amount of water used in mixing. a_{ef}: it is the difference between the total water present in the fresh concrete and the water absorbed by the aggregates. It takes part in the hydration reaction of the cement and the workability of the concrete.

2.2.1 Compressive strength

Four Ø150x300mm cylindrical specimens were used for each dosage for compression failure tests at 28 and 365 days, following the procedure described by the UNE-EN 12390-3: 2009 standard.

2.2.2 Porosity

The water-accessible porosity of hardened concrete is obtained from (1), following the ASTM C642-13 standard.

$$\% \text{ Porosidad} = \frac{P_{\text{sat}} - P_{\text{seco}}}{P_{\text{sat}} - P_{\text{sum}}} \times 100 \quad (1)$$

The saturated weight is obtained by vacuum saturating a piece of each of the test specimens under compression, following the ASTM C3652-05 standard since it is the most appropriate method according to the comparative study carried out by Safiuddin and Hearn (Safiuddin and Hearn, 2005) on the different techniques of saturation of concrete. A pump is connected to the desiccator and a vacuum is carried out for three hours. After that time, the distilled water tap is opened and the vacuum continues for another hour. The pump is stopped and the vacuum is maintained for 20 ± 2 hours. The samples are taken out and weighed on a hydrostatic balance and superficially dry. They are then dried at 110°C for 24 hours, allowed to cool, and the dry weight is obtained.

2.2.3 Air permeability

The air permeability tests are carried out at 28 and 365 days on central sections of cylindrical specimens of Ø150mm that were cut with a height of 50mm. As a conditioning method, the one proposed by Antón et al. (Antón et al., 2013) that allows reaching a specific interior humidity inside the specimen, thus guaranteeing that the six concretes studied are at the same degree of saturation (65% in this case) to be able to be compared with each other.

The procedure consists firstly in obtaining the absorption capacity of the concrete to be tested by means of the ASTM C642-13 standard. Knowing the absorption, it is possible to determine the mass of the specimen corresponding to a specific degree of saturation. The test tubes are then saturated with distilled water under vacuum, according to the ASTM C3652-05 standard. The next step is to protect the lateral surfaces of the test tubes with insulating tape to avoid the formation of humidity gradients in them and they are dried at 50°C until the objective degree of saturation is achieved. Drying at 50°C minimizes microstructural modifications by exposure to elevated temperatures. When the specimens reach the target degree of saturation (GS), they are sealed with a polyethylene film that is impervious to water vapor, which guarantees their watertightness, and they are reintroduced into the oven at 50°C for 7 days in the case of the concretes studied. . This is done to redistribute the moisture inside the concrete, according to the work developed by Parrott (Parrot, 1994).

The air permeability coefficient (kT) in concretes with a GS of 65% is obtained with the Proceq Torrent Permeability Tester equipment. This equipment consists of a cell with a double vacuum chamber and a pressure regulator that ensures that the air flows at the correct angle from the surface to its internal chamber (see Figure 2). This allows the calculation of kT through a rapid and non-destructive test that can be carried out both in the laboratory and on site. Measurements are made on 3 specimens on both sides for each dosage studied.

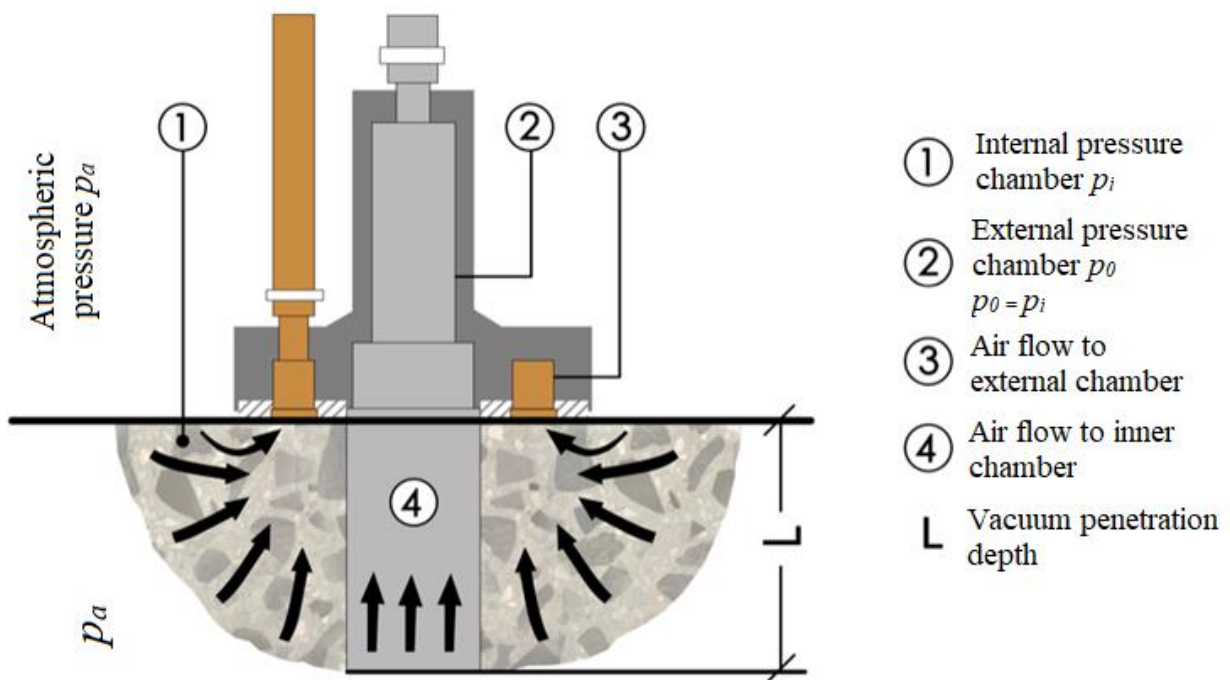


Figure 2. Permeability test with the Torrent Permeability Tester equipment and the equipment's operating diagram.

2.2.4 Resistance to chloride penetration

An accelerated method based on the migration of chlorides by electric field is used following the Nordic Standard NT Build 492 that allows a comparative approximate evaluation of the resistance to chloride penetration. The test is carried out on $\varnothing 100 \times 50$ mm test tubes that have been saturated in a saturated $\text{Ca}(\text{OH})_2$ solution, following the procedure described in the standard. In this procedure, an external electrical potential is applied axially through the sample that forces the chloride ions to migrate towards the interior of the sample, as shown in Figure 3. After a certain test time, the graduated cylinder and a silver nitrate solution is sprayed onto one of the newly divided sections. Chloride penetration depth can be measured from the formation of the white silver nitrate precipitate and with this penetration depth the non-steady state chloride migration coefficient (D_{nssm}) is calculated, through the following simplified formula (2)

$$D_{\text{nssm}} = \frac{0.0239 (273 + T)L}{(U - 2)t} \left(x_d - 0.0238 \sqrt{\frac{(273 + T)Lx_d}{U - 2}} \right) \quad (2)$$

where U is the absolute value of the applied voltage, in volts; T is the mean value of the temperature in the anode solution in $^{\circ}\text{C}$, measured at the beginning and end of the test; L is the thickness of the specimen in mm; x_d is the mean value of the penetration front in mm; and t is the duration of the test in hours.

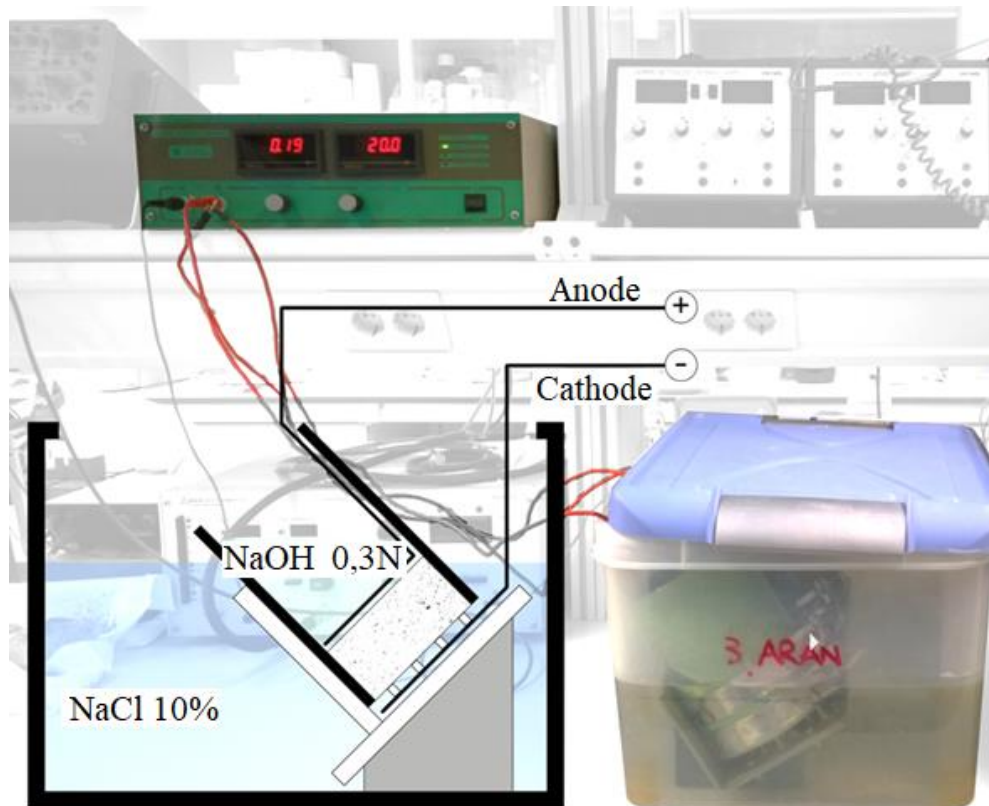


Figure 3. Chloride migration in concrete. Test scheme according to the NT Build 492 standard.

3. RESULTS AND DISCUSSION

Regarding the mechanical characterization of the concretes, the mean value of four specimens has been used for the analysis of the compressive strength. Figure 4 shows the values obtained for compressive strength, where the expressed percentage, followed by *AR*, refers to the amount of recycled aggregate present in the mixture; *CP*, refers to the cementitious matrix composed of *CEM* I 52.5 R; and *MA* to the alternative cementitious matrix (35% fly ash, 15% catalytic cracking catalyst and 50% *CP*). In general, it is observed that all concretes exceed the limits established by the EHE-08 to be used as structural concrete (25 MPa) and as concrete in atmospheric areas exposed to a marine environment (30 MPa), although it is notable that the values compressive strength are lower in all concretes with respect to the pattern (0% *AR-CP*), both at 28 and 365 days. The results show that as the percentage of substitution of natural aggregate for recycled aggregate increases, there is a decrease in resistance, coinciding with the results obtained by other authors (Hansen, 1992, Poon, 2004, Etxebarria et al., 2007, Corinaldesi, 2010). This happens in both, concrete with *CP* and in those made with *MA*. The use of recycled aggregates affects this property due to its greater porosity and the weak behavior of the microstructure, due to the existence of different interface zones. In addition to the paste-aggregate junction that the recycled aggregate presents, another contact zone appears between the recycled aggregate paste and the new paste.

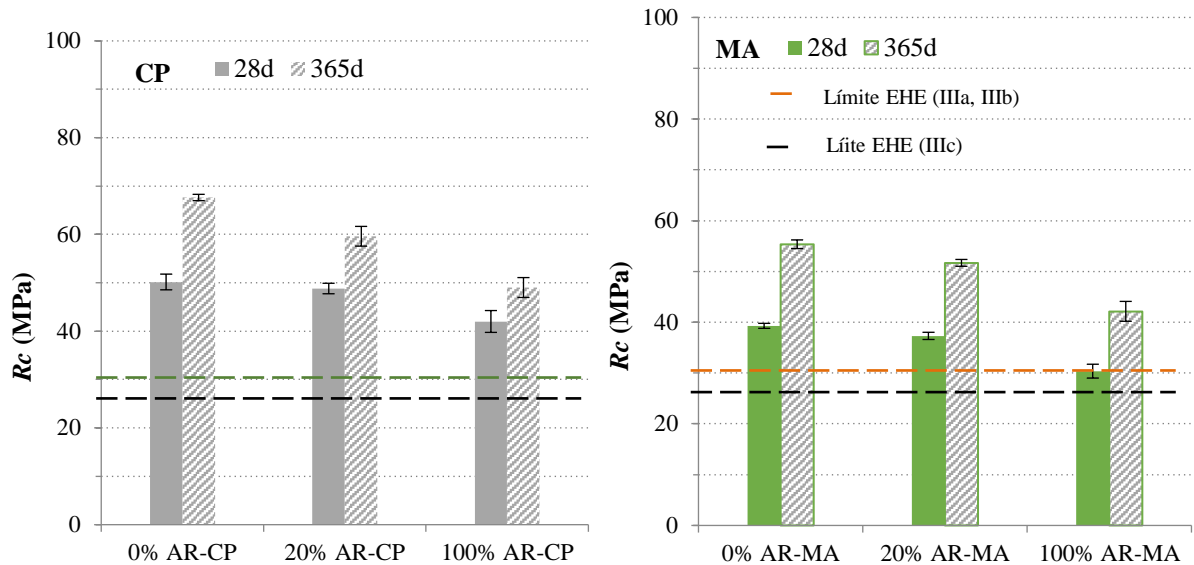


Figure 4. Compressive strength values at 28 and 365 days for the different concretes studied.

In the different percentages of substitution of AN by AR (0%, 20% and 100%) it is clear that the resistance of concretes with CP is higher than those made with MA (Safiuddin and Hearn, 2005), since the contribution of these pozzolanic materials to compressive strength is more relevant in the long term. It is also observed that at 365 days the compressive strength increases in all cases, this increase being more significant in those concretes with 0% and 20% substitution of NA by AR made with the alternative cementing matrix (0% AR-MA and 20% AR-MA), with a 25% increase compared to 28-day resistance in both cases.

Regarding porosity (Figure 5), it increases as the substitution of AN by RA increases (Chaofeng et al., 2021, Kou et al., 2011). This increase is due in large part to the greater porosity of the recycled aggregate (Etxebarria et al., 2006). It is clearly observable in the results at 28 days that the most porous concretes are those with total replacement of natural aggregate by recycling (100% AR-CP and 100% AR-MA) and that the porosity remains practically constant in both cases, without distinction of the cementitious matrix.

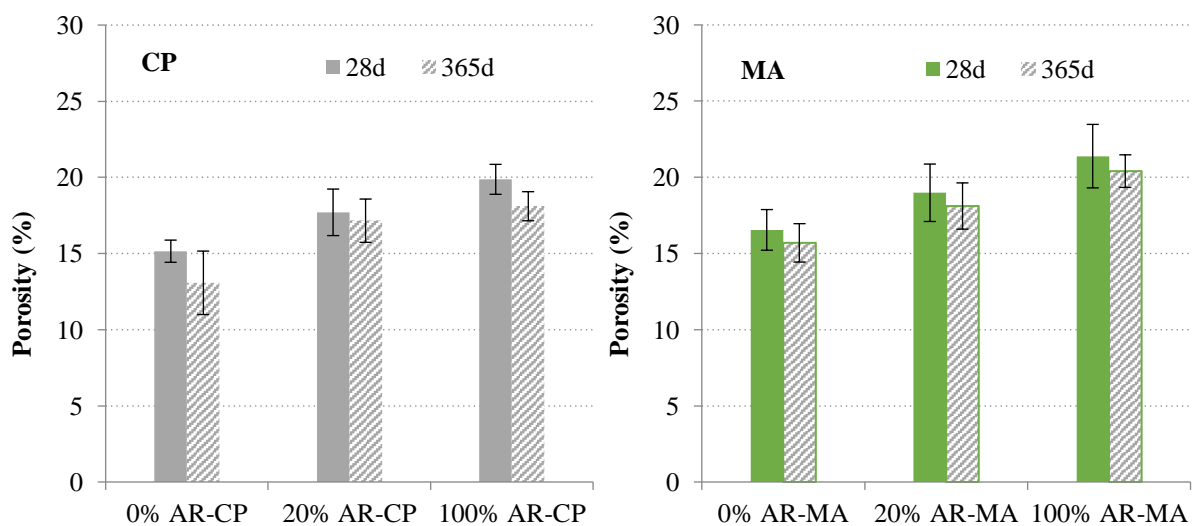


Figure 5. Porosity values at 28 and 365 days in the concretes studied.

In the case of concretes with substitutions of 20% and 0% of **NA** by **RA**, this is lower than that of the previous ones and an apparent relationship between porosity and cementing matrix is observed, since, although it decreases, the highest values are observed for concretes with alternative matrix (20% **AR-MA** and 0% **AR-MA**). At 365 days, porosity decreases in concretes with only one type of aggregate, either natural or recycled (substitutions of 0% and 100%) and no significant increase is observed in those with a combination of aggregates (20% **AR-CP** and 20% **AR-MA**). This is due to a greater complete development of the hydration reactions, with the consequent decrease in capillary porosity. At this age, it is also observed that porosity increases as the amount of recycled aggregate in the mix increases and that, for the same percentage of substitution, the value is higher in the concretes made with the alternative matrix, even in those with 100% of substitution. Figure 6 shows the chloride migration coefficient values obtained in concrete cured for 28 days and measured according to NT Build-492.

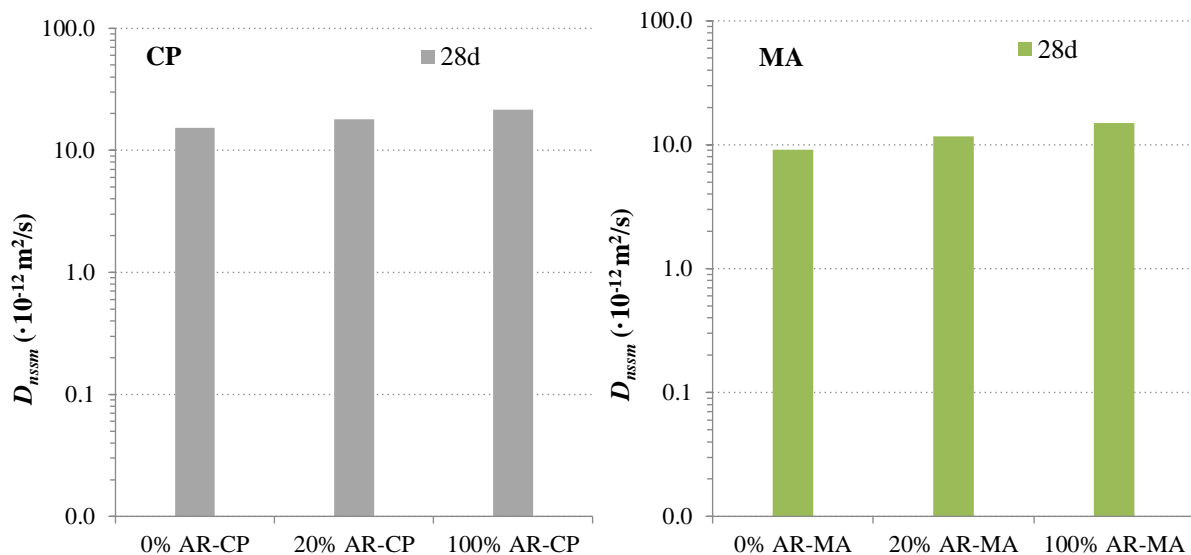


Figure 6. Chloride migration coefficient at 28 days.

The plot shows that there is an increase in the migration coefficient when the amount of **AR** in the mixtures increases, regardless of the type of cementitious matrix used, due to the higher porosity of the **AR**, coinciding with what was found by Kou and Poon (Kou and Poon, 2010) and Kou et al. (Kou et al., 2011). The migration coefficient is lower in all concrete with **MA**, so it can be stated that the presence of **CV** and **FCC** in the cementitious matrix leads to important improvements in the porous structure, both for concrete with **AR** and with **AN**. In cases where there are no substitutions of recycled aggregate (0%), the migration coefficient increases when the matrix is composed only of **CP**, which means that the alternative matrix combined with natural aggregate (0% **AR-MA**), behaves even better than the standard (0% **AR-CP**).

The air permeability coefficient of concrete (kT) was obtained using the Torrent method (Torrent, 1999), allowing the quality of the coating to be classified as good ($0,01 < kT < 0,1$), normal ($0,1 < kT < 1$) and bad ($kT > 1$).

The results obtained are presented in Figure 7. These represent the mean value of three samples for each type of concrete.

In general terms, the results obtained indicate that air permeability tends to increase with the degree of substitution of the aggregates in both cementitious arrays. In addition, it can be observed that the alternative matrix presents a greater resistance to oxygen than the cement matrix, both at short and long term. This behavior is due to the fact that a part of the **CVs** that do not react act as fillers

in the alternative matrix. However, all concretes present air permeability coefficients lower than 1, therefore, they fall within the “normal” classification, both at 28 and 365 days.

Regarding the results obtained at 28 days, in concrete with **CP** matrix, the substitution of 20% and 100% of the aggregate produces increments in permeability of 27% and 25% with respect to the standard; while in concrete with **MA** matrix the increments are 15% and 13% with respect to its pattern. At 365 days, the trend for all concretes is the same, that is, the permeability coefficient tends to increase with the amount of recycled aggregate in the mix.

Regarding the evolution of this property, it is observed that the permeability values of all the concretes decrease with the curing time, due to the complete development of the microstructure.

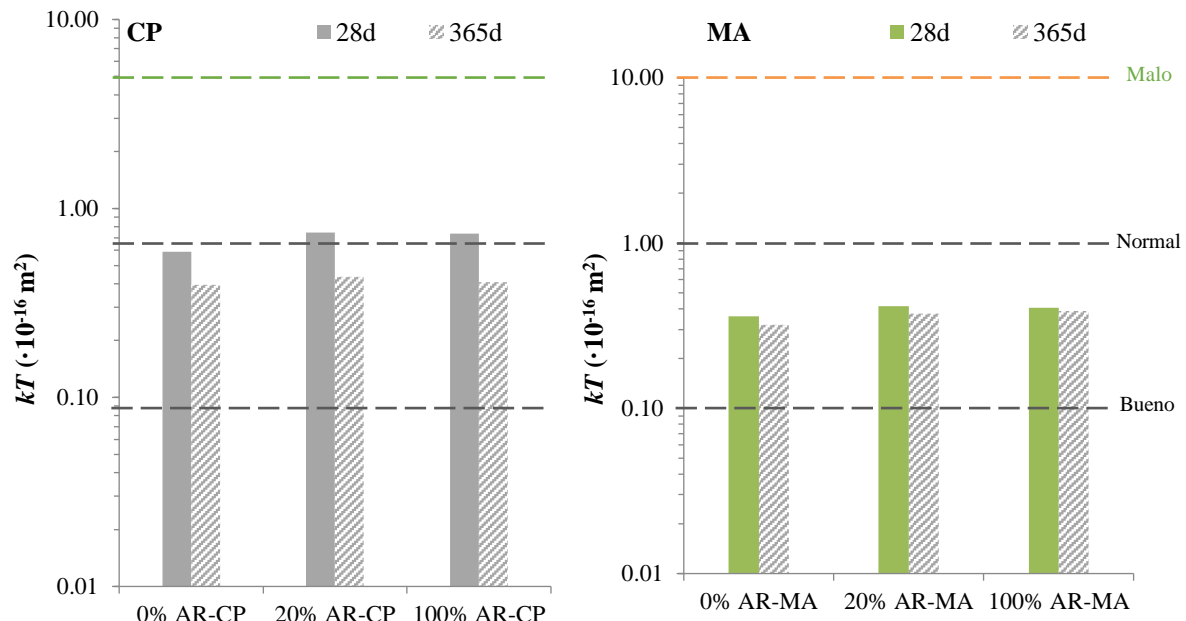


Figure 7. Air permeability coefficients at 28 and 365 days.

The results of this research indicate that all the changes applied to the concretes with respect to the pattern (**substitutions of AN for AR and of CP for MA**) reduce their mechanical behavior. This is due, in the case of aggregate substitutions, to the high porosity of the recycled aggregate and to the substitution percentages; while in the case of the cementitious matrix, it is attributed to the high degree of substitution of **CP for CV and FCC**, which can limit the development of the pozzolanic reaction. Regarding porosity, two trends are observed: porosity depends on the cementing matrix when the **AR** substitutions are low; and when these substitutions are high, the influence of the porosity of the aggregate over the total porosity of the concrete prevails.

In terms of durability, the results obtained from the air permeability and chloride migration tests show that concretes with an alternative matrix are the ones that present the greatest resistance to attack by external aggressive agents; behaving even better than standard concrete. Its effectiveness against the attack of external agents is associated with the porosity reductions produced by the pozzolanic additions used (**CV and FCC**). However, these results cannot be conclusive at an early age, so they need to be completed with long-term data that allow the complete development of the microstructure.

In addition to the porosity values studied, the presence of other factors that influence the permeability and resistance to the passage of chlorides of the concretes is detected, such as the influence of the size and connectivity of the pores, whose study will be carried out through tests of mercury intrusion porosimetry (**PIM**). In addition, the study of the influence of the matrix-aggregate interface on the migration of chlorides by means of the X-ray diffraction technique

(XRD) will be studied in depth in order to determine the existence of Friedel's salt.

It can be stated that, although there are variations in the properties of the concretes studied that depend on the type of substitution (aggregate or matrix), they are all suitable to be used as structural concrete since they exceed the limits set by the EHE.

4. CONCLUSIONS

Once the influence of the partial replacement of cement by additions (CV and FCC) and of natural aggregates with recycled aggregates on the physical, mechanical and durability properties of concrete has been evaluated, the following conclusions can be established:

- 1.- All the changes applied to the concretes with respect to the pattern (substitutions of AN for AR and of CP for MA) reduce their mechanical behavior.
- 2.- Porosity depends on the cementing matrix when AR substitutions are low; and when these substitutions are high, the influence of the porosity of the aggregate over the total porosity of the concrete prevails.
- 3.- Concrete with an alternative matrix are those that have the greatest resistance to attack by external aggressive agents; behaving even better than standard concrete.
- 4.- It can be stated that, although there are variations in the properties of the concretes studied that depend on the type of substitution (aggregate or matrix), they are all suitable for use as structural concrete since they exceed the limits set by the EHE.

5. REFERENCES





- Antón, C., Climent, M. A., de Vera, G., Sánchez, I., Andrade, C. (2013), *An improved procedure for obtaining and maintaining well characterized partial water saturation states on concrete samples to be used for mass transport tests*. *Materials and Structures*, 46, 1389–1400. <https://doi.org/10.1617/s11527-012-9981-4>
- Borrachero, M. V., Payá, J., Monzó, J., Soriano, L., Tashima, M. M. (2021), *Inorganic binders from petrochemical industry waste: The case of fluid catalytic cracking catalyst residue*. *Waste and Byproducts in Cement-Based Materials (Innovative Sustainable Materials for a Circular Economy)*, Woodhead Publishing Series in Civil and Structural Engineering. Pages 283-334. <https://doi.org/10.1016/B978-0-12-820549-5.00003-6>
- Chaofeng, L., Zhedong, C., Huixia, W., Jianzhuang, X., Yuming, Z., Zhiming, M. (2021), “*Chloride transport and induced steel corrosion in recycled aggregate concrete: A review*”. *Construction and Building Materials*, vol 282, 122547. <https://doi.org/10.1016/j.conbuildmat.2021.122547>
- Corinaldesi, V. (2010), “*Mechanical and elastic behaviour of concretes made of recycled-concrete coarse aggregates*”. *Construction and Building Materials*, 24 (9), pp. 1616-1620. <https://doi.org/10.1016/j.conbuildmat.2010.02.031>
- Corinaldesi, V., Moriconi, G. (2009), “*Influence of mineral additions on the performance of 100% recycled aggregate concrete*”. *Construction and Building Materials*, 23 (8), pp. 2869-2876. <https://doi.org/10.1016/j.conbuildmat.2009.02.004>
- Garcés, P., Glasser, F.P., Brew, D.R.M., Zornoza, E., Payá, J. (2011), “*Pozzolanic activity of a spent fluid catalytic cracking catalyst residue*”. *Advances in Cement Research*, vol. 23, pp. 1-7. <https://doi.org/10.1680/adcr.9.00036>
- García de Lomas, M., Sánchez de Rojas, M.I., Frías, M., Mújika, R. (2006), “*Comportamiento científico-técnico de los cementos portland elaborados con catalizadores FCC. Aplicación de la norma vigente*”. *Monografía Materiales*, No. 412, editado por el CSIC, Madrid, pags. 46.

- Bijen, J. “Benefits of slag and fly ash”. *Construction and Building Materials*, 1996, 10 (5), pp. 309-314. [https://doi.org/10.1016/0950-0618\(95\)00014-3](https://doi.org/10.1016/0950-0618(95)00014-3)
- Etxeberria, Vázquez, M. E., Marí, A. 2006, “Microstructure analysis of hardened recycled aggregate concrete”. *Magazine of Concrete Research*, 58 (10), pp. 683-690. <https://doi.org/10.1680/mac.2006.58.10.683>
- Etxeberria, M., Marí, A. R., Vázquez, E. (2007), “Recycled aggregate concrete as structural material”. *Materials and Structures*, vol. 40, pp. 529-541. <https://doi.org/10.1617/s11527-006-9161-5>
- Hansen, T. C. (1986), *Recycled aggregates and recycled aggregate concrete second state-of-the-art report developments 1945–1985*. *Materials and Structures* 19, 201–246. <https://doi.org/10.1007/BF02472036>
- Herath, C., Gunasekara, C., Law, D. W., Setunge, S. (2020), “Performance of high-volume fly ash concrete incorporating additives: A systematic literature review”. *Construction and Building Materials*, vol. 258, 365606. <https://doi.org/10.1016/j.conbuildmat.2020.365606>.
- Hoai-Bao, L., Quoc-Bao, B. (2020), “Recycled aggregate concretes - A state-of-the-art from the microstructure to the structural performance”. *Construction and Building Materials*, Vol. 257, 119522. <https://doi.org/10.1016/j.conbuildmat.2020.119522>
- Hooton, R. D. (2015), “Current developments and future needs in standards for cementitious materials”. *Cement and Concrete Research*, vol. 78, pp. 165–177. <https://doi.org/10.1016/j.cemconres.2015.05.022>
- Kou, S.; Poon, C. (2010), “Properties of concrete prepared with PVA-impregnated recycled concrete aggregates”. *Cement and Concrete Composites*, 32 (8), pp. 649-654. <https://doi.org/10.1016/j.cemconcomp.2010.05.003>
- Kou, S., Poon, C., Agrela, F. (2011), “Comparisons of natural and recycled aggregate concretes prepared with the addition of different mineral admixtures”. *Cement and Concrete Composites*, 33 (8), pp. 788-795. <https://doi.org/10.1016/j.cemconcomp.2011.05.009>
- Kou, S., Poon, C., Etzeberria, M. (2011), “Influence of recycled aggregates on long term mechanical properties and pore size distribution of concrete”. *Cement and Concrete Composites*, 33 (2), pp. 286-291. <https://doi.org/10.1016/j.cemconcomp.2010.10.003>
- Paris, J. M., Roessler, J. G., Ferraro, C. C., DeFord, H. D., Townsend, T. G. (2016), “A review of waste products utilized as supplements to Portland cement in concrete”. *Journal of Cleaner Production*, vol. 121, pp.1-18. <https://doi.org/10.1016/j.jclepro.2016.02.013>
- Poon, C. S. Shui, Z. H., Lam, L., Fok, H., Kou, S. C. (2004), “Influence of moisture states of natural and recycled aggregates on the slump and compressive strength of concrete”. *Cement and Concrete Research*, 34 (1), pp. 31-36. [https://doi.org/10.1016/S0008-8846\(03\)00186-8](https://doi.org/10.1016/S0008-8846(03)00186-8)
- Safiuddin, M.; Hearn, N. (2005), “Comparison of ASTM saturation techniques for measuring the permeable porosity of concrete”. *Cement and Concrete Research*, 35 (5), pp. 1008-1013. <https://doi.org/10.1016/j.cemconres.2004.09.017>
- Sim, J., Park, C. 2011, “Compressive strength and resistance to chloride ion penetration and carbonation of recycled aggregate concrete with varying amount of fly ash and fine recycled aggregate”. *Waste Management*, 31 (11), pp. 2352-2360. <https://doi.org/10.1016/j.wasman.2011.06.014>
- Soriano, L., Payá, J., Monzó, J., Borrachero, M.V., Tashima, M.M. (2016), “High strength mortars using ordinary Portland cement–fly ash–fluid catalytic cracking catalyst residue ternary system (OPC/FA/FCC)”. *Construction and Building Materials*, Volume 106, pp. 228-235. <http://dx.doi.org/10.1016/j.conbuildmat.2015.12.111>
- Torrent, R. J. (1999). *Un método rápido y no-destructivo para medir la permeabilidad al aire del hormigón*. *Materiales de Construcción*, 49 (254), 51–56. <https://doi.org/10.3989/mc.1999.v49.i254.450>

Yin, K., Ahamed, A., Lisak, G. (2018), “*Environmental perspectives of recycling various combustion ashes in cement production – A review*”. Waste Management, vol.78 pp. 401–416. <https://doi.org/10.1016/j.wasman.2018.06.012>

Zornoza, E., Payá, J. Garcés, P. (2008), “*Carbonation rate and reinforcing steel corrosion rate of OPC/FC3R/FA mortars under accelerated conditions*”. Advances in Cement Research, 20 (1), pp. 15-22. <https://doi.org/10.1680/adcr.2007.00008>

Theoretical-experimental behavior of steel fibers as a partial replacement for shear reinforcement in reinforced concrete beams

C. A. Juárez-Alvarado¹, J. M. Mendoza-Rangel^{1*}, B. T. Terán-Torres¹,
P. L. Valdez-Tamez¹, G. Castruita-Velázquez¹
*Contact author: jose.mendozarn@uanl.edu.mx
DOI: <https://doi.org/10.21041/ra.v11i3.548>

Reception: 16/07/2021 | Acceptance: 13/08/2021 | Publication: 01/09/2021

ABSTRACT

It is proposed to partially replace the stirrups with steel fibers and thus improve the shear strength of concrete beams. The variables studied were: water/cement ratios (w/c) = 0.55 and 0.35, and fiber volume (V_f) = 0, 0.3, 0.5, 0.7% and 0, 0.2, 0.4, 0.6% respectively, along with the separation of the stirrups. The results showed that the shear strength of the reinforced fiber and stirrups was greater than the strength of the beams reinforced only with stirrups. Experimental data and the strength prediction models comparison showed that the analytical models adequately predict the effect of the w/c ratio, the V_f , and the contribution of longitudinal and transverse steel. Also, the studied models predicted mainly conservative values with respect to the ultimate shear strength.

Keywords: Fiber-reinforced concrete, beams, shear strength, analytical model, stirrups, steel fibers.

Cite as: Juárez-Alvarado, C. A., Mendoza-Rangel, J. M., Terán-Torres, B. T., Valdez-Tamez, P. L., Castruita-Velázquez, G. (2021), "Theoretical-experimental behavior of steel fibers as a partial replacement for shear reinforcement in reinforced concrete beams", Revista ALCONPAT, 11 (3), pp. 31 – 41, DOI: <https://doi.org/10.21041/ra.v11i3.548>

¹ Universidad Autónoma de Nuevo León, Facultad de Ingeniería Civil, Av. Universidad S/N, Cd. Universitaria, San Nicolás de los Garza, Nuevo León, México.

Contribution of each author

In this work the first author C.A. Juárez-Alvarado contributed with the original idea and the planning of the experiment. C.A. Juárez-Alvarado, J.M. Mendoza-Rangel, B.T. Terán-Torres y P.L. Valdez-Tamez contributed to the redaction of the article, the configuration of tables and graphs, along with the discussion of the results in 25% each. G. Castruita-Velázquez carried out the experimentation and the gathering of data.

Creative Commons License

Copyright 2021 by the authors. This work is an Open-Access article published under the terms and conditions of an International Creative Commons Attribution 4.0 International License ([CC BY 4.0](https://creativecommons.org/licenses/by/4.0/)).

Discussions and subsequent corrections to the publication

Any dispute, including the replies of the authors, will be published in the second issue of 2022 provided that the information is received before the closing of the first issue of 2022.

Comportamiento teórico-experimental de fibras de acero como reemplazo parcial del refuerzo a cortante en vigas de concreto reforzado

RESUMEN

Se propone sustituir parcialmente estribos por fibras de acero para mejorar la resistencia a cortante de vigas. Como variables se usaron: relación $(a/c) = 0.55$ y 0.35 con un volumen de fibras $(V_f) = 0, 0.3, 0.5, 0.7\%$ y $0, 0.2, 0.4, 0.6\%$ respectivamente, y separación de estribos. Los resultados mostraron que la resistencia a cortante con refuerzo de estribos y fibras, fue mayor que la de las vigas control con estribos separados $(d/2)$. La comparativa entre los datos experimentales y modelos de predicción de resistencia, mostró que se predice adecuadamente el efecto de la relación a/c , el V_f , la aportación del acero longitudinal y la presencia de estribos. Los modelos estudiados predijeron en la mayoría de los casos valores conservadores para la resistencia última experimental a cortante.

Palabras clave: concreto fibroreforzado, vigas, esfuerzo a cortante, modelo analítico, estribos, fibras de acero.

Comportamento teórico-experimental de fibras de aço em substituição parcial à armadura de cisalhamento em vigas de concreto armado

RESUMO

Propõe-se a substituição parcial dos estribos por fibras de aço para melhorar a resistência ao cisalhamento das vigas. Como variáveis: relação $(a/c) = 0,55$ e $0,35$ com $(V_f) = 0, 0,3, 0,5, 0,7\%$ e $0, 0,2, 0,4, 0,6\%$ respectivamente e espaçamento de estribo. Os resultados mostraram que a resistência ao cisalhamento com reforço de estribos e fibras foi maior que a das vigas controle com estribos separados $(d/2)$. A comparação entre os dados experimentais e os modelos de predição de resistência mostrou que o efeito da relação (a/c) , (V_f) , a contribuição do aço longitudinal e a presença de estribos está adequadamente previsto. Os modelos estudados previram, na maioria dos casos, valores conservadores para a resistência última ao cisalhamento experimental.

Palavras-chave: concreto reforçado com fibras, vigas, tensão de cisalhamento, modelo analítico, estribos, fibras de aço.

Legal Information

Revista ALCONPAT is a quarterly publication by the Asociación Latinoamericana de Control de Calidad, Patología y Recuperación de la Construcción, Internacional, A.C., Km. 6 antigua carretera a Progreso, Mérida, Yucatán, 97310, Tel.5219997385893, alconpat.int@gmail.com, Website: www.alconpat.org

Reservation of rights for exclusive use No.04-2013-011717330300-203, and ISSN 2007-6835, both granted by the Instituto Nacional de Derecho de Autor. Responsible editor: Pedro Castro Borges, Ph.D. Responsible for the last update of this issue, Informatics Unit ALCONPAT, Elizabeth Sabido Maldonado.

The views of the authors do not necessarily reflect the position of the editor.

The total or partial reproduction of the contents and images of the publication is carried out in accordance with the COPE code and the CC BY 4.0 license of the Revista ALCONPAT.

1. INTRODUCTION

In most reinforced concrete structures, straight corrugated rebars are usually employed, which are proposed in zones subjected to tension in the structural elements to resist normal stresses produced by the shear force and bending moment (V , M). However, when such forces exceed the admissible stresses, diagonal tensile cracks are developed with an inclined orientation due to the shear force. If the concrete is unable to withstand such actions, transverse reinforcement is proposed to reduce the cracking due to shear force (Khuntia et al, 2001).

The failures shown in the structural elements are of great interest due to the risk that they pose to the final users, and one of the most concerning failures is the diagonal tension shear, which presents itself in a fragile form, i.e., there is no warning prior collapse. These failures can be produced by external events, such as seismic forces or impact due to accidental loading.

To counter this type of failure, the structures are reinforced with transverse rebars (stirrups) which, depending on the loads acting on the structure, can become close enough in the zone. This will prevent concrete to flow freely between the steel rebars, causing segregation and weakness in such areas of the structure. One alternative to solve this problem is the use of steel fibers, which provide higher strength to bending moment, impact, cracking, and lower permeability (Shin et al, 1994). The use of steel fibers comes from the basic idea of strengthening the concrete matrix under tensile stresses. The distribution of the fibers as a group with the concrete leads to better behavior since they reduce the fragile nature of the element. As a consequence of the use of the steel fibers, a larger toughness capacity is presented in the composite material since they can absorb energy before reaching the failure of the element and its collapse. The addition of the steel fibers in the concrete helps to transform its fragile characteristic into a ductile one. This is due to the fact that fibers are distributed uniformly and oriented randomly in all directions in the concrete mass (Ashour et al, 1992).

In general, the reinforced concrete elements are designed to resist external loads which produce stresses and displacement of different types, these designs are usually based on construction codes and on technical literature which presents well-established procedures for most structures. Nevertheless, when the reinforcement of the concrete differs from the conventional steel rebars, these procedures and theories must account for the contribution of this additional reinforcement. In most of the technical literature, there is a lack of design procedures for concrete structures that are reinforced with steel fibers, which in contrast, there is plenty of research that shows that steel fibers provide ductility and an increase in the mechanical tensile strength of the concrete (Juárez, et al., 2007). Hence, by taking into consideration the main contribution that steel fibers have, it is convenient to direct such studies towards the behavior under shear stresses in fiber-reinforced concrete beams; this stress is also known as diagonal tensile stress, which is located in the support zones of the beam (Park et al., 1990).

The shear stress leads to sudden failure if the transverse reinforcement in the concrete (stirrups) is not enough, and this failure is usually presented under a lesser load than that for the bending failure. Therefore, if one considers utilizing steel fibers as alternative reinforcement for shear to prevent the sudden failure and increase the ultimate strength, it will be convenient to present theoretical procedures to predict such strength and, by comparing with experimental data, one will be able to identify the contribution of the fiber and hence finding a reliable aid for design. There are several studies that account for this contribution of the steel fibers, Jun et al. (2018) observed that the fiber and the stirrup increase the stiffness, by decreasing the deflection under ultimate load, however, the effect of the fibers decreased with the increment of the amount of stirrups. In addition, it was found out that fiber reduces the strain in the stirrup and the diagonal cracking, due to a bridging of the crack. On the other hand, one of the most recent studies that model the shear was developed by (Mari Bernat et al. 2020), which proposed a multi-action model based on the establishment of

equilibrium equations that include the mechanisms of shear strength that the fibers provide in concrete beams without stirrups.

By considering the aforementioned, a viable and practical solution to this problem, with reinforcement inside the matrix, with the steel fiber addition in the concrete mass, and hence to be able to increase the separation of the stirrups and obtaining a better distribution of the concrete is proposed in this research. This research work proposes the partial substitution of the stirrups by the steel fibers and with that the improve or maintain the mechanical shear strength under diagonal tension of the concrete structures.

The results obtained experimentally showed that the diagonal shear strength of the fiber-reinforced beams, with stirrups, is substantially larger than that estimated by the ACI-318 code. In addition, theoretical procedures to predict the shear strength in fiber-reinforced concrete beams were evaluated, through the comparison of two mathematical models obtained from the literature review (Swamy et al., 1993 and Narayanan et al., 1987), and the experimental data of the 20 beams tested under diagonal tensile shear. It was found out that the two models predict adequately the effect of the w/c ratio, the volume fiber (V_f), the contribution of the longitudinal steel, and the presence of the stirrup under shear ultimate strength. The models of Swamy and Narayanan predicted conservative values with respect to the ultimate shear strength, approaching the reached value of the experimental shear strength.

2. EXPERIMENTAL METHODOLOGY

2.1 Materials

Cement Portland type CPC 30R was used, which satisfies the standard NMX-C-414-ONNCCE-2017, coarse aggregate with a maximum size of 12.7 mm and 4.75 mm for the fine aggregate, which meet the standard ASTM C33-18, the aggregates were of limestone typical of the Monterrey area, with a relative density of 2.59 and 2.71 and with an absorption percentage of 0.72 and 1.82 for each aggregate, respectively. The additive used was a water reducer hyperfluidifier polycarboxylate based, with a liquid content of 56%, mass of 44%, and a density of 1.11 g/cm³. The longitudinal steel reinforcements were four rebars No. 5 (16mm) with $f_y=420$ MPa and for the stirrups, rebars No. 2 (6.4 mm) were used with $f_y = 280$ MPa (ASTM A615-20). Steel fibers were used with 50 mm of length and 1 mm of average thickness, with an aspect ratio of 50, $f_y = 1,152$ MPa, fiber “*Deformed Slit Sheet*” type, according to ASTM A820-16 standard.

2.2 Mixtures composition

In tables 1 and 2, different mixtures of the concrete studied are shown. A total of 8 mixtures were fabricated, four for the ratio w/c = 0.55 and the other four for the ratio w/c = 0.35. In both cases, the variables were: the percentage of fibers volume per cubic meter of concrete and the transverse shear reinforcement using closed-loop stirrups. The beams were fabricated in duplicate for each mixture and each variable.

Table 1 Mixture composition for strength of $f'c = 25$ MPa, in kg/m^3 .

Materials	% of steel fiber			
	0.0	0.3	0.5	0.7
w/c = 0.55				
Total water	157	157	157	157
Cement	280	280	280	280
Coarse A.	792	782.6	766.9	770.1
Fine A.	1139	1124.8	1115.5	1106.1
Fiber	0	23.5	39.2	54.8
Additive	1.1	1.4	1.6	2.2
Air %	2.5	2.5	2.5	2.5

Table 2. Mixture composition for strength of $f'c = 35$ MPa, in kg/m^3 .

Materials	% of steel fiber			
	0.0	0.2	0.4	0.6
w/c = 0.35				
Total water	136	136	136	136
Cement	380	380	380	380
Coarse A.	761	753.9	748.5	742.2
Fine A.	1139	1128.4	1120.2	1110.8
Fiber	0	17.7	31.3	47
Additive	1.9	2.3	2.7	3.4
Air %	2.5	2.5	2.5	2.5

Total water = Reaction water + absorption water + additive water

2.3 Mixing, casting, and curing

The mixtures were fabricated in a concrete mixer with a reversing drum with a capacity of 90 L. The coarse and fine aggregates were homogenized during a minute, with a third of the water of reaction + absorption, afterwards, the cement was added, along with the additive and the remaining water of reaction by mixing for three minutes, then by allowing it to rest for three minutes and by mixing again for two more minutes. When the fibers were required, these were added during the second period of mixing. After the mixing, the consistency was measured through the concrete slump test and the air content according to the standards ASTM C143-20 and ASTM C231-17a, respectively, but only for the mixtures without fibers. The compressive strength was performed by means of the test of six cylinders of the fiber-reinforced concrete of 100 mm of diameter and 200 mm of height, fabricated with each fiber percentage, standardly cured according to the standard ASTM C192-19, and tested at 28 days according to the testing method in ASTM C39-21. In addition, the tensile strength was obtained through diagonal tensile strength test, using six cylinders of 150 mm of diameter and 300 mm of height, cured for 28 days, and tested according to the method ASTM C496-17. On the other hand, the concrete of the beams was poured into metallic falsework, compacted with an electric internal vibrator, which allowed to homogenize the fibers in the concrete mixture, with no agglomeration of them observed. All beams were cured with a water layer inside the falsework up to the age of 7 days, afterwards, they were cured with curing membrane water-based formulated with acrylic spread resins, until the moment of the experiment.

2.4 Fabrication and testing of fiber-reinforced beams

Twenty reinforced concrete beams of 2000x150x250 mm were fabricated, from which, 10 beams were casted with concrete mixture with a water/cement ratio (w/c) = 0.55, to obtain a concrete strength specified of $f'c=25$ MPa, and the remaining 10 beams were casted with the concrete mixture with a ratio $w/a = 0.35$ for a compressive strength specified of $f'c=35$ MPa. The beams were fabricated in duplicate, por each w/c ratio, eight pairs of beams with stirrups, and two pairs of beams without stirrups (see table 3). To evaluate the effect of the fibers with the shear reinforcement in the concrete matrix, steel fibers were added with 50 mm of length and 1 mm of average thickness. Beams were fabricated in duplicate, reinforced with closed-loop stirrup and with the following fiber percentage with respect the total volume of the mixture: 0% (control), 0.3%, 0.5%, 0.7% for the ratio $w/c = 0.55$. In a similar manner, 0% (control), 0.2%, 0.4%, 0.6% for the ratio $w/c = 0.35$. To obtain the same separation of stirrups for both ratios w/c , as observed in table 3, the percentage of fibers must be different, being smaller for the concrete with larger compressive strength. In addition, two pairs of beams were fabricated without stirrups but with the larger percentage of fibers of 0.7% and 0.6% for the ratios $w/c = 0.55$ and 0.35, respectively. The transverse steel reinforcement detailing of the beams and the position for load application can be observed in figure 1. The location of the loads for the test was determined following the criterion used by Park et al., 1990, to define a shear span, which allows to produce high shear forces for diagonal tension at the ends of the beams. All beams were tested at the age of 28 days.

Table 3. Details of the reinforcement of stirrups and fibers of the beams.

w/c = 0.55	Separation of stirrups, mm	150	250	300	350	S/E
	Percentage of fiber, %	0.0	0.3	0.5	0.7	0.7
	Number of specimens	2	2	2	2	2
w/c= 0.35	Separation of stirrups, mm	150	250	300	350	S/E
	Percentage of fiber, %	0.0	0.2	0.4	0.6	0.6
	Number of specimens	2	2	2	2	2

* Nomenclature: S/E = without stirrups



Figure 1. General detailing of the tested beams

In table 4, it is established the designation used for the 20 beams fabricated, along with the amount and distribution of longitudinal reinforcement and the transverse shear reinforcement (stirrups), and the percentage of steel fibers used.

Table 4. Identification of the fiber-reinforced beams

Designation	Concrete strength f'_c , MPa	w/c Ratio	Longitudinal reinforcement Φ 16 mm	Transverse Reinforcement Φ 6.4 mm	Steel fibers, %		
Mva-N-1,0.0	25	0.55	4 rebars	12 stirrups @ 150 mm	0.0		
Mva-N-2,0.0				8 stirrups @ 250 mm	0.3		
Mva-N-3,0.3				8 stirrups @ 300 mm	0.5		
Mva-N-4,0.3				6 stirrups @ 350 mm	0.7		
Mva-N-5,0.5				35	0.35	12 stirrups @ 150 mm	0.0
Mva-N-6,0.5						8 stirrups @ 250 mm	0.2
Mva-N-7,0.7						8 stirrups @ 300 mm	0.4
Mva-N-8,0.7						6 stirrups @ 350 mm	0.6
Mvb-N-9,0.0	25	0.55				Without stirrups	0.7
Mvb-N-10,0.0	35	0.35				Without stirrups	0.6
Mvb-N-11,0.2							
Mvb-N-12,0.2							
Mvb-N-13,0.4							
Mvb-N-14,0.4	25	0.55					
Mvb-N-15,0.6							
Mvb-N-16,0.6							
Mva-N-17,0.7				35	0.35		
Mva-N-18,0.7							
Mvb-N-19,0.6							
Mvb-N-20,0.6							

Nomenclature:

Mva: Beam with $f'_c = 25$ MPa

Mvb: Beam with $f'_c = 35$ MPa

N-1, 2...20: Numeration of the beams

0.0, 0.2, ...0.7: % of fibers with respect to the concrete volume

3. ANALYTICAL MODEL FOR CONCRETE WITHOUT FIBERS

3.1 Model proposed by the Committee 318 of the American Concrete Institute (ACI 318-14)

The nominal shear strength of a transverse section of a reinforced concrete beam is obtained according to the following equation:

$$V_n = V_c + V_s \quad (1)$$

For beams subjected to diagonal tensile shear only, the shear strength provided by the concrete is the following:

$$V_c = \left(0.16\lambda\sqrt{f'_c} + 17\rho_w \frac{V_u d}{M_u} \right) b_w d \quad (2)$$

$$V_c \leq (0.29\lambda\sqrt{f'_c})b_w d \quad (3)$$

$$\frac{V_u d}{M_u} \leq 1.0 \quad (4)$$

$$\rho_w = \frac{A_s}{b_w d} \quad (5)$$

In addition, the shear strength provided by the stirrups is given in the following manner:

$$V_s = \frac{A_v f_y d}{s} \quad (6)$$

Nomenclature:

b_w = Width of the beam (mm).

d = Effective depth of the beam (mm).

f'_c = Compressive design strength given at the age of 28 days. (MPa).

f_y = Yield strength of the stirrups (MPa).

s = Separation of stirrups (mm).

A_s = Area of the longitudinal steel (mm²).

A_v = Area of the stirrups (mm²).

M_u = Ultimate acting moment (kN-mm).

V_c = Shear strength provided by the concrete (kN).

V_n = Theoretical nominal shear strength (kN).

V_s = Shear strength provided by the stirrups (kN).

V_u = Ultimate acting shear force (kN).

ρ_w = Longitudinal reinforcement ratio in the web

λ = Density factor of the concrete = 1.0 for regular weight concrete.

4. CLASSICAL ANALYTICAL METHODS FOR FIBER-REINFORCED CONCRETE

4.1 Swamy model (Swamy et al., 1974)

This model is characterized for being a simple method, it considers that the ultimate theoretical shear strength of a fiber-reinforced beam without stirrups is determined in the following manner:

$$V_u = (0.41\sigma_{ut})b d \quad (13)$$

The approach of the Swamy model was developed to determine the ultimate tensile strength of the fiber-reinforced concrete under bending moment, with the objective to avoid carrying out several tests in the laboratory to determine this result, hence the model proposes the following equation:

$$\sigma_{ut} = 0.97\sigma_m(1 - V_f) + 3.4V_f \left(\frac{L_f}{D_f} \right) \quad (14)$$

$$\sigma_m = 0.62\sqrt{f_{cm}} \quad (15)$$

In the case of the presence of stirrups in the beam, the contribution to the ultimate shear strength obtained from equation (13) is calculated through the following equation:

$$V_w = \left(\frac{A_{sw}}{s} \right) d f_{ywm} \quad (16)$$

Nomenclature:

b = Width of the beam (mm).

d = Effective depth of the beam (mm).

f_{cm} = Compressive strength of fiber-reinforced concrete (MPa).

f_{ywm} = Yield strength of the stirrups (MPa).

s = Separation of the stirrups (mm).

A_{sw} = Area of the stirrups (mm²).

D_f = Diameter of the fiber (mm).

L_f = Length of the fiber (mm).

V_f = Volume fraction of fibers.

V_w = Shear strength provided by the stirrups (kN).

V_u = Ultimate theoretical shear strength (kN).

σ_m = Tensile strength of the fiber-reinforced concrete (MPa).

σ_{ut} = Ultimate tensile strength of the fiber-reinforced concrete under bending moment (MPa).

4.2 Narayanan Model (Narayanan et al., 1987)

This model considers three terms for the computation of the ultimate theoretical shear strength, the first term accounts for the contribution of the fiber reinforcing the concrete, the second term considers the dowel action that provides the longitudinal reinforcement, and the last term proposes the contribution of the strength due to extraction of the fibers during the diagonal cracking. In this manner, the proposed model is the following:

$$V_u = e \left[A' f_{spfc} + B' \rho \frac{d}{a} \right] + V_b \quad (17)$$

$$e = 1.0 \quad \text{when} \quad \frac{a}{d} > 2.8 \quad (18)$$

$$e = 2.8 \frac{d}{a} \quad \text{when} \quad \frac{a}{d} \leq 2.8 \quad (19)$$

$$f_{spfc} = \frac{f_{cuf}}{A} + B + C\sqrt{F} \quad (20)$$

$$A = 20 - \sqrt{F} \quad (21)$$

The identified factors that influence the strength of the fiber-reinforced concrete are the volume fraction of the fiber, the aspect ratio, and the interface that exist between the fiber and the matrix. The next equation considers these three factors:

$$F = \left(\frac{L}{D} \right) \rho_f d_f \quad (22)$$

$$\rho = \frac{A_s}{bd} \quad (23)$$

$$V_b = 0.41(\tau)F \quad (24)$$

Nomenclature:

a = Shear span (mm).

b = Width of the beam (mm).

d = Effective depth of the beam (mm).

d_f = Adherence factor depending on the type of fiber = 0.5 circulars; 0.75 waved; 1 indented.

e = Adimensional factor which accounts for the dowel effect action.

f_{cuf} = Compressive strength of the fiber-reinforced concrete (MPa).

f_{spfc} = Diametral tensile strength of the fiber-reinforced concrete (MPa).

A = Adimensional constant.

A' = Adimensional constant = 0.24

A_s = Area of the longitudinal reinforcement (mm²).

B = Constant = 0.7 MPa

B' = Constant = 80 MPa

C = Constant = 1 MPa

F = Fiber factor.

V_b = Force of extraction of the fiber during cracking (kN).

V_u = Ultimate theoretical shear strength (kN).

ρ_f = Volume fraction of fibers.

ρ = Longitudinal reinforcement ratio.

τ = Ultimate adherence strength = 4.15 MPa

5. RESULTS AND DISCUSSION

5.1 Prediction of the ultimate strength using the analytical models.

In table 5 the results on the nominal shear strength (V_n) are presented, which are obtained through ACI 318-14 models with equations (1), (2), and (6). The strength V_n is used in the design of reinforced concrete beams under shear force, and it includes the strength provided by the concrete, the longitudinal reinforcement, and the stirrups. This model does not consider the contribution of the fibers as concrete reinforcement.

Table 5. Nominal shear strength in concrete beams without fibers, with stirrups equation (1) and without stirrups equation (2) for both w/c ratios

Ratio w/c	f'_c MPa	V_c (eq. 2) kN	f_y MPa	V_s kN	V_n (eq.1) kN
0.55	25	39.5	280	25.8	65.3
0.35	35	44.2	280	25.8	70.0

There are previous studies that propose analytical models based on experimental results (Dinh et al., 2010, Aoude et al., 2012), and others that analyze experimental data coming from diverse sources and use an important number of analytical models for comparison, (Haisam, 2011). The objective of the herein study was to produce its own scientific experiment, which validates the analytical models selected, which are considered as classical in the literature since they have been the foundation of many others, with the merit of the latter based on the personalization of a variable without a substantial modification to the original model.

In table 6, the experimental results of the compressive and tensile strengths of the fiber-reinforced concrete are presented, which were used in the analytical models for the prediction of the ultimate theoretical shear strength. The compressive strengths were taken as f_{cuf} for Narayanan model. In the same manner, the tensile strength was considered as f_{spfc} for Narayanan model. These values were obtained in a standardized manner as previously indicated, hence, there was no significant difficulty in their determination for the application of the models studied.

Table 6. Compressive and tensile strength of the fiber-reinforced concrete specimens at the age of 28 days

Designation	Compressive strength MPa	Tensile strength MPa	Designation	Compressive strength MPa	Tensile strength MPa
Mva-N-1,0.0	28.5	2.5	Mvb-N-9,0.0	44.9	3.4
Mva-N-2,0.0	31.2	2.7	Mvb-N-10,0.0	46.4	3.8
Mva-N-3,0.3	29.5	3.2	Mvb-N-11,0.2	50.1	3.8
Mva-N-4,0.3	29.6	2.5	Mvb-N-12,0.2	37.2	3.4
Mva-N-5,0.5	30.2	3.2	Mvb-N-13,0.4	45.8	3.5
Mva-N-6,0.5	31.9	3.4	Mvb-N-14,0.4	51.7	3.7
Mva-N-7,0.7	31.5	3.2	Mvb-N-15,0.6	48.2	4.2
Mva-N-8,0.7	32.7	3.6	Mvb-N-16,0.6	46.1	3.9

In table 7, the results obtained from the selected analytical models are presented, to determine the ultimate theoretical shear strength

Table 7. Ultimate theoretical shear strength of fiber-reinforced beams for both w/c ratios.

Designation	Swamy Model kN	Narayanan Model kN	Designation	Swamy Model kN	Narayanan Model kN
Mva-N-1,0.0	-	-	Mvb-N-11,0.2	75.0	76.5
Mva-N-2,0.0	-	-	Mvb-N-12,0.2	75.0	76.5
Mva-N-3,0.3	68.2	70.6	Mvb-N-13,0.4	72.9	75.5
Mva-N-4,0.3	68.2	70.6	Mvb-N-14,0.4	72.9	75.5
Mva-N-5,0.5	66.1	69.9	Mvb-N-15,0.6	71.4	76.6
Mva-N-6,0.5	66.1	69.9	Mvb-N-16,0.6	71.4	76.6
Mva-N-7,0.7	64.7	69.9	Mva-N-17,0.7	53.6	58.9
Mva-N-8,0.7	64.7	69.9	Mva-N-18,0.7	53.6	58.9
Mvb-N-9,0.0	-	-	Mvb-N-19,0.6	60.4	64.6
Mvb-N-10,0.0	-	-	Mvb-N-20,0.6	60.4	64.6

5.2 Effect of the reinforcement with fibers in reinforced concrete beams with respect to the theoretical models.

Table 8 shows the experimental results of the shear strength of the fiber-reinforced concrete beams with and without stirrups, it also shows the average for each pair of tested beams in the laboratory.

Table 8. Experimental shear strength of fiber-reinforced concrete beams, for both w/c ratios.

Designation	Vu_{exp} kN	Average kN	Designation	Vu_{exp} kN	Average kN
Mva-N-1,0.0	68.9	67.3	Mvb-N-11,0.2	74.5	74.7
Mva-N-2,0.0	65.6		Mvb-N-12,0.2	74.9	
Mva-N-3,0.3	75.9	76.1	Mvb-N-13,0.4	80.6	80.9
Mva-N-4,0.3	76.2		Mvb-N-14,0.4	81.2	
Mva-N-5,0.5	83.0	84.4	Mvb-N-15,0.6	87.2	83.2
Mva-N-6,0.5	85.7		Mvb-N-16,0.6	79.1	
Mva-N-7,0.7	83.6	86.7	Mva-N-17,0.7	52.8	56.9
Mva-N-8,0.7	89.7		Mva-N-18,0.7	60.9	
Mvb-N-9,0.0	68.6	69.1	Mvb-N-19,0.6	53.4	51.5
Mvb-N-10,0.0	69.6		Mvb-N-20,0.6	49.6	

The effect in the ultimate shear strength provided by the reinforcement with steel fibers is evident just by comparing tables 5, 7, and 8, however, it is more convenient to make a direct relation between the experimental strength obtained and the analytical strength. In figure 2a, in a graphical manner, these values are presented, which were obtained by dividing column 3 of table 8 by the nominal shear strength (equation 1) for the ratio $w/c = 0.55$, and figure 2b shows the values obtained by dividing column 6 of table 8 by the nominal shear strength (equation 1) for the ratio $w/c = 0.35$.

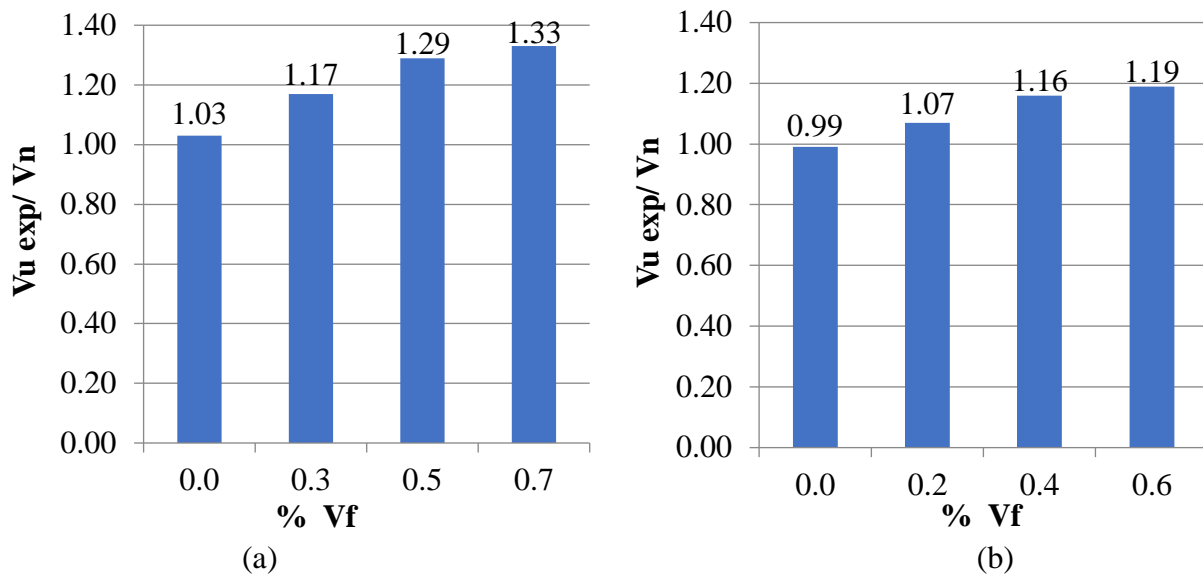


Figure 2. Contribution of the reinforcement with fibers compared with the experimental shear strength of the fiber-reinforced concrete beams with stirrups obtained from table 8 vs the nominal shear strength obtained from table 5. (a) Ratio $w/c=0.55$. (b) Ratio $w/c=0.35$.

For the beams with a ratio $w/c=0.55$, the fiber increases up to 33% of the shear strength in comparison with the nominal strength for $V_f=0.7\%$. In the case of the beams with a ratio $w/c=0.35$, the contribution of the fibers is less significant with a 19% for $V_f=0.6\%$. This behavior shown in both beams may be due to the fibers that allowed for a reduction of the crack width caused by the diagonal tension, which brought about a redistribution of stresses in the stirrups, making them more efficient.

The effectiveness of the reinforcement with fibers together with the use of the stirrups was reported, where it was found out an improvement in the ultimate shear strength and in the ductility (Sarhat et al., 2006). The use of V_f of 0.5 and 1.5% resulted in a larger effectiveness than that resulted by increasing the w/c ratio. In table 8, it is even observed that the beams with ratio $w/c=0.55$, for all volume fibers, reached a higher experimental shear strength than those control beams with ratio $w/c=0.35$, even though the latter has a larger w/c ratio. This implies that at a higher volume of fibers (>0.5) the ratio w/c does not seem to have a significant effect.

It can be noted, in table 9, the experimental results for the ultimate shear strength compared to the theoretical results obtained from the three analytical models studied. The effect of the w/c ratio of the beams can be observed for the experimental as well as for the theoretical results since the shear strength increases at lower w/c values. The best performance produced by the combination of stirrups and fibers, in comparison to the fiber-reinforced beams without stirrups, is also highlighted by the analytical models.

In table 9, it is presented a ratio of the experimental value to the theoretical value, to identify how much the ultimate shear strength is overestimated. The analytical models of Swamy and Narayanan predict values in most of the cases larger than the unit, i.e., they underestimate conservatively the experimental results. The three models show similar values to those from the experiments for both w/c ratios and for the fiber-reinforced beams with stirrups, however, for the beams without stirrups (17, 18, 19, and 20) the shear strength is overestimated for the ratio $w/c = 0.35$. Likewise, the effect of the volume fibers is also modeled adequately since it shows an increment of the ultimate experimental shear strength as V_f of the fiber also increases.

The conceptual criteria for which the three models were established explain the difference in their predictions of the experimental values, while the ACI model considers the contribution to the

ultimate shear strength from the concrete, the fibers, and the stirrups, in the case of having them, and even the force due to the dowel effect. The Swamy model, which is considerably simpler, provides conservative values with respect to the experiments, and only the Narayanan model considers the tensile strength of the concrete. The two latter models consider the effect of the aspect ratio of the fiber and the variation of the V_f . It is worth mentioning that the analytical models studied do not provide information about the ductility and cracking patterns of the fiber-reinforced concrete beams.

Table 9. Ratio between the experimental shear strength and the analytical shear strength obtained for each model

Designation	Vu_{exp} kN	Vn_{ACI} kN	$\frac{Vu_{exp}}{Vu_{ACI}}$	Vu_{Swamy} kN	$\frac{Vu_{exp}}{Vu_{Swamy}}$	$Vu_{Narayanan}$ kN	$\frac{Vu_{exp}}{Vu_{Narayanan}}$
Mva-N-1,0.0	68.9	65.3	1.06				
Mva-N-2,0.0	65.6	65.3	1.00				
Mva-N-3,0.3	75.9			68.2	1.11	70.6	1.08
Mva-N-4,0.3	76.2			68.2	1.12	70.6	1.08
Mva-N-5,0.5	83.0			66.1	1.26	69.9	1.19
Mva-N-6,0.5	85.7			66.1	1.29	69.9	1.23
Mva-N-7,0.7	83.6			64.7	1.29	69.9	1.19
Mva-N-8,0.7	89.7			64.7	1.39	69.9	1.28
Mva-N-17,0.7	52.8			53.6	0.98	58.9	0.89
Mva-N-18,0.7	60.9			53.6	1.14	58.9	1.03
Mvb-N-9,0.0	68.6	70.0	0.98				
Mvb-N-10,0.0	69.6	70.0	0.99				
Mvb-N-11,0.2	74.5			75.0	0.99	76.5	0.97
Mvb-N-12,0.2	74.9			75.0	1.00	76.5	0.98
Mvb-N-13,0.4	80.6			72.9	1.11	75.5	1.07
Mvb-N-14,0.4	81.2			72.9	1.11	75.5	1.08
Mvb-N-15,0.6	87.2			71.4	1.22	76.6	1.14
Mvb-N-16,0.6	79.1			71.4	1.11	76.6	1.03
Mvb-N-19,0.6	53.4			60.4	0.88	64.6	0.83
Mvb-N-20,0.6	49.6			60.4	0.82	64.6	0.78

In similar manner, in table 9, it can be observed that, by analyzing the results of the beams without stirrups, Narayanan models overestimate the values and Swamy model does it similarly, but it is closer to the unit.

The graphical behavior of the aforementioned is presented in figure 3, where it can be observed a relationship between the results of the ultimate experimental shear strength and the results of the analytical models. It is noted that the prediction of the values obtained from the models that approach the diagonal is equal to the experiments, otherwise, all the values that are under this diagonal are slightly conservative. Such is the case for some points of the Narayanan model, which presents a lower degree of approximation with respect to the other analytical models proposed by Swamy and ACI. The majority of the plotted points of the three models show similitude in their results and they are considered conservative since they are over the diagonal.

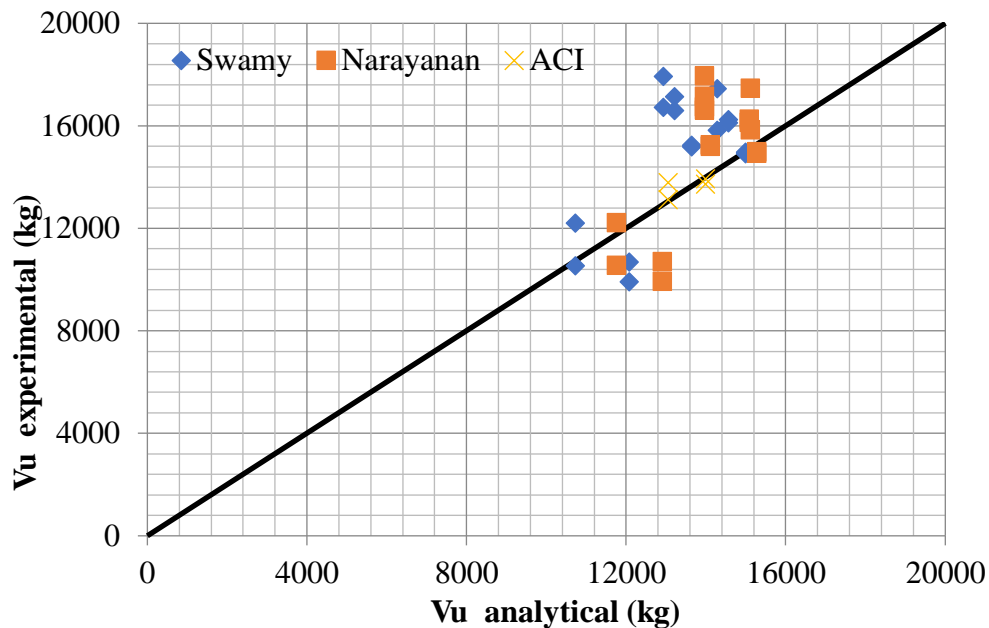


Figure 3. Experimental shear strength vs the ultimate shear strength obtained from the three analytical models proposed, for fiber-reinforced beams with both w/c ratios, with stirrups and without stirrups.

5.3 Effect of the combined action of the reinforcement with steel fibers and stirrups.

Figure 4 shows the results for the experimental shear strength of the fiber-reinforced concrete beams without stirrups, but with the higher fiber content, these are compared to the control beams and the limit values of the three studied models.

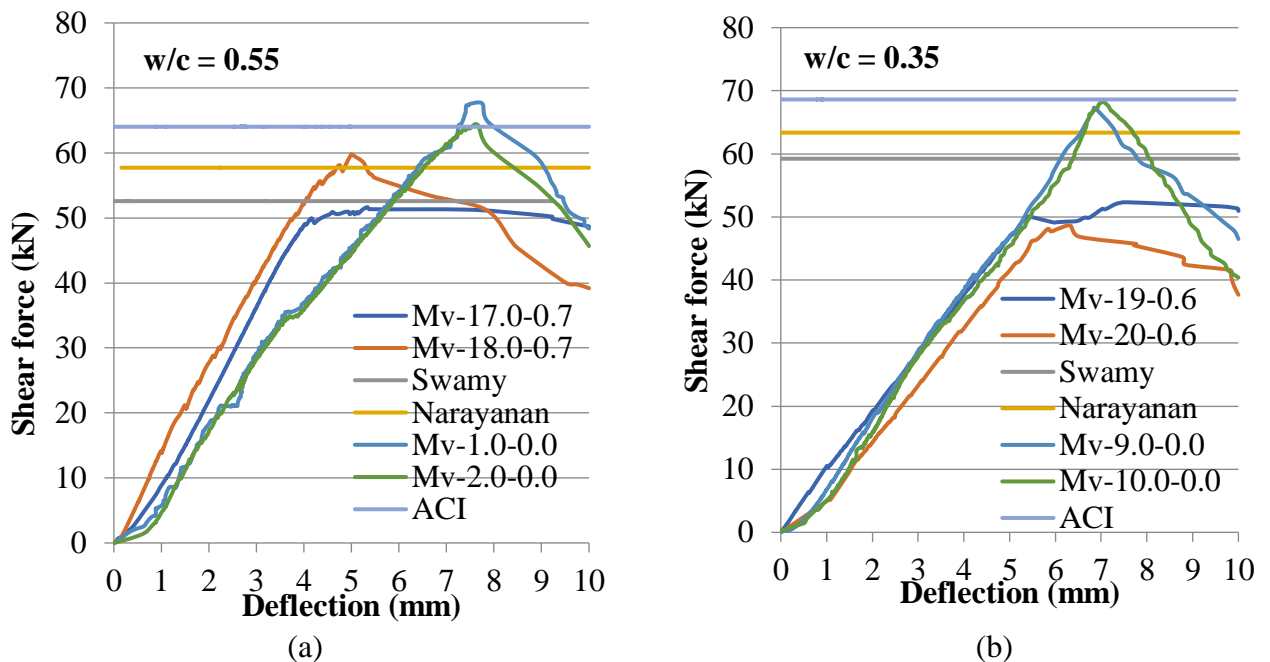


Figure 4. Behavior of the fiber-reinforced beams without stirrups compared to the control beams. (a) Ratio w/c=0.55. (b) Ratio w/c=0.35.

In figure 4, it can be observed that for both w/c ratios the contribution of the maximum content of fiber into the experimental shear strength of the beams without stirrups (17, 18, 19, and 20) was

not sufficient to at least reach the same experimental strength of the control beams (1, 2, 9, and 10) that have no fibers, but which have the higher amount of stirrups. Even just the beams with the ratio $w/c = 0.55$ reach the theoretical strength predicted by the models, this was not the case for the beams with ratio $w/c = 0.35$, this can be attributed to the lower V_f which leads to an insufficient increment of the concrete strength, nevertheless, it can be observed that the post-cracking behavior in the reinforced beams only with fibers had a lower reduction of the shear strength than those with only stirrups, this is due to the fiber-matrix adherence, which allows for the transfer of stresses. The control beams show an appropriate behavior and they reach the predicted value by the ACI. On the other hand, it can be observed in figure 5, where the fiber-reinforced beams with the maximum V_f and with the lesser amount of stirrups had a higher shear strength than the control beams, even they were exceeded significantly for both w/c ratios the limit values of the models. The contribution of the fibers, in combination with half of the area of the transverse steel that the beams have, increased the ultimate shear strength with respect to the theoretical nominal strength, and this resulted to be larger in comparison to the results obtained for the control beams with the greater amount of stirrups.

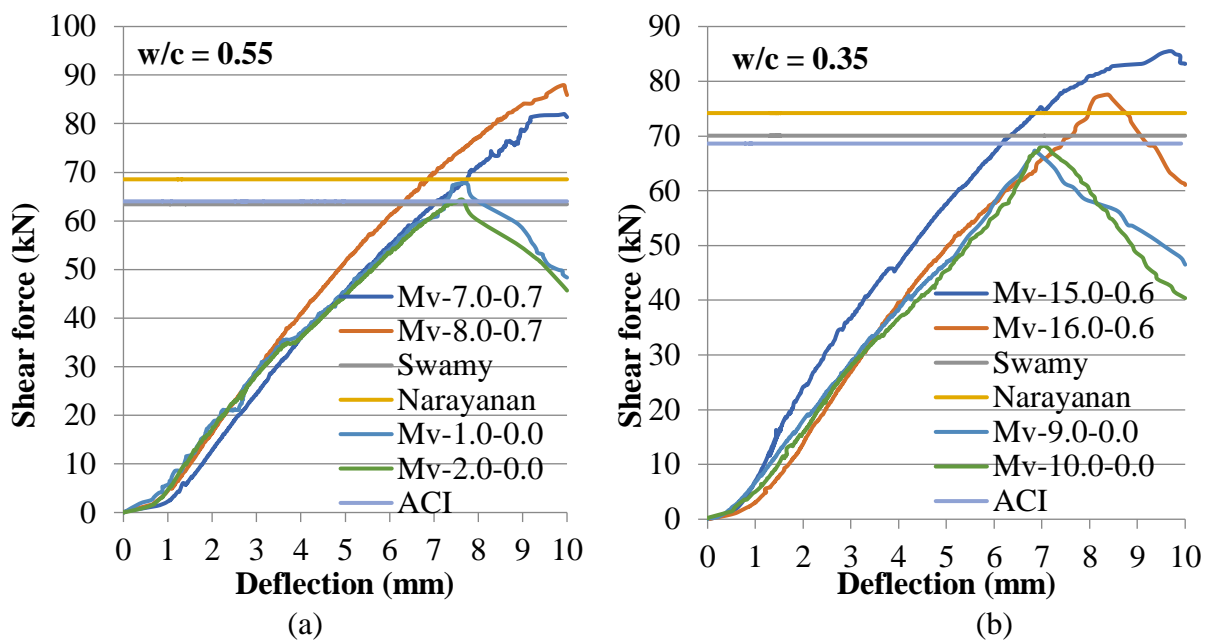


Figure 5. Behavior of fiber-reinforced beams with a minimum amount of stirrups compared with control beams. (a) Ratio $w/c=0.55$. (b) Ratio $w/c=0.35$.

From the reinforced concrete structural behavior point of view, the presence of the steel fibers as additional reinforcement for the beams with stirrups allows to increase in a significant manner the ultimate shear strength, hence, it is justifiable to use analytical models that admit predicting accurately a theoretical shear strength close to that experimentally obtained, and this can be a design aid for these types of structural elements.

The herein research showed that the ultimate shear strength increases substantially when steel fibers are used and that, by knowing analytical models of easy implementation, these can become a useful tool for the analysis and design of fiber-reinforced beams with stirrups and without them. Under this perspective, the conclusions that are applicable according to the results obtained are drawn next.

6. CONCLUSIONS

1. The usage of steel fibers does not produce a decrease in the compressive and tensile strength of the fiber-reinforced concrete for both w/c ratios, on the contrary, both strengths increase.
2. It is suggested to use experimental results for the compressive and tensile strengths obtained from the fiber-reinforced concrete specimens since this will allow the analytical models to have an appropriate prediction of the ultimate theoretical shear strength.
3. The ACI, Swamy, and Narayana analytical models predicted conservative values with respect to the ultimate shear strength since they approach or are less than the experimental shear strength, this implies that they can be used conservatively for the analysis and design of fiber-reinforced concrete beams with stirrups.
4. The use of V_f equal to 0.3, 0.5 and 0.7 in the fiber-reinforced beams with ratio w/c = 0.55 with stirrups resulted in a higher experimental shear strength than the observed for the ratio w/c = 0.35.
5. The fiber-reinforced concrete beams without stirrups with V_f equal to 0.6 and 0.7% have less ultimate shear strength than the control beams for both w/c ratios. In addition, the ultimate shear strength is lesser than the value predicted by the three analytical models.
6. The steel fibers as additional reinforcement in combination with a minimum amount of stirrups allow increasing the ultimate shear strength substantially due to diagonal tension and the ductile behavior in the fiber-reinforced beams.
7. The reinforcement executed only with steel fibers cannot substitute completely the transverse steel reinforcement, but it did show a better post-cracking behavior since it had a lower reduction of shear strength than the beams only with stirrups, this is caused by the fiber-matrix adherence.

7. ACKNOWLEDGEMENTS

The authors would like to thank Consejo Nacional de Ciencia y Tecnología (CONACYT), for the financial support for the master in science student scholarship. Also, they would like to thank the authorities of the Ingeniería Civil “Dr. Raymundo Rivera Villarreal” of the Facultad de Ingeniería Civil at UANL, for their support on the use of the required infrastructure to conduct the experimental tests.

8. REFERENCES

- ACI 318S-14, (2014), *Requisitos de Reglamento para Concreto Estructural y Comentarios*, Instituto Americano del Concreto, ACI.
- Ashour, S. A., Hasanain, G. S., Wafa, F. F. (1992), *Shear Behavior of High-Strength Fiber Reinforced Concrete Beams*, ACI Structural Journal, Vol. 89, No. 2, March-April, pp. 176 – 184.
- Aoude, H., Belghiti, M., Cook, W. D., Mitchell, D. (2012), *Response of steel fiber-reinforced concrete beams with and without stirrups*, ACI Structural Journal, Vol. 109, No. 3, pp. 359-367.
- ASTM International. (2018). *ASTM C33 / C33M-18, Standard Specification for Concrete Aggregates*. Annual Book of ASTM Standards, American Society of Testing Materials. https://doi.org/10.1520/C0033_C0033M-18
- ASTM International. (2020). *ASTM A615 / A615M-20, Standard Specification for Deformed and Plain Carbon-Steel Bars for Concrete Reinforcement*. West Conshohocken, PA. https://doi.org/10.1520/A0615_A0615M-20

- ASTM International. (2016). *ASTM A820 / A820M-16, Standard Specification for Steel Fibers for Fiber-Reinforced Concrete*. West Conshohocken, PA. https://doi.org/10.1520/A0820_A0820M-16
- ASTM International. (2020). *ASTM C143 / C143M-20, Standard Test Method for Slump of Hydraulic-Cement Concrete*. West Conshohocken, PA. https://doi.org/10.1520/C0143_C0143M-20
- ASTM International. (2019). *ASTM C192 / C192M-19, Standard Practice for Making and Curing Concrete Test Specimens in the Laboratory*, Annual Book of ASTM Standards, American Society of Testing Materials. https://doi.org/10.1520/C0192_C0192M-19
- ASTM International. (2021). *ASTM C39 / C39M-21, Standard Test Method for Compressive Strength of Cylindrical Concrete Specimens*. West Conshohocken, PA. https://doi.org/10.1520/C0039_C0039M-21
- ASTM International. (2017). *ASTM C496 / C496M-17, Standard Test Method for Splitting Tensile Strength of Cylindrical Concrete Specimens*. West Conshohocken, PA. https://doi.org/10.1520/C0496_C0496M-17
- ASTM International. (2017a). *ASTM C231 / C231M-17a, Standard Test Method for Air Content of Freshly Mixed Concrete by the Pressure Method*. West Conshohocken, PA. https://doi.org/10.1520/C0231_C0231M-17A
- Dinh, H. H., Parra-Montesinos, G. J., Wight, J. K. (2010), *Shear behavior of steel fiber-reinforced concrete beams without stirrup reinforcement*, ACI Structural Journal, Vol. 107, No. 5, pp. 597-606.
- Dupont, D., Vandewalle, L. (2003), *Shear Capacity of Concrete Beams Containing Longitudinal Reinforcement and Steel Fibers*, ACI Structural Journal, Vol. 216, pp. 79 – 94.
- Haisam, E. Y. (2011), *Shear Stress Prediction: Steel Fiber - Reinforced Concrete Beams without Stirrups*, ACI Structural Journal, Vol. 108, No. 3, May-June, pp. 304 – 314.
- Juarez, C., Valdez, P., Durán, A., Sobolev, K. (2007), *The diagonal tension behavior of fiber reinforced concrete beams*, Cement & Concrete Composites, 29(5):402-408. <https://doi.org/10.1016/j.cemconcomp.2006.12.009>
- Jun Z., Jingchao L., Liusheng C. and Fuqiang S. (2018), *Experimental Study on Shear Behavior of Steel Fiber Reinforced Concrete Beams with High-Strength Reinforcement*. Materials, 11 (9), 1682, pp. 1-19. <https://doi.org/10.3390/ma11091682>
- Khuntia, M., Stojadinovic, B. (2001), *Shear Strength of Reinforced Concrete Beams without Transverse Reinforcement*, ACI Structural Journal, Vol. 98, No. 5, September-October, pp. 648 – 656.
- Marí Bernat, A., Spinella, N., Recupero, A. (2020), *Mechanical model for the shear strength of steel fiber reinforced concrete (SFRC) beams without stirrups*. Materials and Structures. 53(28). <https://doi.org/10.1617/s11527-020-01461-4>
- Narayanan, R., Darwish, I. Y. S. (1987), *Use of Steel Fibers as Shear Reinforcement*, ACI Structural Journal, 84 (3), May – June, pp. 216 – 226.
- Organismo Nacional de Normalización y Certificación de la construcción y Edificación, S.C. (ONNCCE) (2017). *NMX-C-414-ONNCCE: Industria de la Construcción – Cementos Hidráulicos - Especificaciones y Métodos de Prueba*. Norma Mexicana.
- Park, P., Paulay, T. (1990), “*Estructuras de Concreto Reforzado*”, Editoriales Limusa y Noriega, Nueva Edición, pp. 288 – 294. https://www.u-cursos.cl/usuario/7ed3df485e955c4de1ffa12120d4bb52/mi_blog/r/estructuras_de_concreto_reforzado_-_r._park_t._paulay.pdf
- Sarhat, S. R., Abdul-Ahad, R. B. (2006), *The Combined Use of Steel Fibers and Stirrups as Shear Reinforcement in Reinforced Concrete Beams*, SP, American Concrete Institute, vol. 235, pp. 269 – 282.

- Shin, S. W., Oh, J. G., Ghosh, S. K. (1994), *Shear Behavior of Laboratory-Sized High Strength Concrete Beams Reinforced with Bars and Steel Fibers*, American Concrete Institute, Volume 142. pp. 181-200.
- Swamy, R. N., Bahía, H. M. (1985), *The Effectiveness of Steel Fibers as Shear Reinforcement*, Concrete International, Design and Construction, Vol. 7, No. 3, March, pp. 35 – 40.
- Swamy, R. N., Mangat, P. S., Rao, C. V. S. K. (1974), *The Mechanics of Fiber Reinforcement of Cement Matrices*, Symposium Paper, American Concrete Institute, 44, pp. 1 – 28.
- Swamy, R. N., Narayan, J., Roy, Chiam, T. P. (1993), *Influence of Steel Fibers on the Shear Resistance of Lightweight Concrete I – Beams*, ACI Structural Journal, Vol.90, No. 1, January – February, pp. 103 – 114. <https://doi.org/10.14359/4201>

Evaluation of the effect of waste clay from a polyol production process as a partial substitute for cement in reinforced concrete

O. Troconis de Rincón^{1*}, V. Millano¹, W. Suarez¹,
L. Navarro¹, A. De Turrís¹, R. Amesty¹

*Contact author: oladistr@gmail.com

DOI: <https://doi.org/10.21041/ra.v11i3.552>

Reception: 11/07/2021 | Acceptance: 21/08/2021 | Publication: 01/09/2021

ABSTRACT

In this work, the effect of waste clay from a polyol production process was evaluated, as a partial substitute for cement in reinforced concrete, in concentrations of 0%, 5% and 10%. The physico-mechanical characteristics of the concrete and the electrochemical properties of the steel were determined during a period of 356 days (ISO 11474), in 15x10x5 cm specimens, with two steel bars embedded in the concrete. The results indicate that the compressive strength decreased proportionally according to the clay content; increasing for 90 days of curing. However, the capillary sorption of the concrete decreased, which allowed the steel in the marine environment to maintain its passive state for longer than its blank specimen, for the w/c ratios evaluated (0.45 and 0.60).

Keywords: corrosion in reinforced concrete; cement replacement; polyol clay; durability.

Cite as: Troconis de Rincón, O., Millano, V., Suarez, W., Navarro, L., De Turrís, A., Amesty, R. (2021), "Evaluation of the effect of waste clay from a polyol production process as a partial substitute for cement in reinforced concrete", Revista ALCONPAT, 11 (3), pp. 50 – 63, DOI: <https://doi.org/10.21041/ra.v11i3.552>

¹Centro de Estudios de Corrosión, Facultad de Ingeniería, Universidad del Zulia, Maracaibo, Venezuela.

Contribution of each author

In this work, the author Oladis Troconis de Rincon contributed to the generation of the project, direction of the experimental part and analysis of results. He wrote the final work, 30%. Valentina Millano contributed to the generation of the project, direction of the students in the experimental part and analysis of results, 30%. Wilfredo Suarez contributed in the realization of the experimental part, corresponding to the objectives of his postgraduate thesis, Master in corrosion, and generated the first version of the work with contributions of ideas in the development of this, 20%. Luis Navarro contributed in the realization of the experimental part, corresponding to the objectives of his undergraduate thesis, degree in Chemical Engineering, and generated the first version of the work, 10%. Antonio De Turrís contributed 5% to the project's initial proposal before private organizations and the University of Zulia through the Corrosion Studies Center. Roque Amesty contributed to the initial proposal of the project before private organizations and the University of Zulia through the Corrosion Studies Center, 5%.

Creative Commons License

Copyright 2021 by the authors. This work is an Open-Access article published under the terms and conditions of an International Creative Commons Attribution 4.0 International License ([CC BY 4.0](https://creativecommons.org/licenses/by/4.0/)).

Discussions and subsequent corrections to the publication

Any dispute, including the replies of the authors, will be published in the second issue of 2021 provided that the information is received before the closing of the first issue of 2021.

Evaluación del efecto de la arcilla de desecho de un proceso de producción de polioles como sustituto parcial del cemento en concreto armado

RESUMEN

En este trabajo se evaluó el efecto de la arcilla de desecho de un proceso de producción de polioles, como sustituto parcial del cemento en concreto armado, en concentraciones del 0%, 5% y 10%. Se determinaron las características físico-mecánicas del concreto y electroquímicas del acero durante un periodo de 356 días (ISO 11474), en probetas de 15x10x5 cm, con dos barras de acero embebidas en el concreto. Los resultados indican que la resistencia a la compresión disminuyó proporcionalmente según el contenido de arcilla; incrementándose para los 90 días de curado. Sin embargo, la sorción capilar del concreto disminuyó, lo cual permitió que el acero en ambiente marino mantuviera su estado pasivo por más tiempo que sus blancos, para las relaciones a/c evaluadas (0,45 y 0,60).

Palabras clave: corrosión en concreto armado; sustitución del cemento; arcilla poliólica; durabilidad.

Avaliação do efeito da argila residual de um processo de produção de polioliol como substituto parcial do cimento em concreto armado

RESUMO

Neste trabalho foi avaliado o efeito da argila residual de um processo de produção de polióis, como substituto parcial do cimento em concreto armado, nas concentrações de 0%, 5% e 10%. As características físico-mecânicas do concreto e as características eletroquímicas do aço foram determinadas durante um período de 356 dias (ISO 11474), em corpos de prova de 15x10x5 cm, com duas barras de aço embutidas no concreto. Os resultados indicam que a resistência à compressão diminuiu proporcionalmente com o teor de argila; aumentando para os 90 dias de cura. No entanto, a sorção capilar do concreto diminuiu, o que permitiu ao aço em ambiente marinho manter seu estado passivo por mais tempo do que suas metas, para as relações a/c avaliadas (0,45 e 0,60).

Palavras-chave: corrosão em concreto armado; substituição do cimento; argila polióis; durabilidade.

Legal Information

Revista ALCONPAT is a quarterly publication by the Asociación Latinoamericana de Control de Calidad, Patología y Recuperación de la Construcción, Internacional, A.C., Km. 6 antigua carretera a Progreso, Mérida, Yucatán, 97310, Tel.5219997385893, alconpat.int@gmail.com, Website: www.alconpat.org

Reservation of rights for exclusive use No.04-2013-011717330300-203, and ISSN 2007-6835, both granted by the Instituto Nacional de Derecho de Autor. Responsible editor: Pedro Castro Borges, Ph.D. Responsible for the last update of this issue, Informatics Unit ALCONPAT, Elizabeth Sabido Maldonado.

The views of the authors do not necessarily reflect the position of the editor.

The total or partial reproduction of the contents and images of the publication is carried out in accordance with the COPE code and the CC BY 4.0 license of the Revista ALCONPAT.

1. INTRODUCTION

Concrete is the most consumed man-made material in the world (Ghosal, 2015), being a mixture of basically four components; coarse aggregate (gravel), fine aggregate (sand), water and cement. The latter represents the highest economic and environmental cost because its production is one of the largest sources of greenhouse gases, contributing 7 to 8% of these gases (Devi et.al., 2016). The widespread use of cement is due to its versatility, durability, and low maintenance when compared to other commonly used construction materials such as steel, wood, bricks, etc.

In recent decades, efforts have been made to focus on finding materials that partially replace cement in the preparation of concrete, in order to reduce the aforementioned economic and environmental impact. Such efforts have led to the evaluation of different materials among which are: blast furnace ash, marble and granite (Devi et.al., 2016), rice shell ash (Ghosal, 2015), tile dust (Manogna and Srilakshmi, 2015), egg shells (Gowsika et.al., 2014), nickel slag (Montiel, 2012), shrimp shell (Mendoza et.al., 2013), among many others. All these materials have in common being some type of waste from a process other than cement production, so their addition, as a partial substitute for cement in a concrete mix, represents the elimination of an environmental liability. Common elements in these materials are silicates, such as calcium and magnesium silicate, which increase the possibility of pozzolanic activity in these wastes. This type of siliceous or silico-aluminous materials are called natural pozzolans, which, although by themselves have little or no cementing value, react chemically with one of the reaction products of cement in contact with water, portlandite or calcium hydroxide (Ca(OH)_2), which at ordinary temperatures forms compounds with cementitious properties (ASTM C 618-89).

Now, in the Petrochemical industry, there are many processes that produce substances that generate well-being for society, however, they might also generate large amounts of undesirable substances that constitute an environmental liability, which must be disposed of in accordance with the current legal framework (Decree 883. Venezuelan environmental regulations) to be disposed of in soil, air and bodies of water. The production of polyurethanes is one of them, which leaves the accumulation of a residue from the polymerization reaction of the monomers of ethylene and propylene oxides. The waste, known as waste clay, is a mixture of magnesol (synthetic hydrated magnesium silicate), filter material and impregnated polyol, previously used as secondary raw material in the process to deactivate the catalyst (KOH), from the polymerization reaction by means of catalytic adsorption. Reusing this liability, it can help conserve natural resources, by disposing of waste and reducing the demand for conventional raw materials for other production processes.

The characteristic high content of magnesium silicates in Magnesol would be expected to provide remarkable compressive strength as a partial replacement for cement in concretes. In the same way, the alkaline reserve would be favored by the presence of KOH, used as a catalyst, a condition that would benefit the passivation of the reinforcing bars (Oxiteno Andina, 2000).

Thus, the objective of this work was to evaluate the effect of polyol waste clay as a partial substitute for cement, in the preparation of reinforced concrete. This, in order to reduce the consumption of cement, maintaining at least the durability of the concrete without the addition; and also obtaining an economic and ecological benefit, which has not been investigated so far.

2. EXPERIMENTAL PROCEDURE

2.1 Mineralogical characterization of polyol clay

This test was carried out to determine the chemical components that make up the discarded clay from polyol production. To this end, the X-ray spectrometry analysis technique and X-ray fluorescence (XRF) were used. However, due to the caked nature (with polyol residues) of the clay sample, a treatment prior to the application of these test methods was necessary, which consisted of a physical separation of the waste clay from the remaining bulk mass of polyols. The separation process consisted of separating the filter material made up of the powdered mixture of Magnesol and filter aid or rare earths, by means of the total dissolution of the waste impregnated in polyols in an organic solvent such as acetone. Subsequently, the stripping with nitrogen was carried out using a vertical trays filter, which retains the Magnesol-filter aid mixture and the KOH catalyst residue in dry powder; allowing most of the polyol dissolved in acetone to pass through. The dry base of the waste clay (Magnesol, filter aid and KOH) hereinafter polyol clay powder, was subjected to the following tests.

2.2 Physicochemical characterization of polyol clay

- *pH analysis*: the solution prepared with the sample was filtered and the aqueous residue pH was measured, using a pH meter following the ASTM E70-07 standard.
- *Analysis of the chloride ion content*: The analysis of the chloride ion concentration present in the sample was carried out using the potentiometric technique described in the ASTM D512 standard.
- *Pozzolanity Index*: The pozzolanity index of the waste clay was determined according to the procedures described in ASTM C311.

2.3 Mix design

The mix design that was used in the manufacture of the specimens for the tests, contemplated two w/c ratios of 0.45 and 0.60. These mixtures were designed in accordance with ACI 211.1.1991.

2.4 Preparation of specimens

Table 1 shows the number of specimens and dimensions, according to the type of test to be carried out:

Table 1. Distribution of the specimens for the different tests to be carried out.

Test specimen	Programmed test
18 cylinders 10x20 cm	• Capillary sorption
	• Natural Diffusion (D3)
	• Exposition to a natural urban environment
36 cylinders 15x30 cm	• Compressive strength
	• Resistivity
18 prismatic specimens	• Corrosion Potential
	• Corrosion Rate

2.5 Compressive strength test

After a curing period of 28 and 90 days, under conditions of high relative humidity (test specimens wrapped in newspaper and saturated with water) and room temperature (≤ 25 °C), the test was carried out according to the ASTM C39/C39M- standard. 2012.

2.6 Determination of capillary sorption.

Concrete slices of 5 cm thick and 10 cm in diameter were used to carry out this test. The test was based on the procedure described in the DURAR manual (Troconis de Rincón, et.al., 2011), which at the same time it was based on the methodology proposed by Fagerlund (1982) that describes the kinetics of capillary sorption through three coefficients: m (resistance to water penetration), k (capillary sorption coefficient) and ε_e (effective porosity).

2.7 Determination of the carbonation front

The specimens were exposed to an urban environment for 82 days (28 °C and 400 ppm CO₂). Once the specimen was selected, a cross-section cut was made to each one of them and, with its surface free of dust, phenolphthalein (acid-base indicator) was applied by atomization in a uniform way, as indicated in the DURAR manual (Troconis de Rincón, et.al., 2011); thus measuring the carbonate thickness with the use of a caliper.

2.8 Electrochemical evaluation of test pieces exposed to an accelerated marine environment according to the modified ISO 11474 standard.

The corrosion potential was determined twice a week on the reinforcement of the prismatic specimens, using a saturated Cu/CuSO₄ reference electrode and a multimeter. Each prismatic specimen has two carbon steel bars embedded in the concrete, identified as A and B, located 1.5 cm from the exposed face.

Regarding the corrosion rate measurements over time, they were carried out using the Gecorr10 equipment, using the polarization resistance technique. The frequency of corrosion rate measurements was 1 to 2 times per month.

3. RESULTS

3.1 Mineralogical and chemical characterization

The X-ray fluorescence (XRF) test results shown in Table 2 reveal the mineralogical composition of the polyol waste clay powder; discovering that the major constituent is silicon oxide (SiO₂) with 64.86%, followed by potassium oxide (K₂O) with 24.82% and finally magnesium oxide (MgO) with 5.7%, all expressed on a mass basis.

Table 2. Mineralogical composition (oxides) of polyol clay by XRF.

REFERENCE	SiO ₂	K ₂ O	MgO	Al ₂ O ₃	SO ₃	Fe ₂ O ₃	TOTAL
SAMPLE	64.86	24.82	5.7	3.02	0.82	0.79	100.01

In these results, the absence of calcium or its oxide within the composition of the clay is observed. This is not only essential for the formation of calcium silicates, whose reaction with water produces hydrated calcium silicates responsible for the compressive strength of concrete, but also for its alkalinity; which influences its durability. The high concentration of SiO₂ would promote the formation of these silicates if there was a source of Calcium. This source can come from the cement itself, since one of the products of the hydration reaction of calcium silicates is calcium hydroxide. However, as mentioned before, the waste used in the manufacture of concrete is a clay impregnated in polyol, with a pasty appearance. The equipment and techniques used for its analysis only accept powder samples, which is why the waste was separated from the polyol by washing with an organic solvent (Acetone). As a result of this separation process, 51.9% of the sample is made up of polyol, which has a viscous appearance, comparable to oil, and the remaining 48.1% by weight is made up of the filter material (Magnesol, Filter aid and KOH), this is a very fine white powder, which will

be later identified as “clay powder”. Because polyol represents more than 50% of the waste used in the manufacture of concrete, the impact of this dust on the durable properties of concrete cannot be predicted based on the mineralogical composition / chemical analyzes presented.

Table 3 compares the mineralogical composition of the polyol waste clay with that found in the type II portland cement, used in this investigation, by means of X-ray spectrometry. The clay powder is basically composed of magnesium silicate (magnesol), with 72.88% of SiO₂ that could be capable of reacting with free lime (CaO) forming hydraulic compounds that contribute to the development of the mechanical resistance of concrete, that is to say that this concentration range could cause a positive impact by producing long-term pozzolanic activity (Calleja, 1983). Additionally, it is observed that the alkali and MgO content of the powder is high, which could negatively influence the mechanical properties of concrete.

Table 3. Chemical constituents present in Portland cement and polyol waste clay used to make concrete.

Reference Component	Polyol manufacturing waste (Powder clay)	Portland II cement
L.F	2.18	3.46
SiO ₂	72.88	20.16
Al ₂ O ₃	1.05	4.23
Fe ₂ O ₃	0.03	3.05
CaO	1.12	64.38
MgO	9.63	0.87
SO ₃	0.90	1.87
K ₂ O	9.04	0.47
TiO ₂	0.12	0.26
Mn ₂ O ₃	0.01	0.37
Na ₂ O	2.14	0.00
Total	99.10	99.12

L.F. Lost to Fire

When analyzing the amount of chloride ions in the polyol waste clay, it was found that it was low (338.85 ppm), which does not affect the durability of the rebar.

3.2 Pozzolanic activity

Following the guidelines of the ASTM C-311 standard, the degree of pozzolanicity of the polyol waste clay in the manufacture of mortars was studied. For this, the compressive strength values of a mortar with substitution (20% polyol clay) were compared against a blank specimen. The results in Table 4 show that the polyol waste clay exhibits a pozzolanic activity index of 58.34% as a function of its compressive strength. The results in Table 4 also show the limited pozzolanic nature of the waste clay; since it does not exceed the 75% established by the ASTM C311. Since the pozzolanic action is an interaction phenomenon in which the surface (total and specific) of the active material greatly influences, it must be ground to great fineness or possess it by itself, in any case, it must be much finer than clinker. In this case, the material used in the research, (dry clay without the polyol), despite having high SiO₂ content does not have the specified texture to develop pozzolanic action, because the polyol constitutes 51.9% of the material, turning it into a viscous-looking mass, and preventing the interaction of the active surface of the material with the phases and hydration products of the cement.

Table 4. Pozzolanicity activity of polyol waste clay.

Pozzolanicity activity index test (ASTM C-311)	
Pozzolanicity activity index, %	58.34
Strength, kg/cm ²	
Blank	314.64
Substituted Mortar	183.57
Air content, %	13.95
Fluidity, %	81.84
Water Requirement, %	82.64

3.3 Mix design

To prepare the mix design, the procedure described by the ACI C211.1.1991 standard for water/cement ratios (w/c) of 0.45 and 0.60 was followed. Based on this, it was designed for compressive strengths of 380 Kg/cm² and 260 Kg/cm² for w/c of 0.45 and 0.60, respectively, and a slump of 10 ± 2 cm. Table 5 shows the results of the mix design for 1 m³ of concrete, for the mentioned w/c ratios.

Table 5. Mix design for 1 m³ of concrete for w/c ratios of 0.45 and 0.60 and slump of 10±2 cm.

w/c (Ratio)	0.45			0.60			Unit
Substitution %	Blank	5%	10%	Blank	5%	10%	-
Mix water	202.51	202.51	202.51	197.71	197.71	197.71	kg/m ³
Cement content	450.02	427.52	405.02	323.23	307.07	290.91	kg/m ³
Polyol waste clay content	0	22.501	45.002	0	16.16	32.32	kg/m ³
Coarse aggregate content	886.49	886.49	886.49	919.72	919.72	919.72	kg/m ³
Fine aggregate content	793.46	793.46	793.46	888.61	888.61	888.61	kg/m ³

3.4 Evaluation of the fresh mix

Figure 1 shows that for mixtures with clay addition, an increase in workability proportional to the increase in clay is observed as a partial replacement for cement (13-14cm, 21cm and 23-24cm slump for 0%, 5% and 10%, respectively). However, in none of the evaluated cases (with/without clay), significant differences were observed between the mixtures with w/c ratios of 0.60 and 0.45; which may be due to the excellent quality of the aggregates used.

For the 0.45 and 0.60 mixtures with 5% substitution, a slump of 21 cm was recorded for both fresh mixtures, with an approximate increase of 8 cm with respect to the values recorded for the reference mixtures (blanks). For the 0.45 and 0.60 mixtures with 10% substitution, 23 and 24 cm of settlement were recorded, respectively, with an increase of 10 cm compared to their reference mixtures. These results show an effect on the workability of the fresh mix due to the addition of clay as a partial substitute for cement, the effect being more noticeable with respect to blank specimens for the lower dosages of clay, since the difference in workability of the mix between 5 and 10% substitution is minimal (2 cm slump approximately).

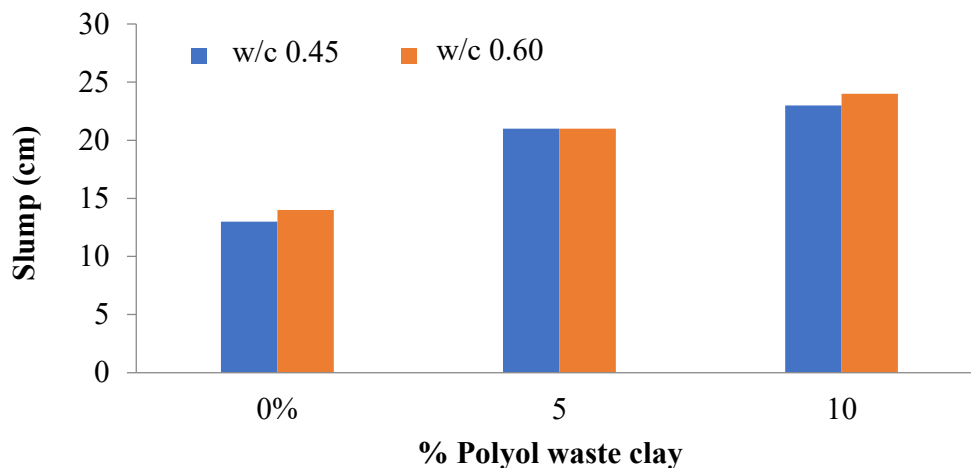


Figure 1. Results of the slump test in concrete fresh mix.

These results show the increased plasticizing property on the fresh mixture, apparently contributed by the polyol, which, since it is a branched polymer with an approximate molecular weight of 3500 g/mol and which constitutes 51.9% by weight of the polyol waste clay, softens and provides greater workability without the need to add water. This is especially beneficial in mixtures with a low w/c ratio, which by nature have poor fluidity and are difficult to work with, providing greater workability without the need to modify the w/c ratio and maintaining the durable properties of concrete.

3.5 Compressive strength test

For w/c = 0.45 (Figure 2), a decrease in compressive strength is observed proportional to the increase in clay concentration. For 28 days of curing, only the blank specimen managed to reach the design resistance. On the other hand, for the 90 days of curing a slight increase in this typical property of mature concrete was observed; even though the polyol clay concretes increased their compressive strength a little more (16% compared to 11% for the blank). However, none of the substituted mixes achieved design strength. The same behavior was obtained for w/c = 0.60 (Figure 3), where only the blank specimen managed to achieve the design compressive strength. It has been determined (Smaoui, et.al., 2005) that the increase in the alkali content in the mix can decrease the compressive strength of concrete. However, even when the K₂O content is very high in the ash (Table 3), the equivalent Na₂O is <0.6 for both mixtures; which would not affect the compressive strength of the prepared concrete.

On the other hand, the polyol waste clay powder has 9.63% MgO (Table 3), which could cause the expansion of concrete by reacting delayed with water (ACI 211.1, 1991); reaction that can even involve months with respect to the setting and hardening of the mixture. This reaction is exothermic, similar to the hydrolysis of CaO, for which it generates heat and a significant increase in volume, thus producing the expansion of the concrete and long-term fracture. However, given the low concentration of the ash used in the mixture, the MgO content is of the order of 0.14%, which would not affect this property either; in such a way that the polyol would be responsible for the decrease in the compressive strength of concrete.

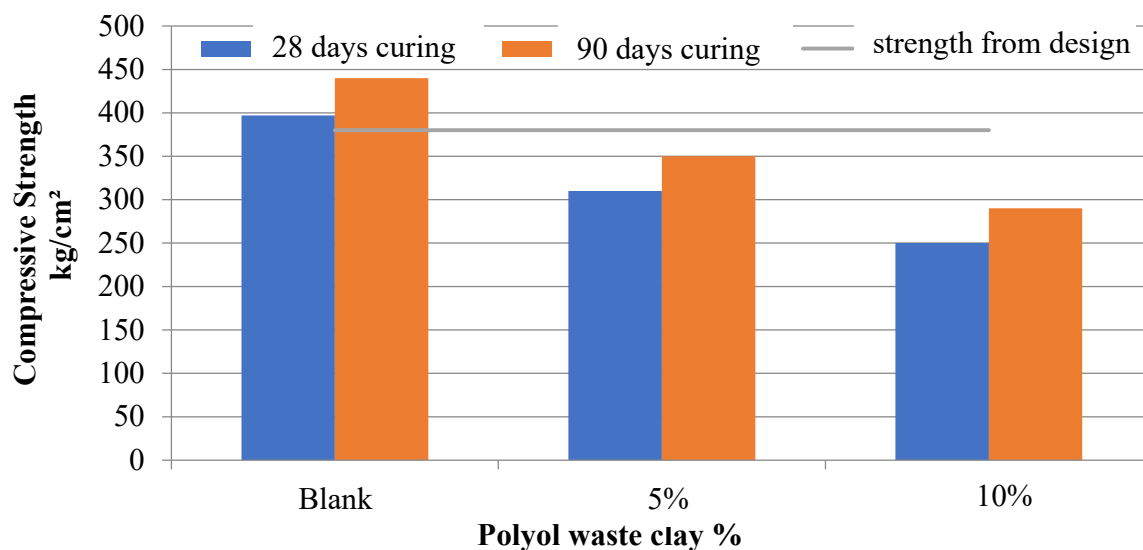


Figure 2. Compressive strength for w/c ratio of 0.45.

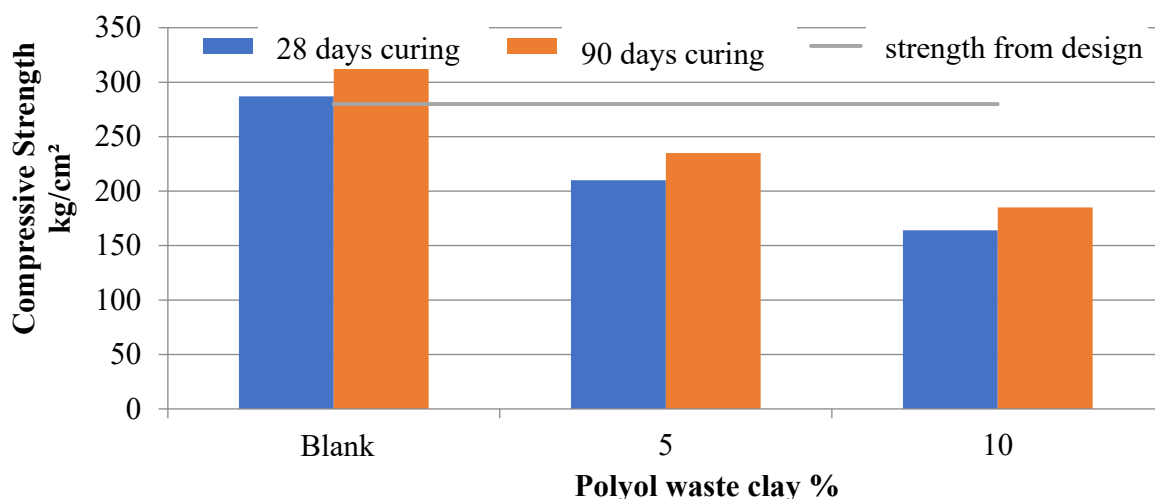


Figure 3. Compressive strength for R a / c 0.60.

3.6 Capillary sorption

Table 6 shows the results obtained for the main kinetics properties, with the addition of polyol clay the water gain in the concrete (k) decreased; observing an increase in resistance to water penetration m (s/m^2). This behavior was evidenced for both w/c ratios (0.45 and 0.60).

In Figure 4 it is observed that the blanks in both w/c ratios are very similar, however, the slopes change drastically for w/c of 0.45 when substituting clay; a marked difference is also noticeably between the mixtures with partial replacement of the polyol waste clay (with w/c 0.45 and 0.60) with regard to the water gain (k); where this value is represented by the slope of the linear region of the curve. With these results it is evident that the use of polyol clay offers greater resistance to water penetration. This property confers a greater resistance to the penetration of aggressive ions such as chloride ion (Cl^-). However, the effective porosity (ξ), slightly increased with the clay content, independent of the w/c ratio; Therefore, it seems that the polyol exerts a hydrophobic effect on the mixture.

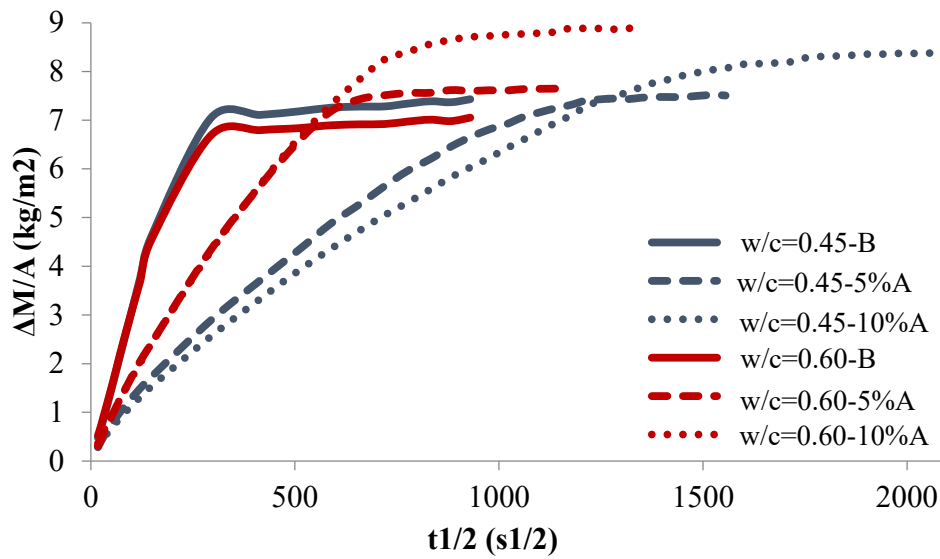


Figure 4. Capillary absorption profile

Table 6. Main kinetic properties for capillary sorption.

w/c (Ratio)	0.45			0.60		
Polyol Clay substitution	Blank	5%	10%	Blank	5%	10%
k (kg/m ² s ^{1/2})	0.0319	0.0117	0.0104	0.0309	0.0169	0.0159
$t^{1/2}$, s ^{1/2}	225	613	767	220	440	541
t , s	50515	375986	588773	48323	194054	293858
m , s/m ²	2.02E+07	1.50E+08	2.36E+08	1.93E+07	7.76E+07	1.18E+08
S , m/s ^{1/2}	2.23E-04	8.16E-05	6.52E-05	2.28E-04	1.14E-04	9.26E-05
ξ , %	14.3	14.3	15.9	13.6	14.9	17.3

3.7 Natural carbonation test results

Figure 5 shows the effect of clay on the natural carbonation rate. It can be seen that the increase in the polyol clay concentration is accompanied by an increase in the carbonation front for the two w/c ratios; which matches the results of effective porosity.

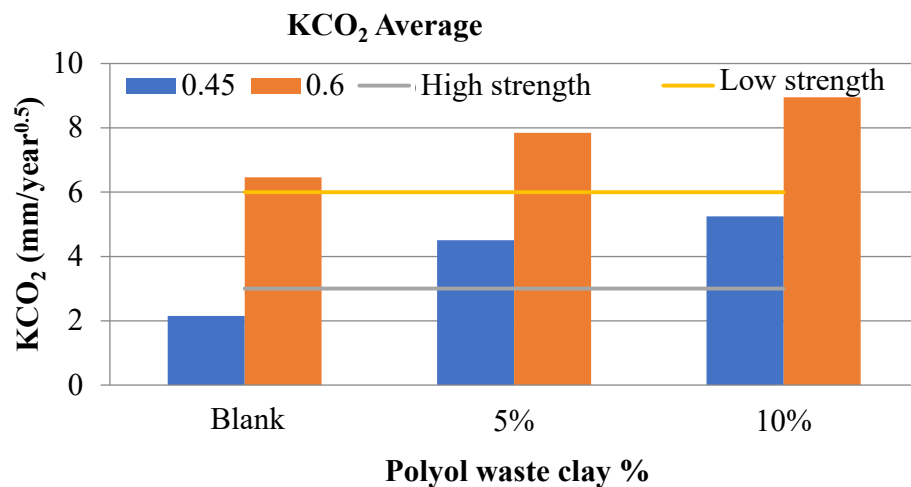


Figure 5. Natural carbonation rate.

The results in the carbonation chamber (accelerated) were similar to those obtained under natural conditions.

3.8 Potentials and corrosion rates over time for specimens exposed to an accelerated marine environment (ISO 11474).

Figure 6 shows the average corrosion potentials and rates as a function of time, after 350 days of exposure to this accelerated test. Note the beneficial effect of polyol clay on the corrosion rate, where the bars for both w/c ratios were active for the blanks in the time where the specimens with partial substitution of cement for polyol clay were passive. Moreover, when the bars in the specimen with w/c 0.45 were activated, those located in the specimen with w/c 0.60 and polyol waste clay had not yet been activated. This effect was expected, given the greater resistance to water penetration in the clay specimens.

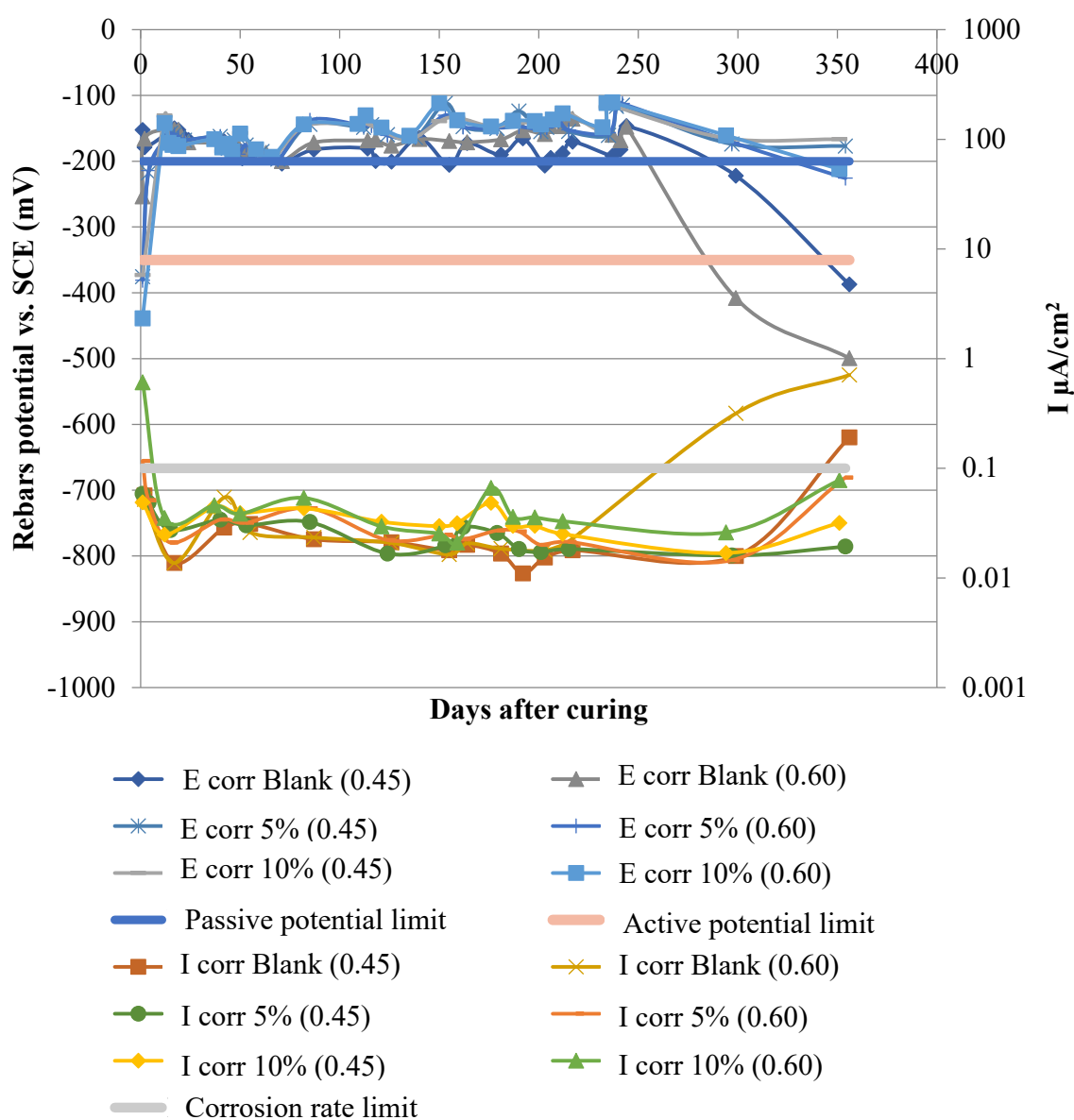


Figure 6. Variation of the corrosion rates and potentials as a function of time, of the steel in the specimens exposed to the ISO 11474 accelerated test.

3.9 Effect of polyol clay on the Durability of reinforced concrete.

Table 7 collects all the results of the different properties for evaluating the durability of steel in concrete for comparison and analysis; where the green boxes indicate that the limit value recommended by the DURAR manual for each property has not been reached. On the other hand, the red boxes indicate that the property has negatively exceeded the limit established as acceptable and finally a third yellow color code was introduced that indicates an intermediate or regular state of the aforementioned property with respect to the established limit.

At first glance, it is observed that only the blank with w/c 0.45 mostly possesses its properties within acceptable limits, with the exception of capillary sorption which is 2.8 times higher than recommended, which makes it susceptible to the penetration of aggressive ions such as Chloride. However, for the purposes of this investigation this concrete is considered to be of acceptable durability.

For the case of concrete with 5% polyol clay, it was found that it has adequate porosity and its capillary sorption improves compared to that of the blank specimen, which makes it less susceptible to the penetration of chloride ions; where the corrosion rates, which indicate the passive condition of the steel, in these specimens support this assumption. It was determined that the compressive strength is 58 kg/cm² below the design, however, it is possible to improve this property due to the high extra workability provided by the polyol clay, with a 60% increment compared to that obtained with the blank. That is, it is possible to reduce the amount of mixing water, counting on the workability provided by the polyol clay, with said decrease a substantial increase in compressive strength would be expected due to the decrease in the inherent w/c ratio.

For the mixtures with 10% polyol clay, the electrochemical results show that the bars took longer to activate, a behavior expected in concretes with low capillary sorption such as that exhibited. However, the compressive strength decreases to values as low as 251 kgf/cm², 130 kgf/cm² below design. However, again a high workability is noted, 78% higher than that exhibited by the blank. This, as mentioned before, allows a decrease in the mixing water, as a consequence an increase in the compressive strength could be obtained.

For w/c of 0.60 a similar behavior was observed, observing the positive effect of polyol clay substitution on capillary sorption (CS); decreasing it as the % polyol clay in the mix is increased. This effect was manifested when exposing the specimens to an accelerated marine environment (ISO 11474); where these were the last specimens where the rebar was activated.

Table 7. Summary of the effect of polyol clay on the Durability of the concretes studied during the 356 days of experimentation

w/c Ratio	Property	Porosity (%)	Capillary Sorption (m/s ^{1/2})	CS (kg/cm ²)	KCO ₂ (mm/a ^{1/2})	% extra-Workability
0.45	limit	10ϵ<15	S<0.0000833	CS>=380	KCO ₂ <3	-
	Blank	14.3	0.000223	407.6	2.151	0
	5%	14.3	0.000082	322	4.506	60
	10%	15.9	0.000065	251.1	5.249	78
0.60	limit	10ϵ<15	S<0.0000833	CS>=260	KCO ₂ <3	-
	Blank	13.6	0.000228	297	6.463	0
	5%	14.9	0.000114	209	7.847	50
	10%	17.3	0.000093	166	8.949	71

4. CONCLUSIONS

- The polyol clay demonstrated high fluidizing power in concrete; increasing its workability in a high proportion.
- Compressive strength tests of concrete after 28 days of curing reveal that the use of polyol clay exerts an adverse effect on this property
- The polyol waste clay has a positive effect on the kinetic properties of the capillary sorption of concrete, improving its resistance to water penetration by more than double, independent of the w/c ratio.
- The resistance to carbonation is negatively affected with the use of clay, independent of the w/c ratio.
- In a marine environment, the electrochemical results (corrosion potential and rate) show a beneficial effect on the steel bars embedded in concrete added with 5 and 10% of the polyol clay, regardless of the w/c ratio and its concentration.
- The steel bars in the specimens with w/c 0.45 partially substituted with 5% and 10% polyol clay, remained passive throughout the evaluation period.
- The steel bars in the specimens with w/c 0.60 partially substituted with 5% and 10% polyol clay, were activated after the blanks.
- The high workability produced by the replacement of the polyol clay allows the reduction of the mixing water to adjust the compressive strength to values more appropriated to the mechanical requirements demanded by the specific structure.
- The polyol in the waste clay is the ingredient that positively affects some properties of concrete, allowing for greater concrete fluidity and resistance to corrosion in marine environments.

5. ACKNOWLEDGMENT

Our most sincere thanks to the company OXITENO ANDINA CA, for the technical support and financial contributions to the development of this research and to the company CEMENTOS CATATUMBO CA, for the technical support provided.

6. REFERENCES

- American Concrete Institute, always advancing (2002), *ACI 211.1-91: Standard Practice for Selecting Proportions for Normal, Heavyweight, and Mass Concrete (Reapproved 2009)*.
- ASTM International (2018), *C311/C311M-18 Standard test methods for sampling and testing fly ash or natural pozzolans for use in Portland-cement concrete*. Retrieved from https://doi.org/10.1520/C0311_C0311M-18.
- ASTM International (1989), *ASTM C 618-89. Standard specification for fly ash and raw or calcined natural pozzolan for use as a mineral admixture in Portland cement concrete*. Section 4, Volume 4.01, 1989, Pp. 296-298. Retrieved from <https://doi.org/10.1520/C0618-19>
- ASTM International (2012), *C39/C39M-12a Standard Test Method for Compressive Strength of Cylindrical Concrete Specimens*. Retrieved from https://doi.org/10.1520/C0039_C0039M-12A
- ASTM International (1999), *D512-89(1999) Standard test methods for chloride ion in water*. Retrieved from <https://doi.org/10.1520/D0512-89R99>
- ASTM International (2007), *E70-07 Standard test method for pH of aqueous solutions with the glass electrode*. Retrieved from <https://doi.org/10.1520/E0070-07>
- Calleja, J. (1983). *Adiciones y cementos con adiciones. Materiales de construcción*. (CSIC), Vol

33, Issue 190-191. Madrid: 25-52.

Devi, S., Gandhi, N., Jat, M., Marmat, N., Manda, B., Vaishnav, M. (2016). *Utilization of marble and granite waste as partial replacement of cement in concrete*. SSRG International Journal of Civil Engineering (SSRG-IJCE). 3 (5): 193-197. ISSN: 2348-8352.

Fagerlund, G. (1982). "On the Capillarity of Concrete". Nordic Concrete Research, No. 1, Oslo, Ppe No. 6.

Ghosal, S. (2015). *Use of rice husk ash as partial replacement with cement in concrete*. International Journal of Engineering Research. 4 (9): 506-509.

Gowsika, D., Sarankokila, S., Sargunan, K. (2014). *Experimental investigation of egg shell powder as partial replacement with cement in concrete*. International Journal of Engineering Trends and Technology (IJETT). Vol. 14 (2): 65-68. <http://dx.doi.org/10.14445/22315381/IJETT-V14P214>

ISO (1998). *ISO 11474 Corrosion of Metals and Alloys - Corrosion Tests in Artificial Atmosphere - Accelerated Outdoor Test by Intermittent Spraying of a Salt Solution (Scab Test)*.

Manogna, P., Srilakshmi, M. (2015). *Tile powder as partial replacement of cement in concrete*. International Research Journal of Engineering and Technology (IRJET). 2(4): 75-77.

Mendoza, K., Millano, V., Troconis, O., Romero, N. (2013). *Evaluación de un biopolímero en la calidad del concreto: evaluaciones preliminares*. Gaceta Tecnica UCLA. 10.:37-41.

Montiel, M. (2012). "Evaluación de la durabilidad del concreto Armado en ambientes marinos, utilizando escoria de níquel como sustituto parcial de cemento". Thesis. Universidad del Zulia. Maracaibo. Venezuela.

Normativa ambiental Venezolana reguladora de los desechos de la actividad industrial. (1995). *Decreto 883*. Gaceta Oficial 5.021 Extraordinario 18/12/1995.

Oxiteno Andina. (2000). *Operations manual*. Induction program for the production area, Venezuela.

Smaoui, N., Bérubé, M. A., Fournier, B., Bissonnette, B., Durand, B. (2005). *Effects of alkali addition on the mechanical properties and durability of concrete*", Cement and Concrete Research. 35.:203– 212. <https://doi.org/10.1016/j.cemconres.2004.05.007>

Troconis de Rincón, O. et al. (2011). *Manual de inspección evaluación y diagnóstico de corrosión en estructuras de concreto armado*. Red iberoamericana XV.B (DURAR) 5 Ed. Editorial. Vice Rectorado Académico.

Corrosion sensor for monitoring reinforced concrete structures: Tests on reinforced concrete specimens

A. Calvo Valdés¹ , M. H. F. Medeiros*¹ , G. Macioski¹ 

*Contact author: medeiros.ufpr@gmail.com

DOI: <https://doi.org/10.21041/ra.v11i3.529>

Reception: 19/01/2021 | Acceptance: 03/08/2021 | Publication: 01/09/2021

ABSTRACT

The aim of the research was to evaluate the effectiveness of a galvanic multi-electrode sensor to detect the probability of corrosion in reinforced concrete prisms subjected to drying and wetting cycles in a NaCl solution. The corrosion potential (E_{corr}) readings obtained using a copper sulfate copper electrode (Cu/CuSO₄) were analyzed along with the galvanic current (I_{gal}) and galvanic potential (E_{par}) readings. The sensor developed showed sensitivity to detect the chloride front and to predict the possibility of corrosion of the reinforcement. The parameters E_{corr} , E_{par} and I_{gal} presented distinct behaviors in terms of its use as parameters for corrosion monitoring.

Keywords: corrosion; potential; galvanic sensor; galvanic current.

Cite as: Calvo Valdés, A., Medeiros, M. H. F., Macioski, G. (2021), "Corrosion sensor for monitoring reinforced concrete structures: Tests on reinforced concrete specimens", Revista ALCONPAT, 11 (3), pp. 64 – 87, DOI: <https://doi.org/10.21041/ra.v11i3.529>

¹ Universidade Federal do Paraná, Rua XV de Novembro, 1299 - Centro, Curitiba - PR, 80060-000, Brasil.

Contribution of each author

In this work, the authors Analiet Calvo Valdés and Marcelo H. F. Medeiros contributed to the activities of bibliographic consultation, writing of the text and development of the experimental program, a total number of 33.3% each. Or author Gustavo Macioski with bibliographic review and consultation activity, completing the remaining 33.3%.

Creative Commons License

Copyright 2021 by the authors. This work is an Open-Access article published under the terms and conditions of an International Creative Commons Attribution 4.0 International License ([CC BY 4.0](https://creativecommons.org/licenses/by/4.0/)).

Discussions and subsequent corrections to the publication

Any dispute, including the replies of the authors, will be published in the second issue of 2022 provided that the information is received before the closing of the first issue of 2022.

Sensor de corrosão para monitoramento de estruturas de concreto armado: Testes em corpos de prova de concreto armado

RESUMO

O objetivo do trabalho foi avaliar a eficácia de um sensor galvânico de múltiplos eletrodos na detecção da probabilidade de corrosão em prismas armados de concreto submetidos a ciclos de secagem e molhagem em uma solução de NaCl. Se analisaram as leituras de potencial de corrosão (E_{corr}) obtidas por meio de um eletrodo de referência de cobre sulfato de cobre (Cu/CuSO₄) com as leituras de corrente galvânica (I_{gal}) e potencial galvânico (E_{par}). O sensor desenvolvido apresentou sensibilidade para detectar a frente de cloretos e prever a possibilidade de corrosão das armaduras. As grandezas E_{corr} , E_{par} e I_{gal} apresentaram comportamentos distintos como parâmetro de monitoramento da corrosão.

Palavras-chave: corrosão; potencial; sensor galvânico; corrente galvânica.

Sensor de corrosión para monitorear estructuras de hormigón armado: Ensayos en especímenes de hormigón armado

RESUMEN

El objetivo del trabajo fue evaluar la efectividad de un sensor galvánico multi-electrodo en la detección de la probabilidad de corrosión en prismas de hormigón armado sometidos a ciclos húmedos y secos en una solución de NaCl. Se analizaron lecturas de potencial de corrosión (E_{corr}), obtenidas utilizando un electrodo de cobre de sulfato de cobre (Cu/CuSO₄), lecturas de corriente galvánica (I_{gal}) y potencial galvánico (E_{par}). El sensor desarrollado mostró sensibilidad para detectar el frente de cloruro y predecir la posibilidad de corrosión de la armadura. Las variables E_{corr} , E_{par} e I_{gal} presentaron comportamientos diferentes como parámetros para monitorear la corrosión.

Palabras clave: corrosión; potencial; sensor galvánico; corriente galvánica.

Legal Information

Revista ALCONPAT is a quarterly publication by the Asociación Latinoamericana de Control de Calidad, Patología y Recuperación de la Construcción, Internacional, A.C., Km. 6 antigua carretera a Progreso, Mérida, Yucatán, 97310, Tel.5219997385893, alconpat.int@gmail.com, Website: www.alconpat.org

Reservation of rights for exclusive use No.04-2013-011717330300-203, and ISSN 2007-6835, both granted by the Instituto Nacional de Derecho de Autor. Responsible editor: Pedro Castro Borges, Ph.D. Responsible for the last update of this issue, Informatics Unit ALCONPAT, Elizabeth Sabido Maldonado.

The views of the authors do not necessarily reflect the position of the editor.

The total or partial reproduction of the contents and images of the publication is carried out in accordance with the COPE code and the CC BY 4.0 license of the Revista ALCONPAT.

1. INTRODUCTION

The degradation of concrete structures due to corrosion affects civil construction throughout the world, with repercussions depending on the volume of registered cases, the precocity with which they occur, and the amount of resources involved in their evaluation and repair (Meira, 2017).

The annual cost of corrosion worldwide exceeds 3% of the world's Gross Domestic Product (GDP), approximately USD 2.2 trillion (Hays, 2020). Depending on when the intervention is carried out, the costs can be compounded (Meira, 2017), and may even exceed the original cost of construction (Dong et al., 2011).

Corrosion reduces the yield strength of steel, weakens the bonding properties between reinforcement and concrete, and affects the seismic performance and static load capacity of reinforced concrete structures. Iron oxidation (with Fe_2O_3 as the main component) is produced by the corrosion of steel bars, which causes the expansion of volume and tensile stress in the concrete, and subsequently causes the concrete to deform and crack (Zhao et al., 2017).

Corrosion of the steel bar inside the concrete essentially occurs for two reasons: first, due to the reduction in the alkalinity of the concrete caused by carbonation, and second, due to the presence of chlorides, which even with high pH, depassivate the reinforcement causing an intense and localized attack (France, 2011).

Investigation of affected structures usually involves an assessment of their durability (Wu et al., 2017). Durability is the result of the interaction of concrete structures with the environment, and is influenced by conditions of use, operation and maintenance processes. To assess the performance of constructions, visual inspections associated with field and laboratory tests are used (Mota, 2011). Systematic visual inspections certainly reduce the level of uncertainty regarding the state of the structure, but this technique has important limitations, as it is based on superficial observations of the structure over short periods of time (Inaudi, 2009), which can result in dangerous errors and inefficient use of resources for the maintenance of the structures.

Through sensors, it is possible to obtain data on a regular basis, ensure simultaneous readings at different points and, consequently, make different measurements compatible (Santos, 2014). Sensors are able to provide real-time information (Zhao et al., 2017) that feeds mathematical models to predict life cycle (Araújo et al., 2013) in order to estimate two fundamental stages of the corrosion phenomenon: the initiation phase and the corrosion propagation phase, according to the phenomenological model proposed by Tuutti (1982) (Figueiredo and Meira, 2013).

In this way, it is possible to carry out forecasts of the monitored structures and reduce the costs associated with restoration or replacement work. In Brazil, for example, according to a study by the Institute for Applied Economic Research (IPEA), by the year 2025 just over 89 million Brazilian reais must be earmarked for the maintenance of 15 bridges in 12 states of the Federation. Part of this money will be invested in monitoring systems, since the use of sensors can provide greater durability and sustainability of public infrastructure works (M. Torres-Luque et al., 2014). In the US, according to the Federal Highway Administration (FHWA), in accordance with a report by the American Society of Civil Engineers (ASCE) for the year 2013, 20.5 billion dollars a year must be invested by 2028 in the maintenance of public infrastructure works. In Europe, the estimated annual cost of maintenance on reinforced concrete bridges is around 1 billion euros (Zoghi, 2013).

Therefore, industrialized electrochemical sensors have attracted attention (Zhao et al., 2017), including: embedded electrodes, macro corrosion current probes, linear polarization sensors, electrical resistance sensors, corrosion potential sensors and galvanic sensors (Dong et al., 2011; Chen et al., 2017).

In the context of chloride corrosion induction, a galvanic sensor is probably the best option for monitoring (Klassen and Roberge, 2008). Its installation in the structure provides measurements of

galvanic current intensity and corrosion potential that allow monitoring the depth of the chloride penetration front (McCarter and Vennessland, 2004; Andrade et al., 2008; Araújo et al., 2013). These sensors are formed by two metals with different electrical potentials (anode and cathode) (Andrade et al., 2008), spatially separated (Angst and Buchler, 2015).

The galvanic macrocell created by the metals will result in a current flow (I_{gal}) between the metal acting as the anode and the metal acting as the cathode in the pair. This flow can be measured without the application of an external current, which is the main advantage of this type of sensor, as this guarantees the simplicity of the sensor and measurement systems, reducing associated costs. The current flow within the macrocell can be measured using a zero resistance ammeter. According to Ohm's law, this current flow between the mentioned regions is limited by the electrolyte resistance, the anodic polarization resistance (AR) and the cathodic polarization resistance (CR) (Andrade et al., 2008; Baltazar et al., 2007). Therefore, the current induced by the coupling of the anode and cathode is proportional to the dissolution of iron in the macrocell anode (McCarter and Vennessland, 2004).

I_{gal} should not be confused with the corrosion current density (I_{corr}), which can be obtained through the Stern-Geary equation from the value of the polarization resistance (R_p) (Martínez and Andrade, 2009) or by the electrochemical impedance spectroscopy (EIS) technique, which is still a technique widely used in the laboratory (McCarter and Vennessland, 2004) due to the overlapping of arcs from simultaneous phenomena and measurement noise associated with the heterogeneity of concrete structures in service (Ribeiro et al., 2015).

Direct estimation of the actual values of R_p from the relationship between the potential variation and the induced change in current ($\Delta E/\Delta I$) is generally not feasible in large concrete structures. This is because the applied electrical signal tends to disappear as the distance increases between the counter-electrode (CE), needed to register the parameter, and the working electrode (WE). To get around this problem, it is possible to use confinement rings in a certain area of the WE surface (Feliú et al., 1990). However, it is unfeasible to make a sensor to be embedded in concrete that, in addition to allowing the reading of the R_p , confines a specific area of the reinforcement (Martínez and Andrade, 2009).

A sensor to be embedded in concrete in order to measure R_p and I_{corr} must include in its composition a reference electrode (REF), a counter electrode (CE), and a working electrode (WE) is also required to avoid the effect of distance critical (L_{crit}) between the CE and the main reinforcement in the case that it is in a passive state. In addition to the electrochemical corrosion parameters, a thermocouple should be considered to measure temperature, as well as resistivity meters to consider the effect of varying temperature and moisture content in concrete. Therefore, the costs associated with materials and systems would increase.

The galvanic sensor is one of the most commercialized corrosion sensors on the international market. Even so, a sensor can cost around US\$400, which makes it more expensive and difficult to use in public works, in addition to the limited number of suppliers (Araújo et al., 2013).

In this context, the aim of this work was to evaluate the functioning of a galvanic sensor with multiple electrodes, made with low-cost Brazilian materials. For this, the developed sensors were embedded in reinforced concrete prisms that were exposed to an aqueous solution with the addition of NaCl (3.5% by mass) in alternating cycles of partial immersion and drying. An attempt was made to simulate the service conditions of a tidal variation zone within a marine atmosphere. The work also aims to evaluate how the sensor arrangement, the concrete strength class and the effect of wetting and drying cycles can affect the readings performed.

The manufactured galvanic sensor is based on the CorroWatch Multisensor, but instead of using activated titanium as a cathode, which is ten times more expensive than conventional steel (ISE, 2020), copper was chosen. Thus, the work deals with an investigation related to the solution of problems related to quality control, damaged concrete and construction recovery, an approach that

is a recurrent theme in the Alconpat journal (Real et al., 2015; Hernández et al., 2016; Macioski et al., 2016; Pérez et al., 2018).

2. MATERIALS AND METHODS

2.1 Concrete specimens

The experimental program consisted of the analysis of the behavior of galvanic sensors installed in prismatic reinforced concrete specimens, with dimensions: (150 x 150 x 100) mm and two CA-50 steel bars with a diameter of 6.3 mm (1/4") placed parallel to each other. Figure 1 illustrates the specimen configuration. For each concrete, 4 specimens were produced, totaling 8 samples.

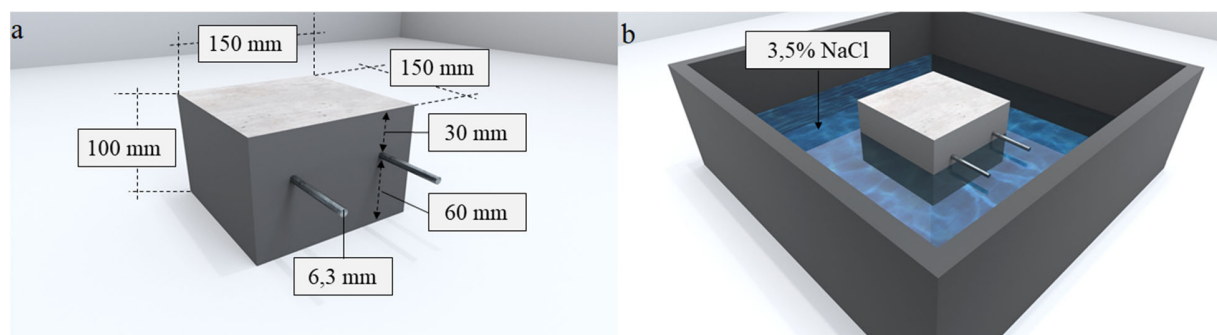


Figure 1. (a) Configuration of the reinforced prismatic concrete specimen. (b) Partially immersed specimen.

In the specimens, the cover of the main bars was defined using NBR 6118:2015 as reference, considering that the structures or some of their elements may be exposed to very strong environmental conditions (Class IV). For Class IV, the standard indicates a minimum cover (c_{min}) of 50 mm, assuming that the specimens are representative of a beam or column. In this context, the cover of the main reinforcement in relation to the surface of the specimen, exposed to the NaCl solution, was 60 mm. On the sides of the specimens and on the surface exposed to air, the bars have a 30 mm cover, as shown in Figure 1(a).

In this experiment, two concretes conventionally used in concrete plants in the region of Curitiba (Brazil) were used, as shown in Table 1. The compressive strength test in concrete ($\varnothing 10 \times 20$ cm cylinders) was carried out in accordance with NBR 5739 (2018). The average strength for this test was obtained from three samples for each series. The average compressive strength (f_{cm}) of concrete with (w/c) 0.75 was 20.62 MPa, and the f_{cm} of the concrete with (w/c) 0.45 was 39.36 MPa. The test was carried out with the specimens in saturated condition with a dry surface.

Table 1. Mixing ratios used for molding the specimens.

Concrete	Cement [kg/m ³]	Sand [kg/m ³]	Gravel [kg/m ³]	w/c [kg/kg]
15 MPa	242.11	970.86	997.50	0.75
30 MPa	410.04	758.58	1053.82	0.45

The 15 MPa mix simulates structural concrete from old buildings. It should be noted that structures built a few decades ago allowed characteristic strengths (f_{ck}) below 20 MPa. Furthermore, standards such as ACI 318-14 recommend a minimum f_{ck} of 17 MPa for reinforced concrete structures exposed to moisture and an external source of chlorides (Class C2). The Brazilian standard NBR 6118:1980 only established that the concrete should present a f_{ck} characteristic strength greater than 9 MPa, compatible with that adopted in the project, as well as meet the quality control criteria

provided for in ABNT NBR 12655. However, the standard NBR 6118:1980 did not include durability criteria for the execution of structural concrete according to the level of aggressiveness of the environment to which the concrete would be exposed.

The 30 MPa mix corresponds to Class III (marine or industrial atmosphere) according to NBR 12655:2006 and the updated version of NBR 6118:2014, similar to the concrete recommended by ACI 318-14 ($f_{ck} = 30$ MPa – $w/c = 0.40$) for the same exposure conditions. For the execution of the reinforced concrete specimens, the cement used was blended cement CP-II-F-32, which has up to 25% carbonaceous material (NBR 16697:2018). The fine aggregate was a fine sand, and gravel was used as the coarse aggregate. The physical characterization of the aggregates and the standards considered for this are presented in Table 2.

Table 2. Physical characterization of aggregates.

Aggregate	Maximum characteristic dimension	Fineness module	Powder content	Specific mass
Coarse (Gravel)	19.00 mm	1.83	0.39%	2.66 g/cm ³
Fine (Fine sand)	0.600 mm	2.40	9.06%	2.50 g/cm ³
Standard	ABNT NM 248:2003			ABNT NBR NM 52:2003 ABNT NBR NM 53:2003

The consistency of the concrete was measured using the slump test method, as recommended by the Brazilian standard NBR 7223: 1992. For both concretes, a fluidity in the range of 80 ± 10 mm was adopted in order to maintain a plastic consistency for molding all specimens, which did not require the use of chemical admixtures. After molding, the specimens were subjected to a curing process by immersion in water saturated with lime as indicated in the NBR 5738:2003 standard for a period of 91 days.

A cure period longer than that recommended by the standard NBR 5738:2003 (28 days) was chosen to simulate the concrete of a real structure that will have the need for field tests after a certain number of years of service. Therefore, no electrochemical readings were taken during the hardening of the concrete or during the concrete curing period. Since the objective is to simulate the interior of a real structure to evaluate the performance of the sensor, a period of stabilization of the concrete outside the curing chamber was not considered. Similar considerations were made in the work by Rocha (2012) and by Dotto (2006).

Finally, after the 91-day curing process, the specimens were placed in an oven to dry at 50°C for 5 days. Then, the lateral surfaces of the specimens were isolated from exposure to chlorides with an epoxy paint with the intention of making the contamination front only advance along the face with the 60 mm cover. To induce corrosion of the steel embedded in the concrete, an accelerated aging process that involves the absorption and diffusion of chloride ions in the cement matrix was used. Accelerated aging followed a partial immersion system alternated in cycles. The cycles consisted of drying in an oven at 50°C for 5 days and partial immersion of the specimens in water with 3.5% NaCl by mass for 2 days, as shown in Figure 1(b). This approach was adopted based on other works that used the same alternating immersion system (Freire, 2005; Dotto, 2006; Silva, 2010; Rocha, 2012; Silva, 2017).

In addition, the adopted system and the salt concentration try to reproduce service conditions similar to a tidal variation zone within a marine atmosphere. In this region, there is contact with water contaminated with chlorides, with wetting and drying cycles. This characterizes a critical exposure condition in terms of reinforcement corrosion. The main degradation mechanism present in these conditions is the corrosion of the reinforcement by the action of chloride ions (Lima and Morelli, 2004), which is the attack considered to evaluate the performance of the sensors in this research.

2.2 Sensor configuration

The galvanic macrocell considered in the study is formed by copper and carbon steel. Carbon steel bars 60 mm in length and 6.3 mm (1/4") in diameter (anode) were used at different heights and installed on a copper plate (cathode) 50 by 50 mm and 4 mm thick. All metals were polished with steel brush. Then, they were rinsed with distilled water, immersed in alcohol and air dried. The area of the copper plate that acts as the cathode (A_c) in the galvanic sensor designed in the work was configured so that it was equal to the sum of the surface area of the anodes (A_a) that make up the galvanic macrocell for an A_c/A_a ratio = 0.97. Figure 2 shows a drawing of the galvanic sensor used in the study.

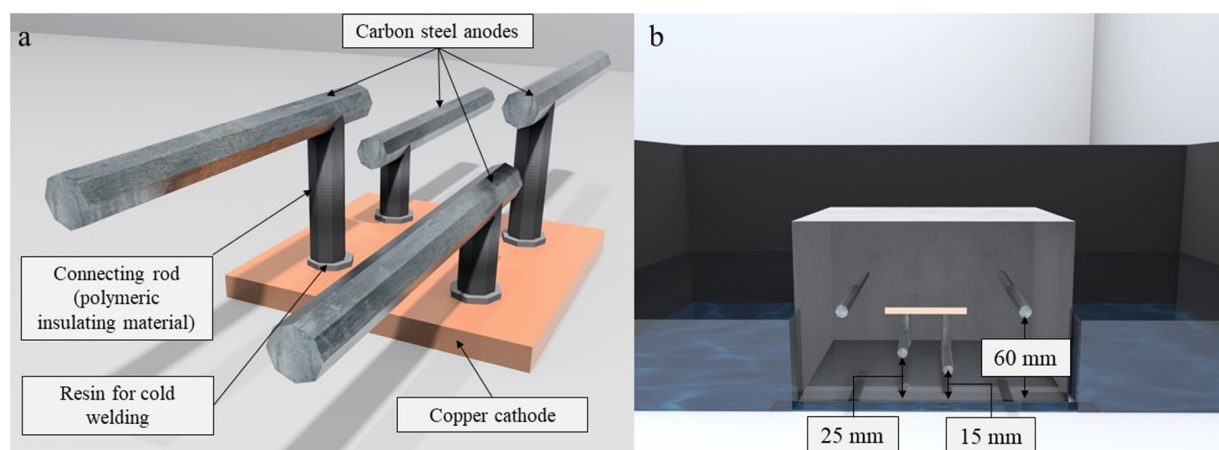


Figure 2. a) Galvanic sensor used in the study. b) Galvanic sensor installed inside the specimen. Source: Author.

Two of the sensor anodes were at a depth of 15 mm and the remaining two at a depth of 25 mm, with respect to the surface of the specimen exposed to the NaCl solution. These are the depths at which the sensor must produce the reinforcement depassivation information by the ingress of chlorides, as shown in Figure 2(b). Figure 3 shows the molding of the prismatic specimens and sensor installation.

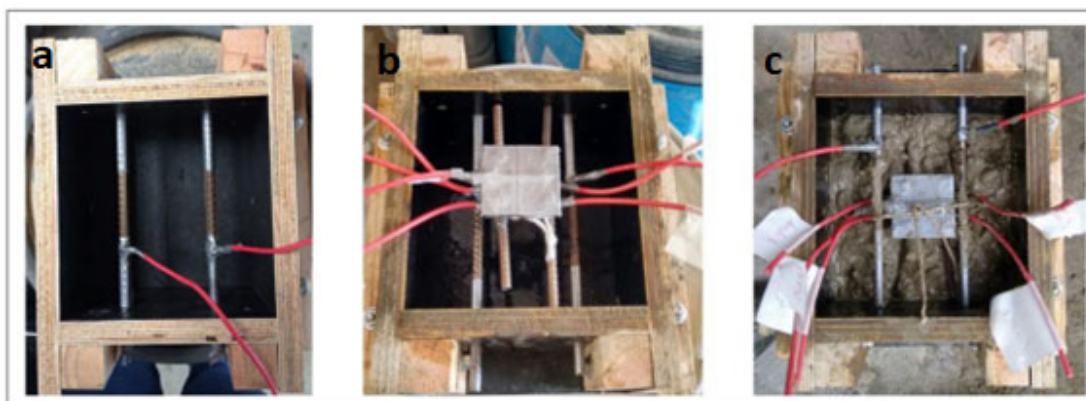


Figure 3. a) Installation of main bars. b) Molds coated with oil and with the sensor positioned. c) Molding with the sensor embedded. Source: Author.

To fit the carbon steel bars to the copper plate, 4 holes 8.0 mm in diameter (> 6.3 mm) were made, as shown in Figure 4. The carbon steel bars were fixed to the copper plate with resin for cold welding in order to avoid an unwanted galvanic couple that could compromise the proper functioning of the sensor, in addition to exposing the device to premature degradation. For the external electrical circuit that connects the electrodes and allows the flow of electrons, a copper cable insulated with a PVC film and a 2.5 mm^2 cross section was used, which was welded to the metals involved. The welding points were protected with insulating polymeric material.

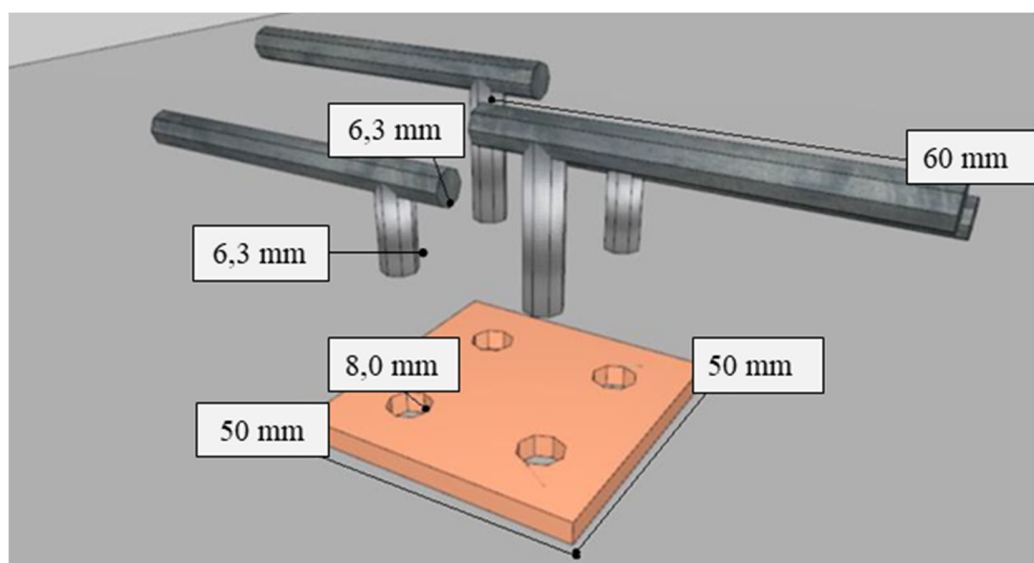


Figure 4. Sensor assembly diagram.

The choice of metals (electrodes) for the construction of the galvanic sensor was a function of the predetermined irreversible equilibrium potential (E_{eq}). Irreversible equilibrium potentials are electrode potentials that have changed under the influence of polarization or external factors. They are experimentally determined and are commonly called corrosion potentials (Gentil, 1996). To determine them, a reference electrode is used, such as a standard hydrogen electrode. E_{eq} indicates the tendency of the electrode to undergo reduction or oxidation in a given medium. The greater the corrosion potential of the electrode in a table of potentials, the greater the tendency of the electrode to undergo oxidation, that is, to behave like an anode (Gentil, 1996; Pawlick et al., 1998; Souza, 2014).

The irreversible equilibrium potential of iron immersed in an electrolyte simulating sea water with reference to a hydrogen electrode is in the range of (-0.34 to 0.50) V. However, the corrosion potential of copper is in the range of (-0.02 to 0.05) V (Akimov, 1957). In the study, the corresponding experimental procedure was not carried out to determine the irreversible potential value of the cathode and anode separately.

Finally, in order to make the sensor more practical, protect the copper cables and consequently improve the recording of electrochemical readings, electrical pin connectors were placed at all ends, as shown in Figure 5(b).

2.3 Characterization tests and electrochemical techniques

At each exposure cycle, electrochemical readings were conducted on the second day of partial immersion in water with 3.5% NaCl. In order to determine the potential of the sensor pairs throughout the aging process, the LabVIEW 8.5 data logger was used, which recorded the polarization potential difference (E_{pair}), as shown in Figure 5.

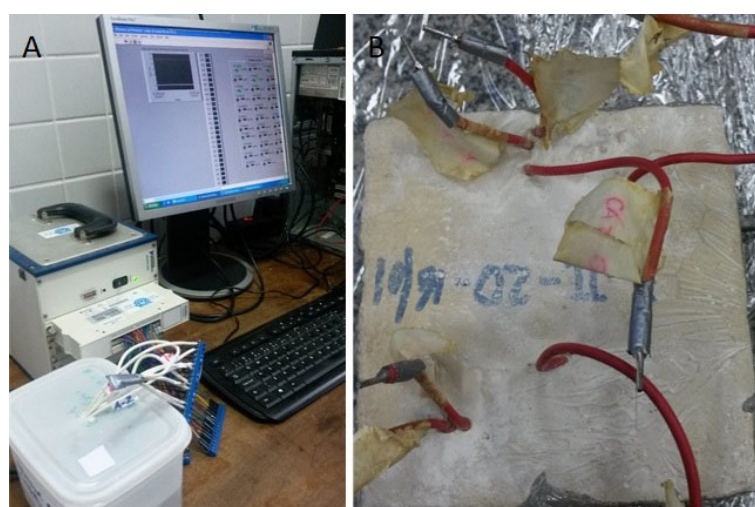


Figure 5. a) LabVIEW 8.5 data logger reading E_{pair} . b) Specimen with electrical pin connectors. Source: Calvo, (2018).

Theoretically, the potential of a galvanic couple (E_{pair}) is the result of the combination of the potentials of the metals involved. It is a spontaneous process caused by the different nature of the electrodes that leads to the polarization of both metals to a combined potential (E_{pair}) (Gentil, 1996; Pawlick et al., 1998). That is, it is obtained from the difference between the positive potential corresponding to the cathode ($E_{cathode}$) and the negative potential (E_{anode}) corresponding to the anode, as shown in Equation (1) (Pawlick et al., 1998) in the environment in which they are inserted.

$$E_{pair} = E_{cell} = E_{cathode} - E_{anode} \quad (1)$$

In practice, $E_{cathode}$ is the polarization potential of the cathode and E_{anode} is the polarization potential of the anode. The polarization potential is the result of the displacement (η) of the metal's irreversible equilibrium potential (E_{eq}) by the formation of the galvanic couple. Thus, Equation 1 can be written in the form of Equation (2).

$$E_{pair} = (E_{eq} + \eta)_{cathode} - (E_{eq} + \eta)_{anode} \quad (2)$$

As no external current is applied to the galvanic macrocell, the polarization potential of the electrodes (anode and cathode) is always in the range of the natural potential of the metals inside the concrete (Mccarter and Vennesland, 2004). Therefore, the E_{pair} value will fluctuate as a function of environmental conditions (Pawlick et al., 1998). Thus, the E_{pair} value must be obtained empirically (Sousa, 2014), and its value includes the values of E_{pair} and η , dispensing with the determination of these factors separately.

Thus, the data logger generated an individual reading corresponding to each of the anode-cathode pairs of the projected sensor. Each pair is recognized by the logger as an individual reading channel. It was analyzed whether the potential difference reading remains stable over time, as well as the type of reaction it indicated: galvanic ($E_{\text{pair}} > 0$) or electrolytic ($E_{\text{pair}} < 0$).

To record the galvanic current (I_{gal}), the electrochemical technique was used, using a Zero Resistance Ammeter – ZRA coupled to an SP-200 potentiostat and logging via EC-Lab software. This technique consists of measuring the galvanic current in a pair formed by different metals, one with an anodic behavior and the other with a cathodic behavior.

The technique is also used to perform some types of electrochemical noise measurements and consists of stabilizing the voltage between the working electrode and the counter electrode, and measuring the current and potential versus the reference electrode (EC-LAB., 2011). In this case, the working electrodes are the carbon steel bars of the galvanic sensor. As a counter-electrode, a stainless steel mesh was used and the reference electrode was the copper plate of the sensor.

In order to help validate the behavior of the sensor, the galvanic current and potential readings of the pair were correlated with the open circuit potential (E_{corr}) readings. Due to its simplicity, measuring the corrosion potential, E_{corr} , is the most used method in field determinations (Martínez and Andrade, 2009). From these measurements, potential maps are drawn revealing the zones that are most likely to corrode in the active state (ASTM C876-15).

A reading was taken at each anode, totaling 6 readings per specimen: four on the sensor anodes and two on the reinforcement bars. In the potential difference readings, a Cu/CuSO₄ reference electrode was used. To analyze the results in order to estimate the probability of corrosion in a given structure, the limits found in ASTM C876-15 were considered.

However, there is still no regulation that establishes a fixed range of I_{gal} and E_{pair} values to characterize the active state of steel in concrete. Therefore, it is not the absolute value of the current that should be considered, but the variation of its values over time (Raupach and Schiessl, 2001; Araújo et al., 2013).

Finally, a qualitative test was performed using the colorimetric method by spraying silver nitrate (AgNO₃) to determine the depth of the penetration front of chlorides entering the concrete by absorption and diffusion, although it does not quantify the free chloride content (Real et al. al., 2015; France, 2011, Pontes et al., 2020). The test consists of spraying an aqueous solution of 0.1 M AgNO₃ onto freshly fractured concrete slices. When the silver nitrate solution is sprayed onto the concrete surface, a photochemical reaction takes place. A white precipitate of silver chloride forms where free chlorides are present. In the region without chlorides or with combined chlorides, there is formation of a brown precipitate, silver oxide (Medeiros, 2008; Marcondes, 2012).

To carry out the test, the specimens were broken in the direction of the flow of chlorides just before the test to prevent carbonation from occurring. In parallel, a test with phenolphthalein spray (1% in ethyl alcohol) was also performed on one of the specimens' slices to avoid false positives. In the presence of carbonates there is also the formation of a white precipitate (Jucá, 2002).

After spraying the aqueous solution of silver nitrate, ten measurements of the depth of penetration of chlorides were performed, every 10 mm, following the recommendations of NT BUILD 492 (2000). In this way, gross errors were avoided in reading the depth reached by chlorides. Before spraying the silver nitrate and phenolphthalein, each slice was brushed to remove surface dust.

3. RESULTS AND DISCUSSION

3.1 Corrosion Potential

Figure 6 shows the results of Open Circuit Potential (E_{corr}) in specimens with 15 MPa concrete. Figure 7 shows the data corresponding to specimens with 30 MPa concrete. Both figures show the average of the readings obtained from the anodes of the galvanic sensor installed inside the specimens, with a cover thickness of 1.5 cm and 2.5 cm, respectively. Also represented in these figures are the averages corresponding to the main bars with a cover thickness of 6 cm.

At the end of the first wetting cycle, negative E_{corr} values (< -350 mV) were observed in the anodes installed at 1.5 cm and 2.5 cm, in both concretes. Several studies found more negative values (indicating active corrosion) at the start of corrosion tests (Gurdián et al., 2014; Rocha et al., 2014; Capraro et al., 2016; Jiang et al., 2017; Medeiros et al., 2014; , 2017; Godinho et al., 2018; Godinho et al., 2019; and Capraro et al., 2021). This behavior is related to the process of formation of the passivating film on the reinforcement, which involves the oxidation of the metal surface and, for this reason, generates electronegative readings at the beginning of the test (Poursaee, 2016; Meira, 2017; Ribeiro et al., 2018).

Thus, E_{corr} gradually changes, transitioning from more negative values to more positive values, until it stabilizes and indicates the formation of the passivating film (Sun et al., 2017) in the absence of aggressive agents inside the concrete. Capraro et al. (2021), for example, observed high negative values (-600 mV / -700 mV) from the start of monitoring up to 800 days in all series exposed to dry chamber wetting and drying cycles ($55 \pm 5\%$ R.H. and 23 ± 2 °C). Similarly, Godinho et al. (2018) observed readings in the range of -486 mV to -550 mV up to 100 days.

In order to encourage the formation of passive film on steel bars before molding, Ghods et al. (2010), Nahali et al. (2014), Williamson and Isgor, (2016) and Godinho et al. (2019) suggest the immersion of carbon steel bars in synthetic solutions that simulate the interior of the concrete before molding.

In this work, the monitoring of anodes installed at 1.5 cm and 2.5 cm did not show a stabilization level, but a tendency to become more electronegative as the chloride content inside the concrete increased.

With regard to the durability of concrete, ABNT NBR 6118 (2014) stipulates minimum cover values (c_{min}) on the reinforcement according to the aggressiveness of the environment in which the structure is inserted. In this case, for the galvanic sensor anodes (1.5 and 2.5 cm), these values were intentionally not respected. Adding to this the interconnectivity between the existing pores and micro-cracks in the paste, the efficiency of the physical protection that the cover provides is reduced.

According to Leek (1991) and Ribeiro et al. (2014), even with the alkaline reserve product of the $\text{Ca}(\text{OH})_2$ content in concrete and the passivation film, the presence of chlorides inside the concrete can trigger the dissolution of the passive film and initiate the corrosive process. According to the authors Huafu et al. (2015) and Jin et al. (2017), as the degree of contamination by chlorides increases, the more negative the E_{corr} value tends to become.

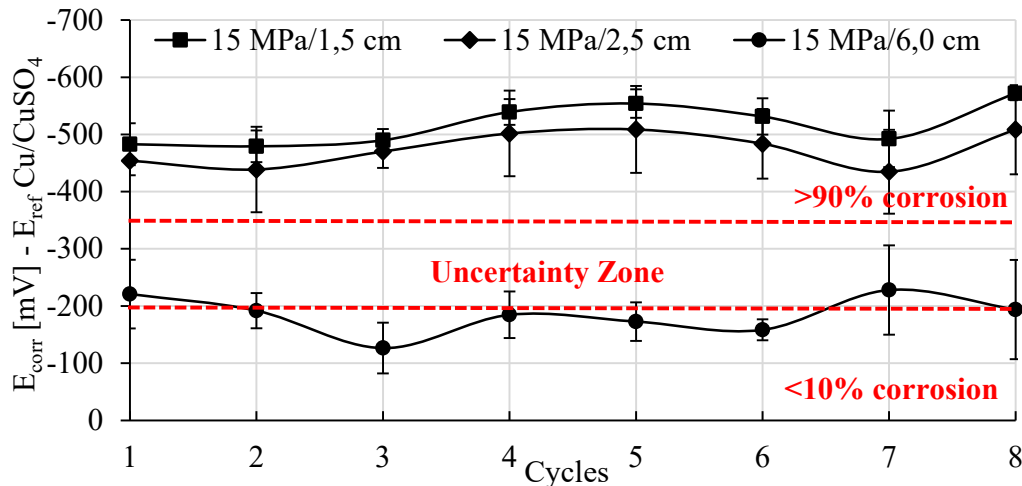


Figure 6. Corrosion potential for the 15 MPa mix. Source: Author.

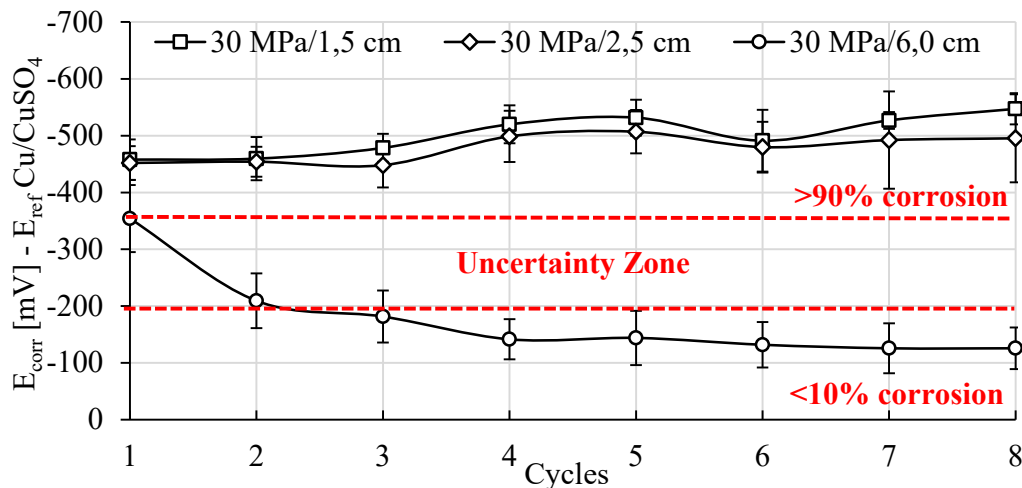


Figure 7. Corrosion potential for the 30 MPa mix. Source: Author.

On the other hand, in the main bars with 6 cm of cover, the probability of corrosion was less than 10% or in the range of (-200 to -350 mV) for both concretes. A similar behavior was observed by the authors Romano et al. (2013), who studied the performance of a sensor with electrodes at different depths in relation to the exposed surface of the specimen, namely: 1.5 and 3 cm. In the study, the electrode placed at a lower depth indicated depassivation before the electrode with a 3 cm cover. In addition, reinforcement bars of the specimen with a 4 cm cover depassivated 100 days after the sensor electrode was placed at a shallower depth.

Theoretically, more electronegative E_{corr} values indicate a critical level of chloride ions around the sensor anodes. If anodes are installed at different depths, anodes closer to the outer surface, through which ion penetration takes place, should present more electronegative values faster than those anodes located at greater depth (Romano et al., 2013).

Finally, the ANOVA analysis of variance and the subsequent Tukey test with 95% confidence indicated that the concrete strength did not influence the results obtained during the corrosion potential test. Therefore, the behavior of this quantity in the specimens of both mixes was the same.

3.2 Pair potential

Figures 8 and 9 show the average potential values of the pair for the six anodes of the system (corrosion sensor + steel bar). For 15MPa concrete, when the potential value of the pair was

negative, the probability of anode corrosion was less than 10% or was in the uncertainty zone according to the open circuit potential readings.

Based on the results observed in this work, 20 mV/min is the potential value of the pair (E_{pair}) for the arrangement and metals used (carbon-copper steel), which characterizes the tested galvanic couple. In parallel, the threshold of 200 mV/min appears to indicate the change to the active state (indicated with a dashed line in Figures 8 and 9).

Thus, when the potential of the pair is in the range of 20 to 200 mV/min, as in the case of anodes with 1.5 cm and 2.5 cm cover in the first cycles, the corrosion is in the active state. From the 4th cycle onwards, the potential of the pair was greater than 200 mV/min, and the anodes were definitely in the active state, regardless of the cover. Positive E_{pair} values indicate that the oxidation process predominates over the reduction process and the anode corrodes (anodic polarization). The greater the potential difference in the galvanic couple, the more intense the anodic polarization tends to be (Pawlick et al., 1998, Sousa, 2014; Fernandes and Martendal, 2015) and the more intense is the corrosion reaction in the pair.

For the 30MPa concrete (Figure 9), a similar behavior was observed for the six anodes at 1.5, 2.5 and 6.0 cm depth. The concrete strength did not influence the results obtained during the pair potential test, according to statistical analysis (ANOVA and Tukey at 95% confidence). It is also noteworthy that the average error of the E_{pair} readings is small when compared to E_{corr} (Figs 6 and 7). Thus, it is possible to prove greater stability in the readings taken with the galvanic sensor.

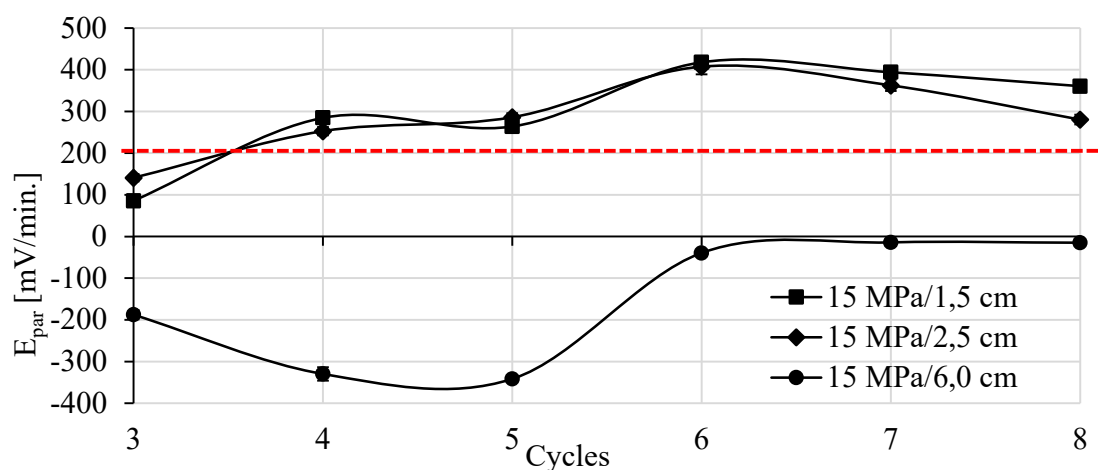


Figure 8. Pair potential for the 15 MPa mix. Source: Author.

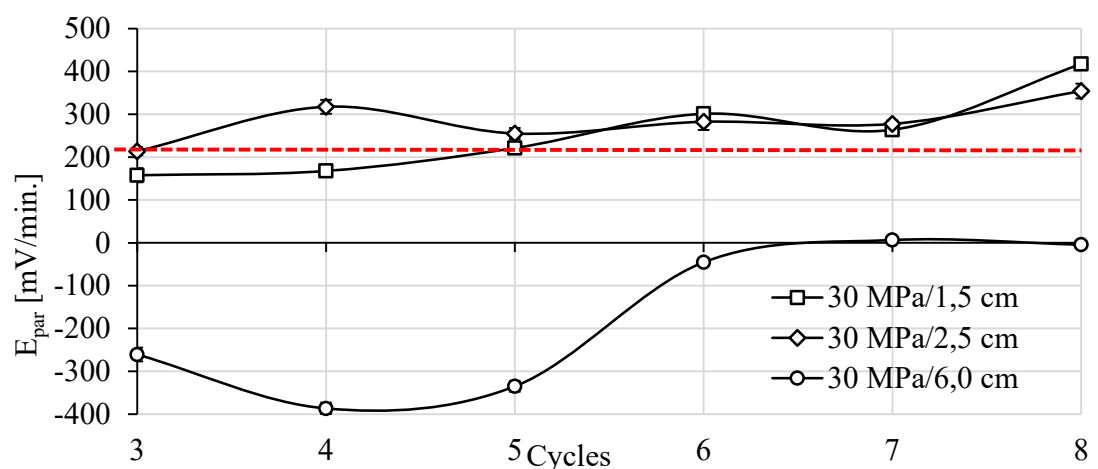


Figure 9. Pair potential for the 30 MPa mix. Source: Author.

Angst and Buchler (2015) expose some intrinsic difficulties in monitoring the mixed potential of a galvanic macrocell (E_{pair}): (i) anodic and cathodic reactions generally occur in the same structural element, (ii) or it is not possible to place reference electrodes near the anode and cathode (iii) or the electrolyte conductivity is too high and therefore the potential difference is too low to be accurately measured.

Note, however, that Angst and Buchler (2015) refer to a macrocell formed on the surface of a steel bar, a product of the penetration of chlorides into the concrete that causes localized corrosion. A galvanic sensor, in a different way, is formed by small pieces of metal with different electrical potentials where one will act as an anode and the other as a cathode, embedded in the concrete at depths always smaller than that of the reinforcement (Andrade et al., 2008; Araújo et al., 2013), which reduces the influence of the conductivity of the electrolyte.

It then remains to consider aspect (ii) mentioned by the authors: the possibility of placing reference electrodes close to the anode and cathode. Thus, in future tests that use the galvanic sensor proposed in this research, it is recommended to install a reference electrode as well. This practice will make it possible to separately determine the anode and cathode potential and thus be able to determine the polarization curve of each electrode, improving the monitoring of the galvanic couple potential. It is also suggested to monitor the behavior of the potential of the pair (E_{pair}) in an environment free of aggressive agents until the parameter reaches an equilibrium point in the range of positive values, as its value is a function of the potentials of the metals that make up the galvanic couple inside the concrete (Pawlick et al., 1998; Mccarter and Vennesland, 2004).

However, the stability of the sensor potential over time is also influenced by the anodic and cathodic current densities. In turn, the anodic and cathodic currents are a function of the anode area and the cathode area, respectively (Pawlick et al., 1998).

Therefore, if the anode has insufficient area, the potential of the pair will shift to higher values with an upper limit represented by the open circuit potential of the metal acting as the cathode. As the area of the cathode in relation to the anode increases, the demand for electrons from the cathode increases, while the area of the anode from which the electrons will be supplied decreases and, therefore, the rate of dissolution of the anode increases (Sousa, 2014). Under these conditions, there is a risk that the anode degrades excessively and shortens the lifetime of the sensor. Therefore, the behavior of the galvanic sensor must be evaluated with a cathode/anode area (A_C/A_A) ratio equal to 1, in order to improve the functioning of the sensor proposed in the work.

Initially, the experimental program did not foresee the realization of this test, but it proved to be extremely important to understand the behavior of the sensor over time.

3.3 Galvanic current

Theoretically, when a corrosive process is established in the bars, the galvanic current increases in the range of positive values due to the variation in the anode potential, which assumes more negative values compared to those obtained initially in its passive state (Araújo et al., 2013; Lacerda and Muller, 2015). An increase in galvanic current accompanied by a decrease in the open circuit potential indicates that a critical level of chloride ions has been reached (Andrade et al., 2008; Araújo et al., 2013).

In Figures 10 and 11 it is possible to observe that during monitoring, the galvanic current (I_{gal}) was negative during seven of the eight cycles in the six monitored anodes (four from the galvanic sensor and the two main bars). For the 15 MPa concrete (Figure 10), positive galvanic current values were observed in cycle 7 after 141 days of monitoring. However, they became negative again in cycle 8. For the 30 MPa concrete, in Figure 11 it is observed that the galvanic current was positive in cycles 7 and 8.

In principle, positive current values are in agreement with the open circuit potential more negative than -350 mV (corrosion probability > 90%), and with the pair potential greater than 200 mV/min, observed at the anodes installed at a lower depth (1.5 and 2.5 cm).

However, in the main bars installed with 6 cm of cover, E_{pair} indicated an electrolytic reaction during the monitoring, which means that the bars were in a passive state in agreement with the measured open circuit potential value. Therefore, the positive galvanic current (I_{gal}) record did not correspond with what was observed in the bars in the previous tests.

However, the galvanic current was close to zero throughout the test. Galvanic current values close to zero are also indicative of the steel's passive condition (Park et al., 2005; Sousa, 2014). Thus, similarly to what happened in the first stage of the experimental program with the sensors soaked in an aqueous solution (Calvo et al., 2017), I_{gal} showed greater inertia to identify the presence of an aggressive agent. Furthermore, according to Ribeiro and Cunha (2014), the galvanic current (I_{gal}) decays throughout the measurement, showing a capacitive behavior which makes monitoring difficult.

The results of galvanic current obtained in the six anodes (1.5, 2.5 and 6 cm) installed in the specimens of the 15 MPa mix were statistically equivalent to the values of galvanic current recorded in the anodes installed in the test specimens of the 30 MPa mix.

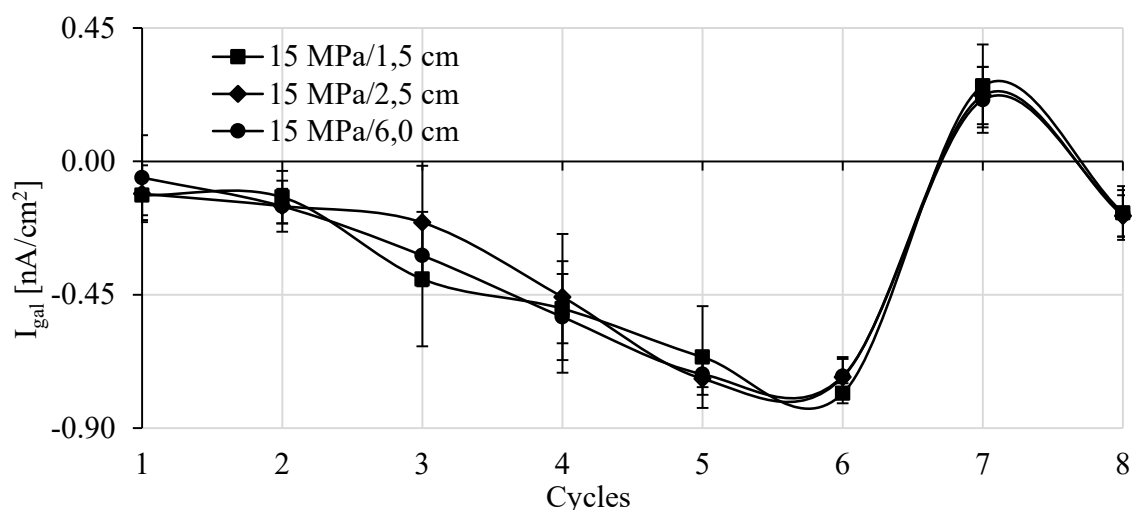


Figure 10. Galvanic current for the 15 MPa mix. Source: Author.

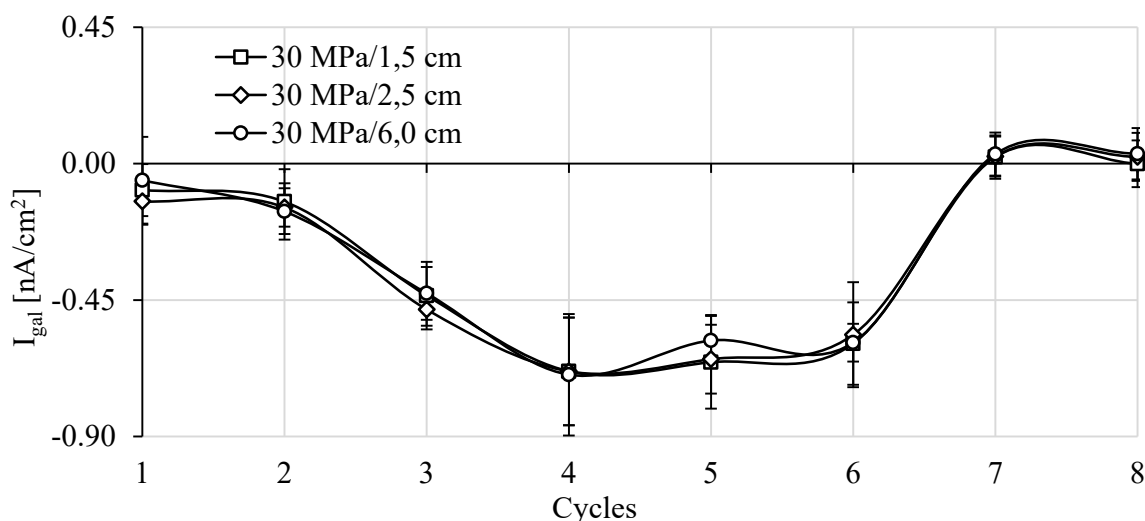


Figure 11. Galvanic current for the 30 MPa mix. Source: Author.

Finally, for data analysis, the linear model was applied, with the determination of R^2 to infer the correlation between the electrochemical techniques considered in the work. No correlation factor (R^2) came close to 0.9; therefore, it cannot be affirmed that there is a positive linear relationship between the electrochemical techniques. That is, the measured quantities differ and do not converge. For this reason, this type of study is important, as the choice of the correct technique, or set of techniques, is essential for the monitoring to be efficient. However, the suggestions made earlier in order to improve the functioning of the sensor are essential in order to be able to understand and estimate the behavior of the quantities evaluated in the field accurately.

3.4 Chloride penetration by the colorimetric method

At the end of the corrosion monitoring, colorimetric tests with silver nitrate (AgNO_3 0.1 M) and phenoltalein were performed. Figure 12 shows the appearance of the specimen slices after spraying the indicators. In none of the eight specimens tested was carbonated concrete observed, as indicated by the pink color in one of the specimen slices. This evidence that there is no carbonation in concrete is important to be sure that the colorimetric test of spraying a solution with silver nitrate will be effective, without indicating the false positive alerted in the works by Pontes et al. (2020). In the slice on the left, it is possible to see two distinct regions in terms of color: one with a brown precipitate corresponding to the region without free chlorides, and another without color in the region affected by free chlorides, which indicates how far the chloride penetration front has reached. In Figure 12, the region without chlorides was delimited with a black line.

After 150 days at the end of the eighth cycle, the chloride penetration front reached an average depth of 7.6 cm in the 15 MPa concrete specimens and 7.2 cm in the 30 MPa concrete specimens. Therefore, in the concrete around the sensor anodes, a critical level of chlorides was reached. The results obtained on the sensor anodes during the E_{corr} and E_{pair} tests indicated a high probability of corrosion at the end of the test.

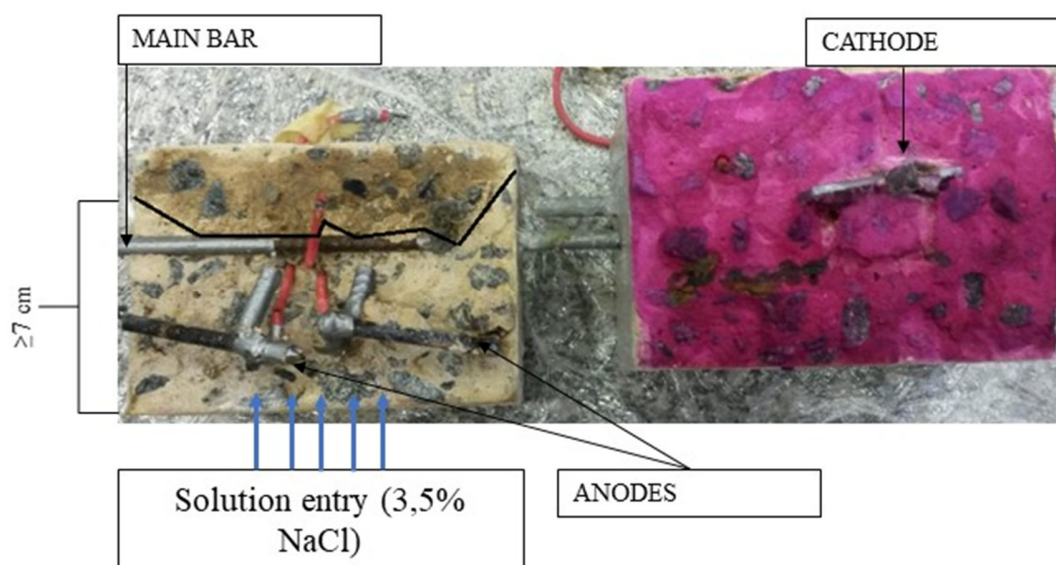


Figure 12. Colorimetric test (chloride penetration and carbonation) in the specimen after the end of monitoring.

It is observed that the depth of penetration of chlorides at the end of the cycles was similar between the 15 MPa and 30 MPa concretes. In this sense, it is necessary to point out that as well as porosity, cracking also provides facilities for aggressive agents to penetrate the concrete and initiate their destructive action in the structure. After the mass hardens, cracks are the result of drying shrinkage,

reinforcement corrosion and alternating wetting and drying cycles, among other factors (Brandão and Pinheiro, 1999). In this work, the three factors acted in combination, providing the appearance of microcracks, as shown in Figure 13.

The appearance of microcracks may have intensified the capillary penetration of water with chlorine ions, causing the concrete to present similar behaviors, different from what was observed under natural exposure conditions. Thus, drying in an oven at 50°C does not seem adequate and should be re-evaluated in other similar studies. However, studies that evaluated the penetration of chlorides in different Brazilian cements observed that concretes with CP-II-F have a high capacity for penetration of chlorine ions when compared to other types of cement, thus reducing the influence of the w/c ratio (Pereira, 2001; Crauss, 2010; Fleet et al., 2018).



Figure 13. Microcracks in specimens.

On the other hand, even though the chloride penetration front reached the main bars (6 cm cover), the critical chloride content for the depassivation of the reinforcement was not reached in the concrete at this depth. This is because the probability of corrosion was less than 10% or in the uncertainty zone, whereas E_{pair} indicated an electrolytic reaction, or at most was in the range -5 to 20 mV/min.

In this sense, it is necessary to point out that the arrival of chlorides in the vicinity of the reinforcement, by itself, does not represent the beginning of the corrosion process. The process will only start when the Cl⁻ ion content around the steel bar reaches the critical content (Jin et al., 2017) in order to depassivate the steel.

Most standards set the permitted Cl⁻ ion contents in relation to the cement mass. Although it is a very controversial point, the value of 0.4% in relation to the cement mass is a consensus in most standards (Casculo, 1997). The NP EN 206 standard, for example, adopts the value of 0.4% (Silva, 2017) and ABNT NBR 12655 (2006) establishes 0.15% in the structure's service conditions.

Furthermore, by breaking the specimens, it was possible to confirm the presence of the corrosion product around the sensor bars, but not around the exposed part of the main bars (6 cm cover). It should be noted that the ends of the main bars were protected with gray insulating tape, so that only 60 mm of the bar was exposed, the same length as the sensor anodes, as shown in Figure 3(a).

4. CONCLUSIONS

The aim of this work was to evaluate the efficiency of a galvanic sensor with multiple electrodes in monitoring the corrosion of reinforced concrete prisms, comparing it with conventional electrochemical methods and with the depth of penetration of chlorides. As the main conclusions of the study, the following can be mentioned:

- The w/c ratio did not influence the tests, with cover being the factor that exerted the greatest influence.
- The open circuit potential and the pair potential indicated an active corrosion state at the sensor anodes (1.5 and 2.5 cm) rather than at the main bars (6 cm).
- For the purpose of this research, 20 mV/min is the potential value of the pair (E_{pair}), which characterizes the tested carbon-copper galvanic steel pair. The 200 mV/min threshold appears to indicate change to the active state.
- The galvanic current showed little variation over time, with capacitive behavior during the 150 days of monitoring.
- The penetration front reached a depth greater than 7 cm, reaching the main bars (6 cm). For this reason, the tests indicated a tendency for the bar to enter the uncertainty zone until sufficient concentrations of chlorides are reached to depassivate the reinforcement and initiate corrosion.
- The developed sensor showed sensitivity to detect the front of chlorides and predict the possibility of corrosion of the reinforcements. Adjustments are still needed, such as monitoring the behavior of the pair potential (E_{pair}) and the corrosion potential (E_{corr}) in a medium free from aggressive agents until the E_{pair} stabilizes. It is considered that the parameters E_{corr} , E_{pair} and I_{gal} behave differently as corrosion monitoring parameters.

5. ACKNOWLEDGMENTS

The authors thank the Laboratory of Materials and Structures of the Federal University of Paraná (LAME-DCC-UFPR), the Graduate Program in Civil Engineering (PPGEC-UFPR), the Center for Studies in Civil Engineering (CESEC-UFPR), the Coordination for the Improvement of Higher Education Personnel (CAPES), the National Water Agency (ANA) and the National Council for Scientific and Technological Development (CNPq).

6. REFERENCES

- American concrete institute (ACI) (2014). ACI 318-14: *Building Code Requirements for Structural Concrete*.
- Associação Brasileira de Normas Técnicas (ABNT) (1980). NBR 6118: *Projeto e execução de obras de concreto armado*.
- Associação Brasileira de Normas Técnicas (ABNT) (2006). NBR 12655: *Concreto de cimento Portland – Preparo, controle e recebimento – Procedimento*.
- Associação Brasileira de Normas Técnicas (ABNT) (2014). NBR 6118: *Projeto de estruturas de concreto – Procedimento*.
- Associação Brasileira de Normas Técnicas (ABNT) (2003). NM 248: *Agregados - Determinação da composição granulométrica*.
- Associação Brasileira de Normas Técnicas (ABNT) (2009). NBR 7211: *Agregados para concreto – Especificação*.

- Associação Brasileira de Normas Técnicas (ABNT) (2003). NM 52: *Agregado miúdo - Determinação da massa específica e massa específica aparente*.
- Associação Brasileira de Normas Técnicas (ABNT) (2003). NM 53: *Agregado graúdo - Determinação de massa específica, massa específica aparente e absorção de água*.
- Associação Brasileira de Normas Técnicas (ABNT) (1992). NBR 7223: *Concreto - Determinação da consistência pelo abatimento do tronco de cone*.
- Associação Brasileira de Normas Técnicas (ABNT) (2003). NBR 5738: *Concreto — Procedimento para moldagem e cura de corpos de prova*.
- Associação Brasileira de Normas Técnicas (ABNT) (2018). NBR 5739: *Concreto — Concreto - Ensaio de compressão de corpos de prova cilíndricos*.
- Associação Brasileira de Normas Técnicas (ABNT) (2018). NBR 16697: *Cimento Portland - Requisitos*.
- ASTM Internacional. (2015). ASTM C876 – 15 *Standard Test Method for Corrosion Potentials of Uncoated Reinforcing Steel in Concrete*. Edição atual aprovada em 1 de novembro de 2015. Publicado em abril de 2016. Originalmente aprovado em 1977. Última edição anterior aprovada em 2009 como C876-09. doi: <https://doi.org/10.1520/C0876-15>
- NT BUILD 492 (2000), *Non-Steady State Chloride Migration (Diffusion Coefficient)*.
- Araújo, A., Panossian, Z., Portella, P. D., Bäessler, R. (2013), Monitoramento da corrosão em estruturas de concreto: sensor galvânico. *Revista Técnica*. Edição 194. Maio/2013. Link: <http://techne.pini.com.br/engenharia-civil/194/artigo294083-1.aspx>
- Andrade, C., Figueiras, H., Félix, C., Coutinho, J. S. (2008), “Desempenho do kit-sensor de corrosão na monitorização da durabilidade de estruturas de betão”, in: Anais do Encontro Nacional Betão Estruturas - BE2008. Guimarães. 5, 6, 7 de novembro de 2008.
- Angst, U., Buchler, M. (2015), On the applicability of the Stern–Geary relationship to determine instantaneous corrosion rates in macro-cell corrosion. *Materials and Corrosion*. 66(10). doi: <https://doi.org/10.1002/maco.201407997>
- Akimov, G. V. (1957), “*Théorie et Méthodes d’Essais de la Corrosion des Métaux*”. Dunod. Paris. p 53.
- Baltazar, M., Almeraya, F., Nieves, D., Borunda, A., Maldonado, E., Ortiz, A. (2007). *Corrosión del acero inoxidable 304 como refuerzo en concreto expuesto a cloruros y sulfatos*. Scientia Et Technica, XIII (36),353-357. Acesso em: 17 de Julio de 2021. ISSN: 0122-1701. Disponible en: <https://www.redalyc.org/articulo.oa?id=84903663>
- Brandão, A. M. S.; Pinheiro, L. M. (1999), *Qualidade e durabilidade das estruturas de concreto armado: aspectos relativos ao projeto*. Cadernos de Engenharia de Estruturas. n.8. EESC. Universidade de São Paulo. São Carlos. 1999.
- BioLogic Science Instruments (2011), EC-LAB Software: Techniques and Applications. Version 10.1x. Fevereiro, Disponível em: <https://www.egr.msu.edu/~scb-group-web/blog/wp-content/uploads/2012/07/EC-Lab-software-Techniques-and-Applications-manual.pdf>
- Cheng, Y., Asad H., Chen, E., Ma, G., Li, Z. (2018), *Simulation of a novel capacitive sensor for rebar corrosion detection*. Construction and Building Materials. 174: 613–624. <https://doi.org/10.1016/j.conbuildmat.2018.04.133>
- Chen, Y., Tang, F., Tang, Y., O’Keefe, M. J., Chena, G. (2017), *Mechanism and sensitivity of Fe-C coated long period fiber grating sensors for steel corrosion monitoring of RC structures*. Corrosion Science. 127: 70–81. <https://doi.org/10.1016/j.corsci.2017.08.021>
- Calvo Valdés, A., Farias Medeiros, M. H., de Jesus Roque, P. (2017). *Sensores de corrosão para monitoramento de pontes e viadutos de concreto armado. Primeira etapa – Testes em solução aquosa*. Revista De Engenharia E Pesquisa Aplicada, 2(3). <https://doi.org/10.25286/repa.v2i3.689>

- Calvo Valdés, A. (2018), “*Sensores de corrosão para monitoramento de pontes e viadutos de concreto armado*”. Dissertação (Mestrado). Programa de Pós-graduação de Engenharia de Construção Civil – PPGCEC. Universidade Federal do Paraná, Setor de Tecnologia, Curitiba.
- Cascudo, O. (1997), “*O controle da corrosão de armaduras em concreto. Inspeção e técnicas eletroquímicas*”. Capítulo 2: Corrosão de armaduras em concreto. p 39-61. Capítulo 8: Potenciais de corrosão p 137-153. Primeira versão 1997.
- Capraro, A. P. B., Gervasio, S., Medeiros, M. H. F., Hoppe Filho, J., Braganca, M., Oliveira, I. (2016), “*Avaliação dos mecanismos de corrosão de concretos contaminados com diferentes teores de pirita (FeS₂)*”, in: Anais do 58o Congresso Brasileiro de Concreto (58o CBC 2016). Instituto Brasileiro do Concreto – IBRACON. Belo Horizonte/MG, 1–16.
- Capraro, A. P. B., Macioski, G., Medeiros, M. H. F. (2021), *Effect of aggregate contamination with pyrite on reinforcement corrosion in concrete*. Engineering Failure Analysis. 120: 1350-6307. <https://doi.org/10.1016/j.engfailanal.2020.105116>
- Crauss, C. (2010), “*Penetração de cloretos em concretos com diferentes tipos de cimento submetidos a tratamento superficial*”. Dissertação de mestrado. Programa de Pós-Graduação em Engenharia Civil Universidade Federal de Santa Maria. 31 de agosto de 2010.
- De Lacerda, M. M., Müller, R. (2015), *Uso de sensor de taxa de corrosão instantânea como técnica de monitoramento da corrosão em estruturas de concreto*. Obra24horas. Acesso em: novembro / 2015. Disponível em: <https://www.obra24horas.com.br/artigos/concreto/uso-do-sensor-de-taxa-de-corrosao-instantanea-como-tecnica-de-monitoramento-da-corrosao-em-estruturas-de-concreto>
- De Lima, Ma. G., Morelli, F. (2004), “*Caracterização da agressividade do ambiente marinho às estruturas de concreto*”. Curso de Pós-Graduação em Engenharia de Infraestrutura Aeronáutica - ITA, São José dos Campos, SP. p 1-20 2004. Disponível em: https://semengo.furg.br/images/2004/07_2004.pdf
- Dotto, J. M. R (2006), “*Corrosão do aço induzida por íons cloreto – uma análise crítica das técnicas eletroquímicas aplicadas ao sistema aço-concreto com ou sem pozolana*”. Dissertação (Doutorado). Escola de Engenharia. Programa de Pós-graduação em Engenharia de Minas, Metalúrgica e de Materiais – PPGEM. Universidade federal do Rio Grande do Sul. Porto Alegre.
- Dong, S.-G., Lin, C.-J., Hu, R.-G., Li, L.-Q., Du, R.-G. (2011), *Effective monitoring of corrosion in reinforcing steel in concrete constructions by a multifunctional sensor*. Electrochimica Acta. 56(4): 1881–1888. <https://doi.org/10.1016/j.electacta.2010.08.089>
- Freire, K. R. R (2005), “*Avaliação do desempenho de inibidores de corrosão em armaduras de concreto*”. Dissertação de mestrado. Programa de Pós-graduação em engenharia de construção civil – PPGCEC. Universidade Federal do Paraná. Curitiba 2005.
- França, Clério Bezerra (2011), “*Avaliação de cloretos livres em concretos pelo método de aspersão de solução de nitrato de prata*”. Dissertação de mestrado. Programa de pós-graduação em Engenharia de Construção Civil. Universidade Católica de Pernambuco. Pró -Reitoria Acadêmica- PRAC.
- Fernandes, K. V., Martenda, P. C. (2015), *Por que os metais sofrem corrosão?* Engenheiro de Materiais. Acesso em: novembro 2015. Disponível em: <http://engenheirodemateriais.com.br/tag/pilha-galvanica/>
- Figueiredo, E. J P., Meira, G. R. (2013), *Boletim Técnico: Corrosão das armaduras de concreto*. Boletín No. 6, Associação Latinoamericana de Controle da qualidade, Patologia e Recuperação da Construção. ALCONPAT Internacional.
- Federal Highway Administration (FHA) (2011). *U.S. Government of Transportation. Bridge preservation guide*. August 2011.
- Feliú, S., González, J. A., Feliú Jr., S., Andrade, M. C. (1990), *Confinement of the electrical signal or in-situ measurement of polarization resistance in reinforced concrete*. ACI Materials Journal. 87 (5):457.

- Frota, W.D.S.; Martins, E. R.; Valerio, P. P. (2018), *Avaliação da difusão de íons cloreto considerando concreto simples constituído por três principais classes de cimento portland convencional*. Sodebras Journal. 13(151): 99-113. doi: <https://doi.org/10.13140/RG.2.2.12429.64486>
- Godinho, J. P., Oliveira, R. L. N., Capraro, A. P. B., Réus, G. C., Medeiros, M. H. F. (2018), “*Influência das condições de limpeza de barras de aço carbono do concreto armado nas leituras eletroquímicas de densidade de corrente de corrosão e potencial de corrosão*”, in: Anais do 3º Encontro Luso-Brasileiro de Degradação em Estruturas de Concreto (3º DEGRADA), São Carlos/SP, 77–92.
- Godinho, J. P., Zermiani, B. N., Oliveira, R. L. N., Medeiros, M. H. F. (2019), *Comportamento eletroquímico do aço carbono inserido no concreto durante a passivação*. Revista Técnico-Científica do CREA-PR. ISSN 2358-5420 –Edição Especial – Setembro de 2019, 1 - 16.
- Gurdián, H.; García-Alcoel, E.; Baeza-Brotons, F.; Garcés, P.; Zornoza, E. (2014), *Corrosion behavior of steel reinforcement in concrete with recycled aggregates, fly ash and spent cracking catalyst*. Materials (Basel). 7(4), 3176-3197. doi: <https://doi.org/10.3390/ma7043176>
- Gentil, V. (1996), “*Corrosão*”. 3a Edição. Rio de Janeiro. Editora LTC. Capítulo 3: “Potencial de eletrodo”. p 14 – 28.
- Ghods, P., Isgor, O. B., McRae, G. A., Gub, G. P. (2010), *Electrochemical investigation of chloride-induced depassivation of black Steel rebar under simulated service conditions*. Corrosion Science. 52(5): 1649–1659. doi: <https://doi.org/10.1016/j.corsci.2010.02.016>
- Ghods, P., Isgor, O. B., McRae, G., Miller, T. (2009), *The effect of concrete pore solution composition on the quality of passive oxide films on black steel reinforcement*. Cement and Concrete Composites. 31(1): 2–11. doi: <https://doi.org/10.1016/j.cemconcomp.2008.10.003>
- Hays, G. F. (2020), *Now is the Time*. Director General da World Corrosion Organization. Acesso em: dezembro de 2020. Disponível em: <http://corrosion.org/Corrosion+Resources/Publications/ /nowisthetime.pdf>
- Pei, H., Li, Z., Zhang, J., Wang, Q. (2015), *Performance investigations of reinforced magnesium phosphate concrete beams under accelerated corrosion conditions by multi techniques*. Construction Building Materials. 93: 982-994. <https://doi.org/10.1016/j.conbuildmat.2015.05.057>
- Hernández, Y., Troconis de Rincón, O., Torres, A., Delgado, S., Rodríguez, J., Morón, O. (2016). *Relación entre la velocidad de corrosión de la armadura y el ancho de fisuras en vigas de concreto armado expuestas a ambientes que simulan el medio marino*. Revista ALCONPAT, 6(3), 272 - 283. <https://doi.org/10.21041/ra.v6i3.152>
- Institut Für Seltene Erden und Strategische Metalle (ISE) (2020), *Preços, ocorrência, extração e uso do Titan*. Acesso em: dezembro de 2020. Disponível em: <https://pt.institut-seltene-erden.de/seltene-erden-und-metalle/strategische-metalle-2/titan/>
- Inaudi, D. (2009), “*Integrated Structural Health Monitoring Systems for Bridges*”. in: Anais do 1o Congresso de Segurança e Conservação de Pontes ASCP'09. Lisboa. 2009.
- Jucá, T. R. P. (2002), “*Avaliação de Cloretos Livres em Concretos e Argamassas de Cimento Portland pelo Método de Aspersão de Nitrato de Prata*”. Universidade Federal de Goiás. Escola Engenharia Civil II.
- Jin, M., Jiang, L., Zhu, Q. (2017), *Monitoring chloride ion penetration in concrete with different mineral admixtures based on embedded chloride ion selective electrodes*. Construction Building Materials. 143: 1-5. 15 julho, 2017. <https://doi.org/10.1016/j.conbuildmat.2017.03.131>
- Jiang, J. -Y., Wang, D., Chu, H. -Y., Ma, H., Liu, Y., Gao, Y., Shi, J., Sun, W. (2017), *The passive film growth mechanism of new corrosion-resistant steel rebar in simulated concrete pore solution: Nanometer structure and electrochemical study*. Materials (Basel). 10(4): 412. doi: <https://doi.org/10.3390/ma10040412>

- Klassen, R. D., Roberge, P. R. (2008), “*Technique for corrosion monitoring*”. Capítulo 5: Zero resistance ammetry and galvanic sensor. p 111-124.
- Leek, D. S. (1991), *The Passivity of Steel in Concrete*. Quarterly Journal of Engineering Geology. 24:55–66. <https://doi.org/10.1144/GSL.QJEG.1991.024.01.05>
- Lv, H., Zhao, X., Zhan, Y., Gong, P. (2017), *Damage evaluation of concrete based on Brillouin corrosion expansion sensor*, Construction and Building Materials, 143: 387-394, ISSN 0950-0618, <https://doi.org/10.1016/j.conbuildmat.2017.03.122>
- Mccarter, W. J., Vennesland, Ø. (2004), *Sensor systems for use in reinforced concrete structures*. Construction and Building Materials. 18(6): 351–358. <https://doi.org/10.1016/j.conbuildmat.2004.03.008>
- Medeiros, M. H. F. (2008), “*Contribuição ao estudo da durabilidade de concretos com proteção superficial frente a ação de íons cloretos*”. Universidade de São Paulo. Escola Politécnica. 2008.
- Medeiros, M. H. F., de Oliveira Andrade, J. J., Helene, P. (2011), “*Durabilidade e Vida Útil das Estruturas de Concreto*”. Capítulo 22, Concreto: Ciência e Tecnologia, Geraldo Cechella Isaia (Editor), © 2011 IBRACON. URL: <http://www.phd.eng.br/wp-content/uploads/2014/07/lc55.pdf>
- Medeiros, M. H. F., Rocha, F. C., Medeiros-Junior, R. A., Helene, P. (2017), *Corrosion potential: influence of moisture, water-cement ratio, chloride content and concrete cover*, Revista IBRACON de Estruturas e Materiais (RIEM). 10 (4):864–885. <https://doi.org/10.1590/s1983-41952017000400005>
- Torres-Luque, M., Bastidas-Arteaga, E., Schoefs, F., Sánchez Silva, M., Osma, J. F. (2014), *Non-destructive methods for measuring chloride ingress into concrete: State-of-the-art and future challenges*. Construction and Building Materials. 68:68-81. <https://doi.org/10.1016/j.conbuildmat.2014.06.009>
- Marcondes, C. G. N. (2012), “*Adição de nanotubos de carbono em concretos de cimento Portland absorção, permeabilidade, penetração de cloretos e propriedades mecânicas*”. Universidade Federal do Paraná. Setor de Tecnologia. Programa de Pós-Graduação em Engenharia de Construção Civil – PPGCEC. 2012.
- Meira, G. R. (2017), “*Corrosão de Armaduras em Estruturas de Concreto - fundamentos, diagnóstico e prevenção*”. 1ª edição, editora do IFPB, João Pessoa-PB, 2017.
- Macioski, G., de Souza, D. J., Capraro Brandão, A. P., de Medeiros, M. H. F. (2016). *Análisis de la corrosión de barras de acero en función de la variación del pH del medio*. Revista ALCONPAT, 6(3), 223 - 234. <https://doi.org/10.21041/ra.v6i3.153>
- Mota, A. C. M. (2011), “*Avaliação da presença de cloretos livres em argamassas através do método colorimétrico de aspersão da solução de nitrato de prata*”. Dissertação de mestrado. Escola Politécnica da Universidade de Pernambuco, Recife, Brasil.
- Martínez, I., Andrade, C. (2009), *Examples of reinforcement corrosion monitoring by embedded sensors in concrete structures*. Cement and Concrete Composites, 31(8): 545–554. doi: <https://doi.org/10.1016/j.cemconcomp.2009.05.007>
- Nahali, H., Dhouibi, L., Idrissi, H. (2014), *Effect of phosphate based inhibitor on the threshold chloride to initiate steel corrosion in saturated hydroxide solution*. Construction and Building Materials. 50: 87–94. <https://doi.org/10.1016/j.conbuildmat.2013.08.054>
- Pérez López, T., Sosa, M. R., Moo-Yam, V. M. J., Chávez, E., Pérez-Quiroz, J. T. (2018). *Análisis de la interfaz concreto-acero en especímenes expuestos a la intemperie e inmersos en agua de mar natural*. Revista ALCONPAT, 8(1), 16 - 29. <https://doi.org/10.21041/ra.v8i1.203>
- Pereira, E. V., Salta, M. M. (2012), “*Monitorização permanente da corrosão em estruturas de betão armado*”. Resultados a longo prazo”, in: Anais do Encontro Nacional BETÃO ESTRUTURAL - BE2012. FEUP, 24-26 de outubro de 2012.

- Pereira, E. V., Figueira, R. B., Salta, M. M. L., Da Fonseca, I. T. E. (2009), *A Galvanic Sensor for Monitoring the Corrosion Condition of the Concrete Reinforcing Steel: Relationship Between the Galvanic and the Corrosion Currents*. Journal of Sensor. 9(11): 8391-8398. doi: <https://doi.org/10.3390/s91108391>; ISSN 1424-8220. 2009.
- Pawlick, L. A., Stoner, G. E., Clemenña, G. G. (1998), *Development of an embeddable reference electrode for reinforced concrete structures*. Contract Research Sponsored by Virginia Transportation Research Council. URL: https://www.virginiadot.org/vtrc/main/online_reports/pdf/99-cr1.pdf
- Park, Z.-T., Choi, Y.-S., Kim, J.-G., Chung, L. (2005), *Development of a galvanic sensor system for detecting the corrosion damage of the steel embedded in concrete structure. Part 2. Laboratory electrochemical testing of sensors in concrete*. Cement and Concrete Research. 35(9): 1814–1819. <https://doi.org/10.1016/j.cemconres.2003.11.027>
- Pontes, C. V., Réus, G. C., Araújo, E.C., Medeiros, M. H. F. (2020), *Silver nitrate colorimetric method to detect chloride penetration in carbonated concrete: How to prevent false positives*. Journal of Building Engineering. (34): 101860. <https://doi.org/10.1016/j.jobe.2020.101860>
- Poursae, A. (2016), *Corrosion of Steel in Concrete Structures*. Elsevier, 1st Edition. Amsterdã, Holanda, 2016.
- Pereira, V. G. A. (2001), “*Avaliação do coeficiente de difusão de cloretos em concretos: influência do tipo de cimento, da relação a/c, da temperatura e do tempo de cura*”. Dissertação de mestrado Programa de Pós-Graduação em Engenharia Civil Universidade Federal de Rio Grande do Sul.
- Real, L. V., Oliveira, D. R. B., Soares, T., Medeiros, M. H. F. (2015). *Método colorimétrico por aspersión de nitrato de plata para la evaluación de la penetración de cloruros en concreto: estado del arte*. Revista ALCONPAT, 5(2), 149 - 159. <https://doi.org/10.21041/ra.v5i2.84>
- Romano, P., Brito, P. S. D., Rodrigues, L. (2013), *Monitoring of the degradation of concrete structures in environments containing chloride ions*. Construction and Building Materials. 47: 827–832. <https://doi.org/10.1016/j.conbuildmat.2013.05.042>
- Ribeiro, V. D., Cunha, T. M. P. (2014), “*Corrosão em Estruturas de Concreto Armado*”. Capítulo 8: Técnicas de avaliação e monitoramento da corrosão em estruturas de concreto armado, p 215.
- Ribeiro, D. V., Helene, P., Cascudo, O., Tutikian, B. F., Sales, A., Souza, C. A. C., Cunha, M. P. T., Lourenco, M. Z., Almeida, F. C. R. (2018), “*Corrosão e Degradação em Estruturas de Concreto: Teoria, Controle e Técnicas de Análise e Intervenção*”. 2a, Elsevier Brasil, Rio de Janeiro-RJ, 2018.
- Rocha, F. C. (2012), “*Leituras de potencial de corrosão em estruturas de concreto armado: influência da relação água / cimento, da temperatura, da contaminação por cloretos, da espessura de revestimento e do teor de umidade do concreto*”. Dissertação de mestrado. Programa de Pós-graduação em engenharia de construção civil – PPGCEC. Universidade Federal do Paraná. Curitiba 2012.
- Rocha, F., Campos, H., de Andrade, T. S., Roquitski, A., Medeiros, M. H. (2014). *Influência da espessura de revestimento e da contaminação por cloretos nas leituras de potencial de corrosão de armaduras*. REEC - Revista Eletrônica De Engenharia Civil, 8(2). <https://doi.org/10.5216/reec.v8i2.26968>
- Raupach M., Schiebl, P. (2001), *Macrocell sensor systems for monitoring of the corrosion risk of the reinforcement in concrete structures*. NDT & E International. 34(6): 435-442. [https://doi.org/10.1016/S0963-8695\(01\)00011-1](https://doi.org/10.1016/S0963-8695(01)00011-1)
- Ribeiro, D. V., Souza, C. A. C., Abrantes, J. C. C. (2015), *Uso da Espectroscopia de Impedância Eletroquímica (EIE) para monitoramento da corrosão em concreto armado*. Revista IBRACON de Estruturas e Materiais. 8 (4): 529-546. Agosto 2015. <https://doi.org/10.1590/S1983-41952015000400007>

- Sousa, C. D. C. A. (2014), “*Corrosão em estruturas de concreto armado: Teoria, Controle e Métodos de Análise*”. Capítulo 2: Princípios da corrosão eletroquímica., p 13-34.
- Silva, P. N. R. (2017), *Ataque em estruturas de concreto por ação de cloretos*. Acesso em: dezembro 2017. Disponível em: <https://www.axfiber.com.br/single-post/2017/01/12/ataque-em-estruturas-de-concreto-por-a%C3%A7%C3%A3o-de-cloretos>
- Silva, E. P. (2010), “*Avaliação do potencial de corrosão de concretos estruturais produzidos segundo as prescrições da NBR 6118, submetido a ensaio de corrosão acelerado*”. Dissertação (Graduação) -Curso de Engenharia Estrutural e Construção Civil de Fortaleza. Universidade Federal do Ceará. Fortaleza 2010.
- Santos, L. O. (2014), “*Monitoramento e ensaio de Pontes*”. in: Anais do Congresso Brasileiro de Pontes e Estruturas. Rio de Janeiro. p 1-14. 21-23 de Maio del 2014.
- Wu, L., Li, W., Yu, X. (2017), *Time-dependent chloride penetration in concrete in marine environments*. Construction and Building Materials. 152: 406-413. <https://doi.org/10.1016/j.conbuildmat.2017.07.016>
- Williamson, J., Isgor, O. B. (2016), *The effect of simulated concrete pore solution composition and chlorides on the electronic properties of passive films on carbon steel rebar*. Corrosion Science. 106: 82–95. <http://dx.doi.org/10.1016/j.corsci.2016.01.027>
- Zhang, J., Lui, C., Sun, M., Li, Z. (2017). *An innovative corrosion evaluation technique for reinforced concrete structures using magnetic sensors*. Construction and Building Materials. 135: 68-75. <http://dx.doi.org/10.1016/j.conbuildmat.2016.12.157>
- Zoghi, M. (2013), “*The International Handbook of FRP composites in civil engineering*”. 1st Edition. CRC Press. ISBN 9780849320132. September 26, 2013. Acesso: Janeiro, 2016. Disponível em: <https://www.crcpress.com/TheInternational-Handbook-of-FRP-CompositesinCivilEngineering/Zoghi/p/book/9780849320132>

Mapping External Mortar Render (EMR) defects: case study in multi-storey residential buildings

R. Dias^{1*} , L. Pagoto¹ , N. Tsutsumoto² , C. Fioriti³ 

*Contact author: rdias07@live.com

DOI: <https://doi.org/10.21041/ra.v11i3.538>

Reception: 18/05/2021 | Acceptance: 09/07/2021 | Publication: 01/09/2021

ABSTRACT

This study aims to identify, map, and quantify the external mortar render (EMR) defects of 22 multi-storey buildings located in the Fernandópolis city, Brazil. Incidence (M-INC) and intensity (M-INT) methods were used to quantify the building defect (BD) of five typified facade regions: continuous wall (1-OCW), around openings (2-OOP), top of parapets and eaves (3-TOP), below balconies, soffits or ledges (4-BCE), and on corners and edges (5-OCE). In addition, three degradation pattern maps were created. We observed 4351 and 481 BDs by M-INT and M-INC, respectively. The most frequent problems were stains and cracks. The most affected regions by M-INT were 2-OOP (34.5%), 1-OCW (23.3%), and 4-BCE (21.6%) while by M-INC were 1-OCW (39.9%), 3-TOP (29.3%), and 2-OOP (16.6%).

Keywords: mortar renders; anomalies; degradation; building pathology; mapping defect.

Cite as: Dias, R., Pagoto, L., Tsutsumoto, N., Fioriti, C. (2021), "Mapping External Mortar Render (EMR) defects: case study in multi-storey residential buildings", Revista ALCONPAT, 11 (3), pp. 88 – 107, DOI: <https://doi.org/10.21041/ra.v11i3.538>

¹Departamento de Engenharia Civil, Faculdade de Engenharia de Ilha Solteira – FEIS/UNESP, Universidade Estadual Paulista, Ilha Solteira, Brasil.

²Instituto Federal de Educação, Ciência e Tecnologia de São Paulo, Campus Avançado Ilha Solteira, SP, Brasil

³Universidade Estadual Paulista, Faculdade de Ciências e Tecnologia – FCT/UNESP, Presidente Prudente, Brasil

Contribution of each author

In this study, the following stages were overcome: research conception, bibliographic survey, data collection, analysis of the field results, writing of the manuscript, translation, text review, and evaluation of the research. Author R. Dias contributed to the research conception (50%), bibliographic survey (50%), data collection (70%), analysis of results (50%), writing (50%), translation (34%), and revision of the text (100%). Authors L. Pagoto and N. Tsutsumoto contributed with data collection (15%), analysis of results (15%), writing (25%), translation (33%), and research evaluation (15%). Author C. Fioriti participated in in research conception (50%), bibliographic survey (50%), analysis of results (20%), and evaluation of the research (70%).

Creative Commons License

Copyright 2021 by the authors. This work is an Open-Access article published under the terms and conditions of an International Creative Commons Attribution 4.0 International License ([CC BY 4.0](https://creativecommons.org/licenses/by/4.0/)).

Discussions and subsequent corrections to the publication

Any dispute, including the replies of the authors, will be published in the second issue of 2022 provided that the information is received before the closing of the first issue of 2022.

Mapeamento de manifestações patológicas em revestimentos argamassados de fachada (EMR): estudo de caso em edifícios residenciais

RESUMO

Este trabalho objetivou identificar, mapear e quantificar as manifestações patológicas (BDs) em revestimentos argamassados de fachada (EMR), de 22 prédios residenciais de Fernandópolis-SP, Brasil. Para quantificação das BDs foram empregados os métodos da incidência (M-INC) e intensidade (M-INT), considerando a localização em cinco regiões tipificadas da fachada: paredes contínuas (1-OCW), entorno de aberturas (2-OOP), topo de parapeitos e beirais (3-TOP), abaixo de varandas/sacadas/ressaltos (4-BCP) e cantos/bordos (5-OCE). Observou-se 4351 e 481 BDs pelo M-INT e M-INC, respectivamente, realizando três mapas padrão de degradação. As BDs mais frequentes foram as manchas e fissuras. As regiões mais afetadas pelo M-INT foram 2-OOP (34,5%), 1-OCW (23,3%), e 4-BCP (21,60%), enquanto para o M-INC foram 1-OCW (39,9%), 3-TOP (29,3%) e 2-OOP (16,6%).

Palavras-chave: Revestimentos de Argamassa; Anomalias; Degradação; Patologia das Edificações; Mapeamento.

Mapeo de manifestaciones patológicas en revestimientos de mortero (EMR): un estudio de caso en edificios residenciales

RESUMEN

Este trabajo tuvo como objetivo identificar, mapear y cuantificar las manifestaciones patológicas (BD) en revestimientos de fachadas de mortero (EMR) de 22 edificios residenciales en Fernandópolis-SP, Brasil. Para cuantificar las BDs se utilizaron los métodos de incidencia (M-INC) e intensidad (M-INT), considerando cinco regiones tipificadas de la fachada: muros continuos (1-OCW), alrededor de huecos (2-OOP), parte superior de parapetos y aleros (3-TOP), debajo de balcones/balcones/voladizos (4-BCP) y esquinas/bordes (5-OCE). Se observaron 4351 y 481 BDs por M-INT y M-INC, respectivamente, realizando mapas estándar de degradación. Los BD más frecuentes fueron manchas y grietas. Las regiones más afectadas por M-INT fueron 2-OOP (34,5%), 1-OCW (23,3%) y 4-BCP (21,60%), y para M-INC fueron 1-OCW (39,9%), 3-TOP (29,3%) y 2-OOP (16,6%).

Palabras clave: Recubrimientos de mortero; Anomalías; Degradación; Patología de la edificación; Mapeo de defectos.

Legal Information

Revista ALCONPAT is a quarterly publication by the Asociación Latinoamericana de Control de Calidad, Patología y Recuperación de la Construcción, Internacional, A.C., Km. 6 antigua carretera a Progreso, Mérida, Yucatán, 97310, Tel.5219997385893, alconpat.int@gmail.com, Website: www.alconpat.org

Reservation of rights for exclusive use No.04-2013-011717330300-203, and ISSN 2007-6835, both granted by the Instituto Nacional de Derecho de Autor. Responsible editor: Pedro Castro Borges, Ph.D. Responsible for the last update of this issue, Informatics Unit ALCONPAT, Elizabeth Sabido Maldonado.

The views of the authors do not necessarily reflect the position of the editor.

The total or partial reproduction of the contents and images of the publication is carried out in accordance with the COPE code and the CC BY 4.0 license of the Revista ALCONPAT.

1. INTRODUCTION

Walls and their renders affect the habitability and healthiness of buildings; therefore, they must meet the minimum requirements for performance and useful life (Terra, 2001; Silva et al., 2013). The anomalies found in mortar facade render (EMR) have various origins, and the presence of a building defect (BD) decreases the functional performance of EMR, thus causing damage to users (Bauer, 2017; Dorfman; Petrucci, 1989).

The facades of the buildings perform differently depending on their geographic orientation. This difference is because of the climatic action (wind, solar charge, and rain) that affects a facade (Fox et al., 2016). However, anomalies owing to thermal in the EMR can be observed for facades that are not directly exposed to solar irradiation (without direct heat flow): they are normally identified in humid places with cracks and/or coating (Takeda; Maker, 2018).

There are various failures that affect EMR, which can originate in different phases of a building triggered either by human error (design strategies, construction, use, and maintenance) or climatic effects (Bauer, 2017; Bauer et al., 2018). The variation in climatic effects affects the durability of the EMR owing to its constant interaction. For temperature, the seasonal and/or daily variations could generate internal stresses in the mortar that could culminate in the gradual formation of microcracks, thus decreasing the performance of the coating and a consequent reduction in useful life (Sentena et al, 2018).

Solar radiation mainly affects the horizontal surfaces and facades of a building; however, many architects and urban planners have dispended significant attention to designing options, thus neglecting thermo-physical performance (Fabbri et al., 2020).

The various factors that affect the durability of buildings and their subsystems, such as EMR, can be subdivided into two categories. The first is related to the durability of the system and the second is related to the aggressiveness of the environment (Souza et al., 2018). Thus, external rendering construction systems need to be evaluated, specifically in different climatic zones (Maciel; Carvalho, 2019).

Considering the distinction of actions according to the geographic location of a building, the mapping of degradation and any other type of anomaly (BD) is crucial in the construction of a database between a laboratory and field, to transform data of research into useful practical notions that will become inducers of appropriate conservation actions (Rodrigues, 2014).

Using the data collected, connections between different parts of a facade and the types of defects that occurred in the mortar lining were established. These links can be expressed graphically through "degradation pattern maps" (Gaspar; Brito, 2005).

Owing to the significance of EMR for buildings, it is necessary to study the BDs that will contribute to the degradation during useful life, which could be minimized when planned during the design or execution of the render (Postinger et al., 2019).

In recent years, various studies have been carried out to develop and/or improve methods for predicting the useful life of buildings and/or their systems, as well as to provide techniques for the prevention, diagnosis, and rehabilitation of buildings (Flores-Colen; Brito, 2010; Silva et al., 2013; Vieira et al., 2015; Silva et al., 2011; Carvalho et al., 2016; Silva et al., 2018; Charisi et al., 2018; Souza et al., 2018; Ferreira et al., 2019; Ansah et al., 2020; Saviz et al., 2020).

In these studies, several variables of the developed methods relate to the BD observed in buildings of a certain location or region. However, the lack of knowledge of the professionals of the productive chain owing to the absence of concise data on the origin of the pathological problems, which are the most common forms of manifestation, as well as the lack of registration and dissemination of data delay the development and improvement of the techniques of designing and building, and preventing previous errors (Thomaz, 2020).

Thus, this study aims to identify, map, and quantify the main BDs that affect 22 multi-story

residential buildings in the municipality of Fernandópolis-SP, Brazil, by inspecting buildings that meet the established criteria.

2. PROCEDURES

Fernandópolis city, Brazil, is a small municipality located in the northwestern region of the state of São Paulo. The municipality is relatively new, approximately 82 years old (Prefeitura De Fernandópolis, 2012). Therefore, the multi-story buildings in the municipality are more recent than their age and with maximum ages varying between 4 and 34 years. Thus, the case study was carried out in all residential buildings above five floors in the municipality of Fernandópolis-SP.

The sample universe of 22 buildings meets this criterion, and they were arranged in different regions of the municipality, as shown in Figure 1. The buildings were named A to Q, and there were two condominiums with four and three towers, named A1, A2, A3, A4, L1, L2, and L3. Notably, because all buildings in the municipality that met these requirements were selected, no technique or recommendation was used for choosing the sample universe. The selected buildings have main structure in reinforced concrete, masonry closures, and some variations in form, dimension and architectural elements of the facade, with the EMR as the predominant finish of the facade.

2.1 Local climate classification

As a typical climate classification, the global Köppen-Geiger system of climatic types has been used, widely used in the areas of geography, climatology, and ecology (Alvares et al., 2013). This classification is based on specific parameters for each global region of the world, so therefore, that the determination of climatic types is carried out considering based on the seasonality as well as average monthly or annual values of air temperature and precipitation.

2.2 Inspection / Data Collection

A practical and objective method was adopted for the analysis of damaged facade systems, specifically EMR; therefore, other architectural finishing elements were neglected. Inspection and registration of visible BDs were carried out with the naked eye and using a binocular. Based on the inspection sequence described by Antunes (2010), the inspection was carried out from left to right, from top to bottom, floor by floor, considering all the levels were covered and that all the problems established in the EMR were noted. Field information was duly noted in an inspection form developed specifically for this study.

2.3 Incidence Method (M-INC) and Intensity Method (M-INT)

These methods were used by Segat (2005), and they are based on two different methods of quantifying the observed pathological cases. In M-INC, each BD is quantified only once per facade, even if it occurs repeatedly, whereas all DBs are quantified in the intensity method (M-INT), regardless of the number of repetitions.

The importance of this form of survey and quantification is because M-INC allows us to highlight, which are the most common and frequent BDs for the sample space, whereas M-INT allows obtaining more information concise about the BDs that are present in greater quantity.



Figure 1. Multi-storey residential buildings studied (panoramic view)

2.4 Quantification of BDs

The total quantification of each BD was carried out preliminarily in a unitary manner for each type, facade, and location. For M-INT, in the presence of extended stains and/or cracks, until there was no physical separation from it, even if it extended over more than one floor or even the entire facade, it was quantified only once. For physical separation (discontinuity), the number of individual BDs was added. To convert the quantification to M-INC and the consequent separation of the results for each method, the following logical rule was used: if the total quantity of a certain BD that occurs in a given facade is equal to or greater than 1, it was admitted with a quantity equal to 1, and if the total quantity is equal to 0, it is assumed that quantity is equal to 0. Therefore, either 0 BD or 1 BD was quantified for each facade and BD.

2.5 Typified facade regions

BDs were also quantified in each region of the facade, that is, according to their location. To assign the location of the BDs, the facade was divided into five areas: (1) in continuous walls-OCW, (2) around openings-OOP, (3) on top of parapets and eaves-TOP, (4) below balconies or ledges-BCP; and (5) in the corners and edges-OCE, as shown in Figure 2.

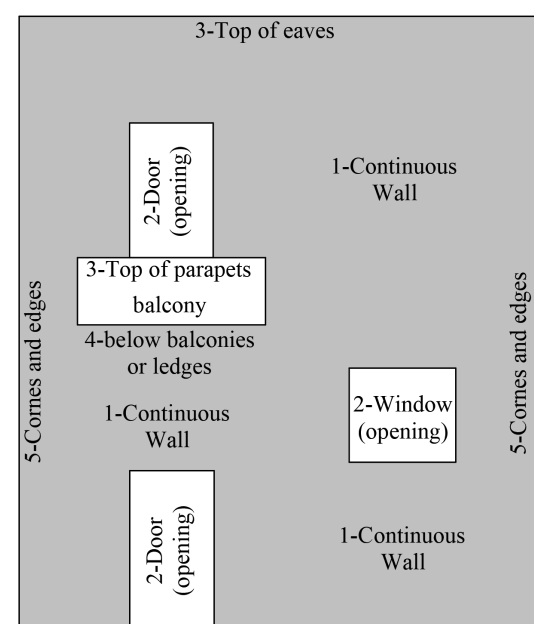


Figure 2. Typified regions of the facade
Source: Gaspar and Brito (2005) - modified by the Author

2.6 Delimitation

The BDs observed refer to the most frequent in the inspected buildings. Thus, less frequent and/or more remote pathological manifestations were excluded. This work was not aimed to evaluate the mortar, its materials and the properties, the composition, the executive method also the thickness of the render.

The approach to the BDs found refers exclusively to the EMR, ignoring defects found in paint and/or other external coating than mortar. Although the inspected buildings are all constituted with a main structure in reinforced concrete and that damage to this structure can manifest BDs in the external mortar render, these structures and their possible BDs were not studied.

3. BDs MAPPING

The mapping of the BDs was carried out using “*degradation pattern maps*”, as reported by Gaspar and Brito (2005). In addition to the regions of the facade, the types of BD with the focus of this research were horizontal crack (HC), vertical crack (VC), leaning crack (LC), mapped crack (BD), detachment with blistering (BD), detachment in plates (PD), detachment with powder (WD), vesicles (VS), light stains (LS), dark stains (DS), and fantomes (FA). When other types of BD were found in the EMR, they were assigned as the designation (OT). Thus, to differentiate the location of similar BDs, they were designated with the numeral of the typified region in front of their type, such as BDHC1 (BD type horizontal crack in region 1 - on continuous wall).

The realization of the mapping consists of assessing not only the occurrence of a certain pathological problem in each specific region of the facade, but also the significance of these problems, thus attributing a corresponding level of degradation to each BD.

In this study, four adaptations were made to the method developed by Gaspar and Brito (2005). The first adaptation involves the framing of the local problems observed in the EMR of the studied buildings and the corresponding level of degradation. Second, owing to the configuration of the buildings studied (few walls at ground level and many parking areas with stilts), pathological problems at ground level were not observed, thus motivating an adjustment in the typified regions of the facades. The third adaptation involves the evaluation of results by geographic orientation of the facade and global, and in the work carried out by Gaspar and Brito (2005), only the global parameters are presented. The fourth adaptation consists of the number of maps produced, that is, “*probability map*,” “*sensitivity map*,” and “*potential degradation map*”.

3.1 Degradation Level

As highlighted by Gaspar and Brito (2005), the level of DB degradation is defined via a qualitative analysis, in which the BDs are classified into five levels: Level 0 (no degradation) to Level 4 (very accentuated degradation), as summarized in Table 1.

3.2 Probability Map

Using the observed data, a connection between a typified region of the facade and the probability of occurrence of some BD could be established. From this connection, a probabilistic relationship is established, which can be the object of the elaboration of a “probability map” that is obtained through the mathematical calculation according to Equation (1). The resulting parameter 0 indicates that there is no probability of BD occurring, whereas parameter 1 indicates that the pathological case will occur in the region.

$$S_{(G,IT)} = \frac{\sum BD_{RG,IT}}{\sum BD_{G,IT}} \text{ or } S_{(G,IC)} = \frac{\sum BD_{RG,IC}}{\sum BD_{G,IC}} \quad (1)$$

where $S_{(G)}$ denotes the sensitivity of the facade for the manifestation of a certain group G of BD (varies between 0 and 1), where 0 represents no sensitivity to the formation of BDs to the specific group and 1 represents total sensitivity to the manifestation of defects:
 BD_{RG} represents the number of BDs in group G that occur in the R region,
 R represents the region of incidence (1 to 5),
 BD_G represents the quantity of all BDs in group G (cracks, stains, or detachments),
 IC and IT correspond to the methods of quantifying BDs, that is, incidence and intensity, respectively.

Table 1. Degradation Levels

Degradation Level	Visual defects observed	Strategic action
Level 0 - No degradation (desirable situation)	➤ No visual degradation was observed	It does not require attention
Level 1 - Very mild degradation signals (suitable condition)	➤ Leve Light superficial staining, without the presence of efflorescences	Periodic visual assessment
Level 2 - Mild degradation signals (acceptable condition)	<ul style="list-style-type: none"> ➤ Linear cracks (vertical, horizontal or linear) isolated or widely spaced, with few repetitions along the facade ➤ Accentuated surface staining, with mild signs of efflorescence or presence of moisture ➤ Localized presence of mold or mildew 	Surface cleaning by brushing and washing
Level 3 - Wide degradation (minimum acceptable condition)	<ul style="list-style-type: none"> ➤ Intense linear cracks (vertical, horizontal or inclined), occurring in several parts, but spaced apart ➤ Isolated mapped cracks ➤ Damaged corners or edges ➤ Localized infiltrations ➤ Light stains (efflorescences) ➤ Fantomes ➤ Alteration of tonality and surface texture 	Repair and protection
Level 4 - Very severe degradation (worst condition / not acceptable)	<ul style="list-style-type: none"> ➤ Linear cracks very intense and not widely spaced (agglomerated) ➤ Mapped cracks agglomerated or with many repetitions ➤ Detachments ➤ Vesicles 	Partial or complete replacement of the damaged element

Source: Gaspar and Brito (2005) - modified by the Author

3.3 Sensibility Map

In addition to the probability of the pathological case occurring, a connection between each typified region of the facade and the possibility of the appearance of a specific pathological case could be established. From this connection, a relationship that expresses the sensitivity of the typified region to a specific BD is established, in which it is possible to elaborate a “*sensitivity map*” or distribution map of the BD, which is the object of the expression resulting from Equation (2). A resulting

parameter of 0 indicates that the region has no sensitivity at all for the manifestation of this pathological case, whereas p indicates that the region is sensitive to the manifestation of the pathological case.

$$S_{(G,IT)} = \frac{\sum BD_{RG,IT}}{\sum BD_{G,IT}} \text{ or } S_{(G,IC)} = \frac{\sum BD_{RG,IC}}{\sum BD_{G,IC}} \quad (2)$$

where $S_{(G)}$ denotes the sensitivity of the facade to the manifestation of a specific group G of BD (varies between 0 and 1), where 0 represents no sensitivity to the formation of BDs to the specific group and 1 represents total sensitivity to the manifestation of defects:

BD_{RG} represents the number of all BDs in group G that occur in the region of BD formation to the specific group, and 1 represents totally sensitive to the manifestation of defects,

R represents the region of incidence (1 to 5),

BD_G represents the quantity of all BDs in group G (cracks, stains, or detachments),

IC and IT represents the methods of quantifying BDs, that is, incidence and intensity, respectively.

3.4 Potencial Degradation Map

A map of degradation potential could be drawn by weighting the BDs by their corresponding level of degradation, that is, which region is more or less degraded, according to qualitative parameters of degradation listed in Table 1 and Equation (3).

$$DP_{(R,IT)} = \frac{\sum BD_{R,IT} \cdot l_{MP,R,IT}}{\sum BD_{IT} \cdot l_{MP,IT}} \text{ or } DP_{(R,IC)} = \frac{\sum BD_{R,IC} \cdot l_{MP,R,IC}}{\sum BD_{IC} \cdot l_{MP,IC}} \quad (3)$$

where $DP_{(R)}$ denotes the degradation potential of a given facade region (varies between 0 and 1), where 0 represents no potential and 1 represents the maximum potential for degradation:

BD_R denotes the amount of BD that occurs in región R,

$l_{BD,R}$ denotes the level of BD degradation that occurs in region R,

R denotes the region of incidence (1 to 5),

BD denotes the quantity of all BDs,

l_{BD} denotes the level of general degradation considering all BDs,

IC and IT correspond to the methods of quantifying BDs, that is, incidence and intensity, respectively.

4. RESULTS

4.1 Local climatic conditions

The local climate is classified as Aw according to the global categorization of the Köppen and Geiger climatic types, where A refers to Group A - Tropical and w represents savanna climate with dry winter. Based on the records of climatic events observed in the period from January 2015 to May 2020 provided by the INMET and CLIMATEMPO climatic portals, the climate is characterized by high daily temperatures, with maximum and minimum peaks of approximately 40 and 5 °C, respectively. The average annual temperature obtained was approximately 25 °C, whereas the thermal amplitude obtained for the same period varied between 10 and 15 °C. Rainfall data, wind direction, and speed were also consulted for the same period. For pluviometry, higher

and lower concentrations of precipitation were observed during summer (hot season) and winter (colder season), respectively, characterizing the seasonality, as highlighted by the Köppen and Geiger classification. The local atmospheric pressure suffers little daily variation, highlighting the average values from 950 to 960 hPa, with the maximum atmospheric pressure peaks following the driest season (winter), while the minimum the wettest season (summer). For the prevailing winds, these are quite present in the cardinal directions combined with the East direction and practically nonexistent in the other directions.

4.2 BDs Overview

In total, 4351 BDs were detected for M-INT and 481 BDs for the M-INC, adding all types, locations, and buildings. Table 2 summarizes the total quantification for each type of BD, while Table 3 summarizes the total quantification for each group of BD and the average number of repetitions. The total of each building is shown in Figure 3. Similar to what was observed by Gaspar and Brito (2005), in which it was established that most of the buildings (93%) of the facades showed some signs of degradation, the BD of the present case study was observed in all (100%) the samples.

Using M-INC, the greatest occurrences were cracks and stains with the same amount and percentage, followed by detachments, as summarized in Table 3. Additionally, Terra (2001), Padaratz et al. (2002) obtained similar results, with more representation of the fissures, followed by the stains and finally the detachments.

Segat (2005) and Mazer et al. (2013) observed the predominance of cracks in the referred method, followed by detachments and stains. One factor to be highlighted is the location of the studies of the aforementioned works, and in the studies whose results were similar. They present a particularity in common, namely, hotter and more humid summers. However, the difference in climate did not change the predominance of cracks in this method.

Stains are much more frequent than other BDs. However, stains and cracks have the same recurrence. Carrying out a regional climatological assessment, in addition to the preferential direction of the winds, the daily cyclical temperature variation, notably observed by the large daily thermal amplitude, is a very significant factor.

Table 2. Number of BDs by type, location and method of quantification

<i>BUILDING DEFECT (BD)</i>	<i>M-INC QUANTIFICATION</i>					<i>M-INT QUANTIFICATION</i>				
	<i>NORT H</i>	<i>SOUT H</i>	<i>EAS T</i>	<i>WES T</i>	<i>TOTA L BD</i>	<i>NORT H</i>	<i>SOUT H</i>	<i>EAS T</i>	<i>WES T</i>	<i>TOTA L BD</i>
BDHC1	11	8	13	13	45	52	74	36	53	215
BDHC2	2	0	5	2	9	2	0	8	4	14
BDHC3	6	4	2	3	15	26	18	2	14	60
BDHC4	0	1	2	1	4	0	1	15	45	61
BDHC5	3	0	0	0	3	4	0	0	0	4
BDVC1	5	6	5	1	17	30	19	14	2	65
BDVC2	3	1	5	1	10	5	2	43	14	64
BDVC3	1	1	1	1	4	1	7	1	3	12
BDVC4	0	0	0	0	0	0	0	0	0	0
BDVC5	5	3	2	2	12	15	6	4	7	32
BDLC1	4	7	8	5	24	21	66	30	18	135
BDLC2	1	1	5	3	10	4	2	80	35	121
BDLC3	3	2	1	1	7	4	3	2	1	10
BDLC4	2	1	0	0	3	13	100	0	0	113
BDLC5	0	0	0	2	2	0	0	0	3	3
BDMC1	6	6	9	7	28	72	8	30	57	167

BDMC2	1	1	1	0	3	1	4	1	0	6
BDMC3	1	1	1	1	4	1	1	2	4	8
BDMC4	0	0	0	0	0	0	0	0	0	0
BDMC5	2	1	1	2	6	12	2	2	10	26
BDLS1	2	5	2	2	11	6	32	7	20	65
BDLS2	0	0	0	1	1	0	0	0	1	1
BDLS3	0	0	1	1	2	0	0	1	9	10
BDLS4	0	0	0	0	0	0	0	0	0	0
BDLS5	1	1	0	0	2	8	1	0	0	9
BDDS1	7	7	8	10	32	45	67	134	37	283
BDDS2	7	10	12	9	38	298	261	442	271	1272
BDDS3	21	21	22	22	86	148	135	166	195	644
BDDS4	5	6	8	5	24	108	61	327	269	765
BDDS5	4	1	2	2	9	16	4	2	4	26
BDFA1	0	0	1	0	1	0	0	3	0	3
BDFA2	0	0	0	0	0	0	0	0	0	0
BDFA3	0	0	0	0	0	0	0	0	0	0
BDFA4	0	0	0	0	0	0	0	0	0	0
BDFA5	0	0	0	0	0	0	0	0	0	0
BDBD1	0	0	2	1	3	0	0	2	1	3
BDBD2	0	0	0	0	0	0	0	0	0	0
BDBD3	0	1	0	0	1	0	8	0	0	8
BDBD4	0	0	0	0	0	0	0	0	0	0
BDBD5	0	0	0	0	0	0	0	0	0	0
BDPD1	0	1	3	1	5	0	2	4	1	7
BDPD2	1	0	1	0	2	3	0	1	0	4
BDPD3	0	1	0	1	2	0	1	0	1	2
BDPD4	0	0	0	0	0	0	0	0	0	0
BDPD5	0	0	0	0	0	0	0	0	0	0
BDWD1	6	3	6	4	19	14	3	20	26	63
BDWD2	0	3	0	1	4	0	15	0	1	16
BDWD3	3	5	4	3	15	4	11	9	9	33
BDWD4	0	0	0	0	0	0	0	0	0	0
BDWD5	0	1	0	1	2	0	1	0	3	4
BDVS1	1	1	4	1	7	1	1	4	1	7
BDVS2	0	1	0	1	2	0	1	0	1	2
BDVS3	3	0	2	0	5	3	0	3	0	6
BDVS4	0	0	0	0	0	0	0	0	0	0
BDVS5	1	0	0	0	1	1	0	0	0	1
BDOT2	1	0	0	0	1	1	0	0	0	1
Total	119	112	139	111	481	919	917	1395	1120	4351

Table 3. Number of BDs by group and method of quantification

<i>BD GROUP</i>	M-INT		M-INC		AVERAGE NUMBER OF REPETITIONS (M-INT/M-INC)
	ABSOLUTE	RELATIVE	ABSOLUTE	RELATIVE	
<i>Cracks</i>	1116	25,65%	206	42,83%	5,42
<i>Detachments</i>	156	3,59%	68	14,14%	2,29
<i>Stains</i>	3078	70,74%	206	42,83%	14,94
<i>Other types</i>	1	0,02%	1	0,21%	1,00
Total	4351	100,00%	481	100,00%	-

Table 4. Number of BDs by solar orientation and quantification method

FACADE	M-INC		M-INT	
N-NORTH	119	24,74%	919	21,12%
S-SOUTH	112	23,28%	917	21,08%
E-EAST	139	28,90%	1395	32,06%
W-WEST	111	23,08%	1120	25,74%
TOTAL	481	100,00%	4351	100,00%

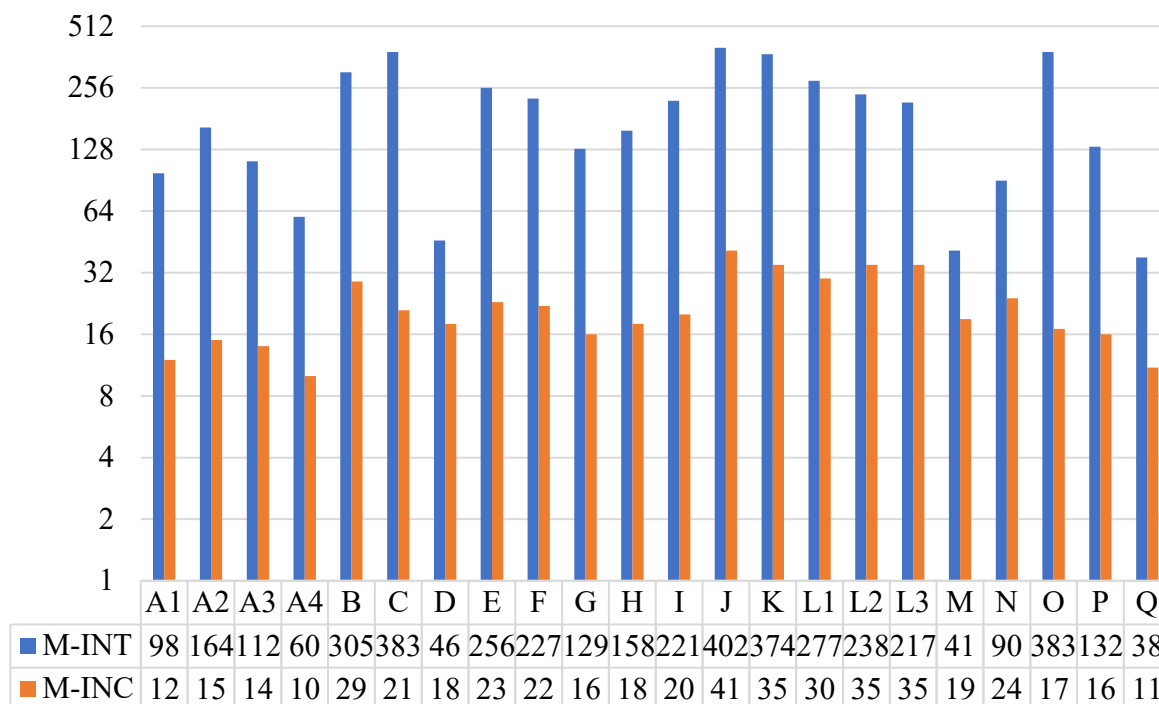


Figure 3. Number of BDs per building and quantification method

Considering solar orientation, in relation to M-INC, the east and north facades were the ones with the most problems, followed by the south and west facades with practically the same quantity and percentage. In the work carried out by Mazer et al. (2013), problems predominated in the north and west facades, followed by the east and south facades. For M-INT, the east and west facades were the most significant, followed by the north and south facades with practically similar quantity and percentage. The number of BDs by solar orientation and the method are listed in Table 4. In the work carried out by Antunes (2010), the distribution of problems occurred in decreasing order on the north, south, west, and east facades, whereas Consoli (2006) observed a greater occurrence on the south facade, followed by the east, west, and north facades.

Considering the location of BDs by M-INT, there was a predominance of stains in the vicinity of openings, tops, balconies, or ledges, whereas cracks predominate in continuous walls and in the corners. The results obtained are close to the parameters reported by Gaspar and Brito (2005) and Freitas (2012), although the study region is in different climates according to the Köppen and Geiger classification, that is, Fernandópolis-SP (Aw), Lisbon, Alcochete, and Tavira (Csa) and Goiania (Aw). The same parameters and representativeness of problems were also verified using M-INC, with the exception of continuous wall stains, which overcame detachments. The results of localization by group of BD and localization are presented in Figures 4 and 5.

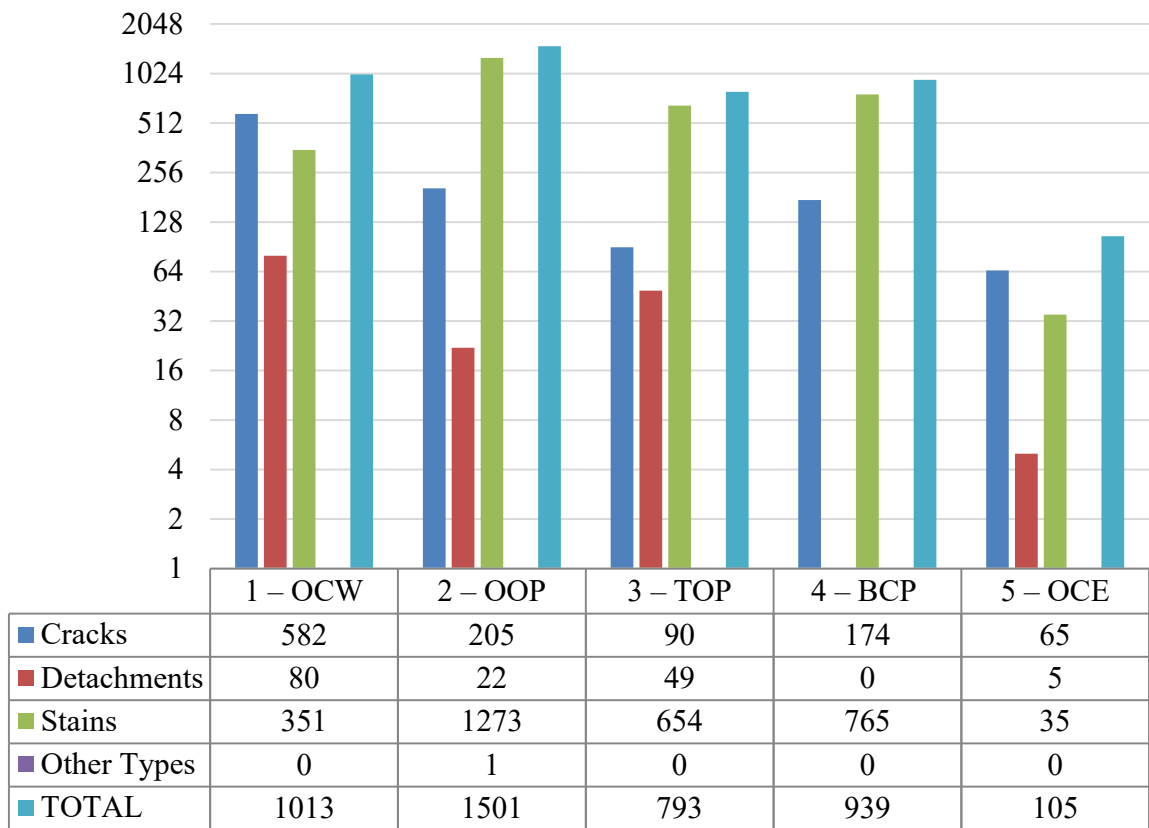


Figure 4. Location of BDs by group and location - Intensity Method

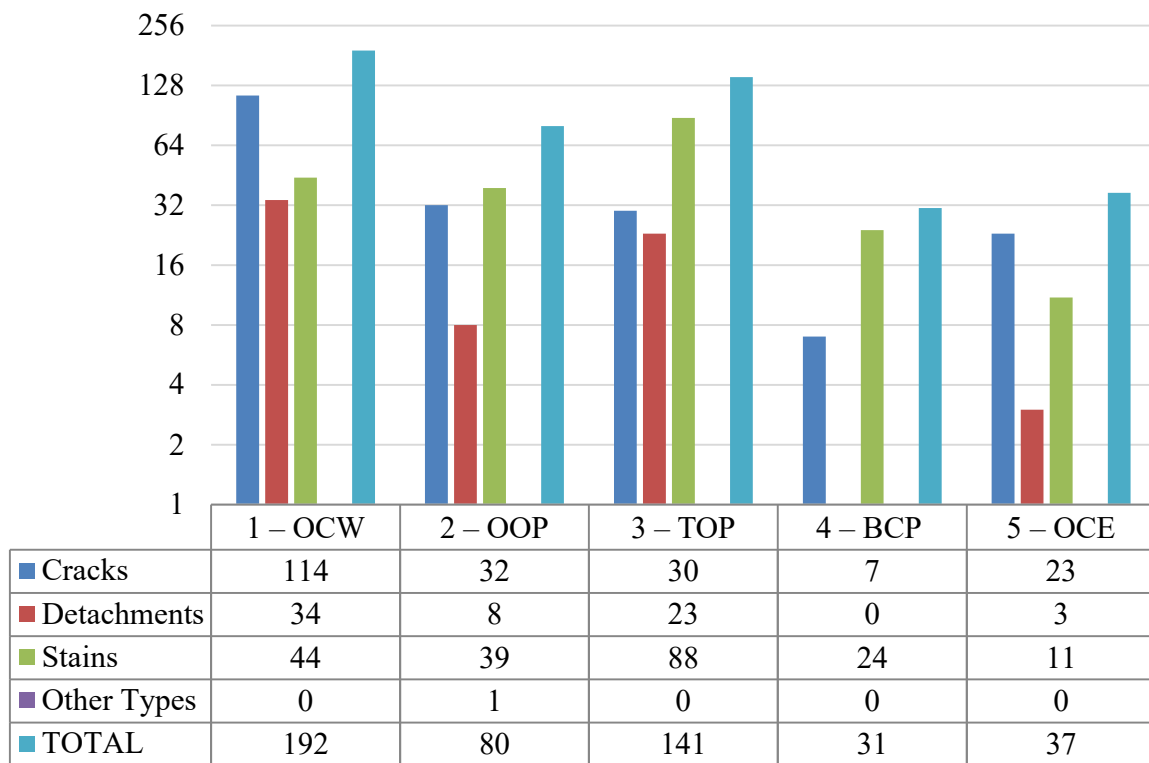


Figure 5. Location of BDs by group and location - Incidence Method

4.3 Probability of occurrence of BD and its Degradation Potential

The probability of defects occurring in each typified region of the building for each specific and general solar orientation as well as intensity and incidence methods is shown in Figures 6 and 7. The values on the right indicate the average level of degradation for each typified region of the facade. In general, for both quantification methods, the highest probability of occurrence of BD occurs in regions 1–in continuous walls, region 2–around openings, and region 3–at the top (parapets and eaves), as observed by Gaspar and Brito (2005), Antunes (2010), Freitas (2012), and Souza et al. (2019). Nevertheless, the levels of degradation were more significant in these regions. Except for the parameters obtained by Gaspar and Brito (2005), the degradation levels of regions 2 and 4 were shown to be more significant in this study.

In general, there are significant differences between the results of each method applied in the quantification for the determination of the degradation potential (PD). Therefore, the recurrence of effects for each specific method occurs in a different way, that is, one for the total number of repetitions and another for the number of times it occurs, without considering the repetitions for the same facade. In this way, potentialization of effects can be identified for each method and BD. As highlighted in Table 3, although there is the same recurrence for stains and cracks, there is a much higher number of repetitions of stains against cracks, hence the importance of considering them independently and, nevertheless, interpreting their results.

Considering all solar orientations, there is a greater potential for degradation in region 1–in continuous walls than in region 3–at the top (parapets and eaves) for M-INC. For M-INT, there is a greater potential for degradation in region 2 (around openings), followed by region 1 (continuous walls). Gaspar and Brito (2005) also observed a crucial degradation in region 1 in continuous walls. The degradation potential (PD) in each typified region of the building for each specific and general solar orientation as well as intensity and incidence methods is shown in Figures 8 and 9.

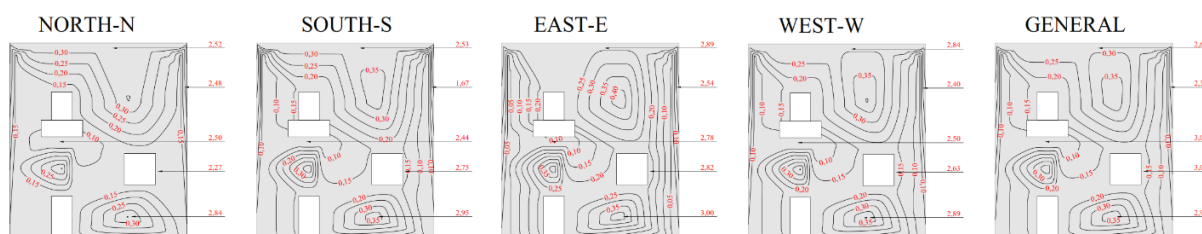


Figure 6. Map of Probability of occurrence of BDs - Incidence Method
 OBS: values on the right represent the average level of degradation of each typified region

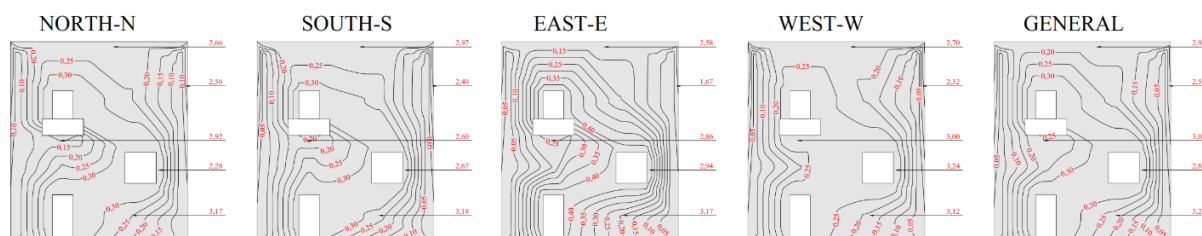


Figure 7. Map of Probability of occurrence of BDs - Intensity Method
 OBS: values on the right represent the average level of degradation of each typified region

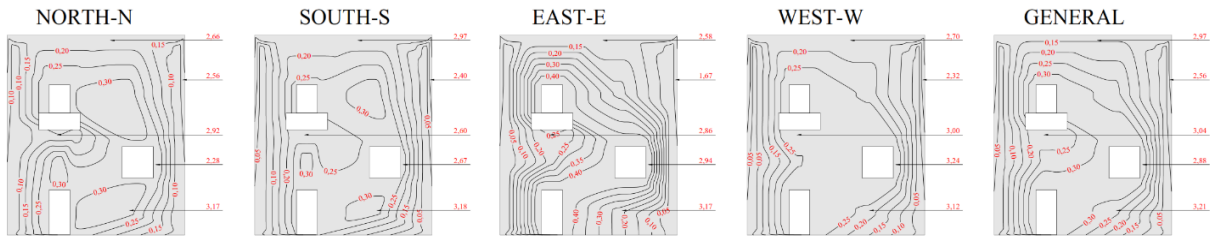


Figure 8. Potential Map of Degradation of the Region - Incidence Method
 OBS: values on the right represent the average level of degradation of each typified region

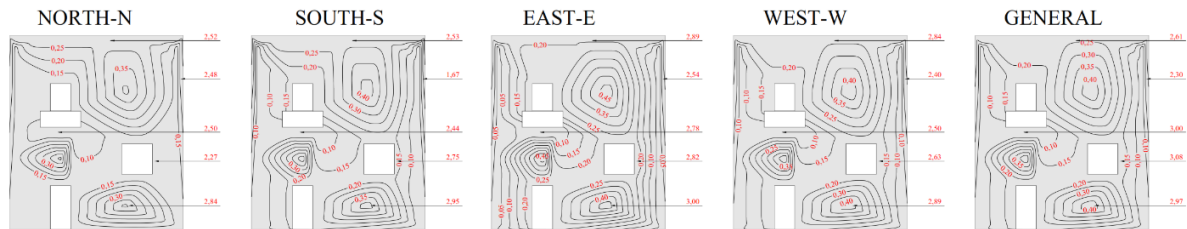


Figure 9. Potential Map of Degradation of the Region - Intensity Method
 OBS: values on the right represent the average level of degradation of each typified region

4.4 Sensitivity to the manifestation of BDs

Sensitivity to the formation of BD refers to the sensitivity of each typified region to the formation of a specific type of BD, in which it is presented by the “*Sensitivity Map*”

4.4.1 Facade sensitivity to crack formation

In decreasing order, there is a greater predisposition to the formation of cracks in regions 1, 2, and 5. Cementitious matrices are easily affected by hygrothermal movements due to important variations in temperature and humidity. In the presence of large masses or strain restrictions, cracking is inevitable if the mortar used does not have specific properties for this purpose.

In the present case study, a large daily temperature range (about 15°C), cyclic variations in humidity as well as atmospheric pressure with small daily and seasonal variations (practically constant for a short period) was observed. These particularities certainly contribute to the hygrothermal movement of the EMR, especially in the continuous walls (region 1), which are restricted to free deformation by the mortar itself, as well as representing the largest exposed surface, therefore, more subject to the effects of temperature and humidity, justifying being the most affected region.

In addition, even if there was no such important daily thermal amplitude, the temperature between EMR and air are different and, in the presence of constant atmospheric pressure, there is a contribution to the condensation of water vapor inside the mortar matrix, also causing hygrothermal movements.

The cracks present in these regions tend to obtain levels of degradation above 2.00 and highlighting average levels above 3.00, which is the minimum acceptable. Such observations were also reported by Gaspar and Brito (2005), Antunes (2010), Freitas (2012), and Souza et al. (2019). Sensitivity maps of crack-formation for the two quantification methods are presented in Figures 10. and 11.

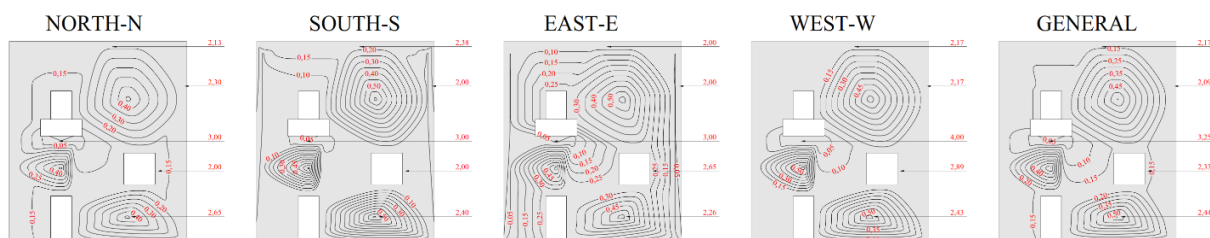


Figure 10. Sensitivity to crack formation - Incidence Method
 OBS: values on the right represent the average level of degradation of each typified region

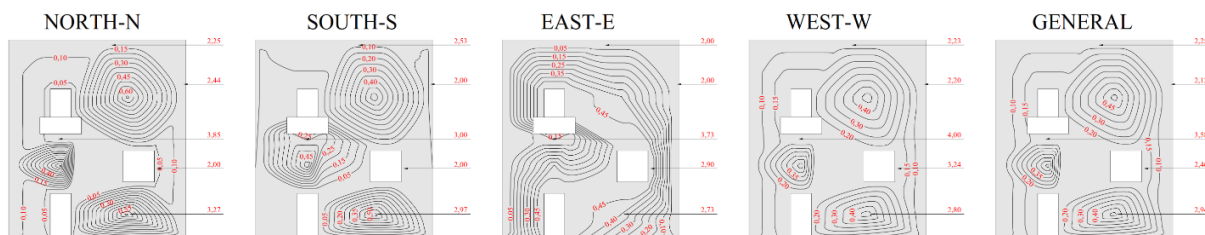


Figure 11. Sensitivity to crack formation - Intensity method
 OBS: values on the right represent the average level of degradation of each typified region

4.4.2 Facade sensitivity to stain formation

In decreasing order, there is a greater predisposition to the formation of dark stains in regions 3, 1, and 2. Light stains are rare and recurrent; therefore, there is a large predominance of dark stains. There are too many stains on facades with solar orientation facing the prevailing wind dimensions (combined with the cardinal east direction). This could indicate that the atmospheric air in the region may have a high number of solid particles in suspension and hence the “easy sensitivity” to this predisposition. The aforementioned regions have differences and similarities regarding the mechanisms of action in the formation of BDs, and they have the same type of sensitivity. Gaspar and Brito (2005) attributed the sensitivity to the action of directed rain, specifically in those that are minimally protected by covers and overhangs. None of the study buildings have outstanding coverings for the facade panels, and this situation could also cause the problem. Figures 12 and 13 show the sensitivity maps for the formation of stains for each quantification method.

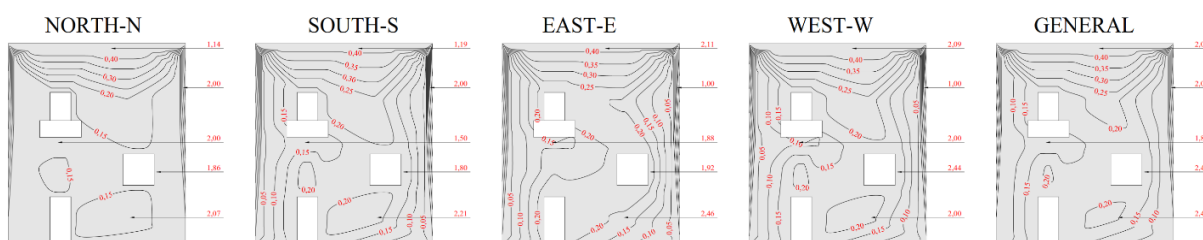


Figure 12. Sensitivity to staining - Incidence method
 OBS: values on the right represent the average level of degradation of each typified region

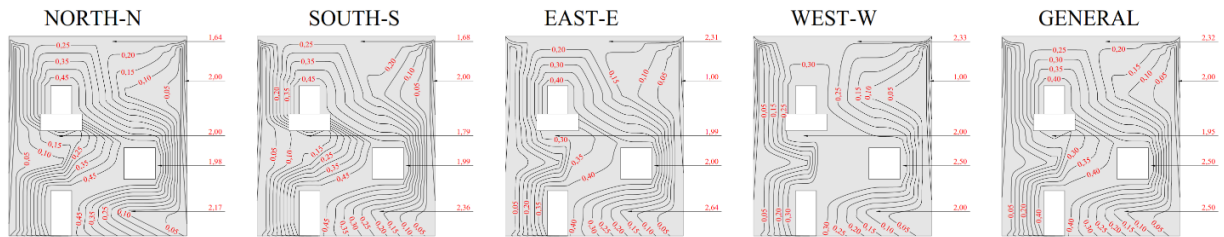


Figure 13. Sensitivity to staining - Intensity method
 OBS: values on the right represent the average level of degradation of each typified region

4.4.3 Facade sensitivity to detachments

The predisposition for the formation of detachments is more prevalent in regions 1, 3, and 2. This condition was also verified by Antunes (2010) and Souza et al. (2019). The detachments present in all the most sensitive regions were those with powder. This BD occurs for various reasons, but its application at high temperatures should be considered. According to a survey of the local climate, temperatures in the region are normally high at all times of the year, in addition to a high daily thermal amplitude, on the order of 15 °C. Therefore, when applying or improving the mortar property to resolve these effects, this condition must be observed.

Parallel to detachment, cracks are more recurrent and frequent also in Region 1 which, when present, contribute to the accumulation of aggressive agents in this location, favoring the potentialization of problems translated into detachment formation (highest degradation).

In addition to powdery detachment, there is a predominance of vesicles and plate detachments, manifestations commonly associated with late expansive reactions, either owing to a deficiency in the composition of the mortar trace or in the presence of impurities. Notably, these BDs in the vicinity of regions 2 and 3 occur in supposedly more humid locations and with a predominance of superficial staining.

Sensitivity maps for the formation of displacements for each typified region of the facade and the quantification method are shown in Figures 14 and 15.

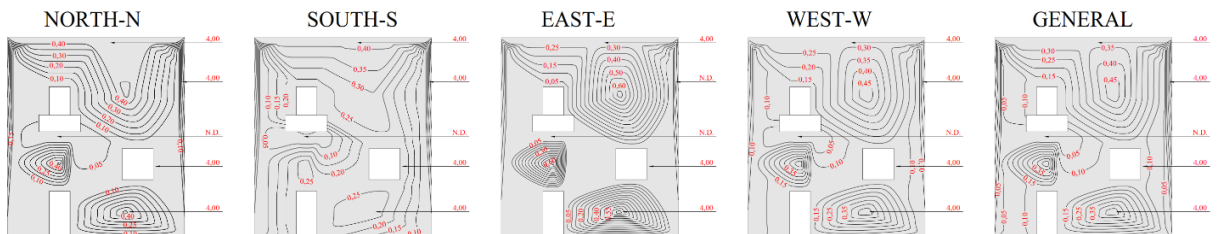


Figure 14. Sensitivity to the formation of detachments - Incidence Method
 OBS: values on the right represent the average level of degradation of each typified region

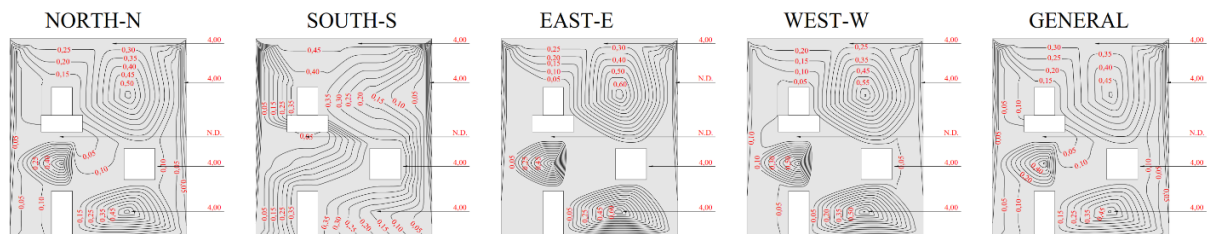


Figure 15. Sensitivity to the formation of detachments - Intensity method
 OBS: values on the right represent the average level of degradation of each typified region

5. CONCLUSIONS

Based on the results obtained, the following conclusions were observed, highlighting the climate and BD parameters:

- The local climate is characterized by a large daily thermal amplitude (on the order of 15 °C) on average.
- Increased humidity and rainfall accompany the hottest season (summer).
- Winds are more frequent and faster in the cardinal directions and the east direction (E).
- The local atmospheric pressure is practically constant in all seasons of the year.
- The relative humidity of the air concomitantly declines with the decline in daily temperatures, observing drier weather in winter and more humid in summer.
- BDs was established in all the buildings observed.
- There is the same recurrence of stains and fissures; however, the stains are repeated more significantly, and then more intense when compared to the fissures.
- The detachments are less recurrent and frequent than the other BDs studied in this case study.
- The quantification of BDs using the different methods was effective.
- The comparison of the quantity of BDs between the quantification methods allows us to observe those that are more recurrent and with more repetitions of problems, indicating the possibility of problems located in specific buildings.
- The same recurrence of stains and cracks was observed, although the spots are repeated with much more significance, causing an excessively high number of stains predominated in the east and west directions.
- There is strong evidence that the local direction of the winds (combined with the cardinal east direction) favors the formation of stains for these facades.
- The large daily thermal amplitude is also another strong indication that the local climate favors the formation of cracks and detachments, whether by hygrothermal movements or even the temperature at which the mortar is applied.
- The results were more similar to studies with climates of the same particularity (dry winter and wet summer).
- Considering the number of problems, given the number of repetitions of stains in the east and west directions, for the intensity method, a greater number of anomalies was observed in the aforementioned facades, followed by the north and south facades, whereas the predominance was on the east facade, followed by north, south, and west for M-INC.
- As for the typified regions of the facade, a greater probability of occurrence of BDs was observed in regions 1, 2, and 3 than in regions 2, 4, and 5.
- The potential for degradation in each region varies according to the method, and the most significant degradations are found in regions 1, 2, and 3.
- Regions 1, 2, and 5 were more sensitive to the formation of cracks and fissures than the other regions.
- There was a greater sensitivity to the formation of stains in regions 3, 1, and 2 than in the other regions.
- Significant detachment sensitivity was observed in regions 1, 3, and 2 than in the other regions.

6. ACKNOWLEDGEMENTS

We acknowledge the Dias & Cardozo company for partial financing this research, a very important private initiative in fostering research.

7. REFERENCES

- Alvares, C. A., Stape, J. L., Sentelhas, P. C., de Moraes Gonçalves, J. L., Sparovek, G. (2013), *Köppen's climate classification map for Brazil*. Meteorologische Zeitschrift. 22(6):711-728. <https://www.doi.org/10.1127/0941-2948/2013/0507>.
- Ansah, M. K., Chen, X., Yang, H., Lu, L., Lam, P. T. I. (2020), *An integrated life cycle assessment of different façade systems for a typical residential building in Ghana*. Sustainable Cities and Society. 53:1-13. <https://doi.org/10.1016/j.scs.2019.101974>.
- Antunes, G. R. (2010), “*Estudo de manifestações patológicas em revestimentos de fachada de Brasília – Sistematização da incidência de casos*”, Dissertação (Mestrado em Engenharia Civil), Faculdade de Tecnologia, Universidade de Brasília.
- Bauer, L. A. F. (2017), “*Materiais de Construção*”. Volume 2. 5ª ed. Revisada. LTC Editora. Rio de Janeiro. 538p.
- Bauer, E., Milhomem, P. M., Aidar, L. A. G. (2018), *Evaluating the damage degree of cracking in facades using infrared thermography*. Journal of Civil Structural Health Monitoring. 8:517-528. <https://doi.org/10.1007/s13349-018-0289-0>.
- Carvalho, C. G., Flores-Colen, I. e Faria, P. (2015), *Rehabilitation of renders of old buildings in Portugal: Survey, supporting methodology proposal and case study*. Structural Survey. 33(4/5):337-353. <https://doi.org/10.1108/SS-04-2015-0024>.
- Charisi, S., Thiis, T. K., Stefansson, P., Burud, I. (2018), *Prediction model of microclimatic surface conditions on building façades*. Building and Environment. 128:46-54. <https://doi.org/10.1016/j.buildenv.2017.11.017>.
- Consoli, O. J. (2006), “*Análise da durabilidade dos componentes das fachadas de edifícios sob a ótica do projeto arquitetônico*”, Dissertação (Mestrado em Engenharia Civil), Programa de Pós-Graduação em Engenharia Civil, Universidade Federal de Santa Catarina.
- Dorfman, G., Petrucci, H. M. C. (1989), “*Recomendações para fachadas com vistas a sua maior durabilidade e facilidade de manutenção*”, Simpósio Sobre Patologia das Edificações, CPGEC/UFRGS, Porto Alegre: RS(BR), pp. 251-261.
- Fabbri, K., Gaspari, J., Bartoletti, S., Antonini, E. (2020), *Effect of facade reflectance on outdoor microclimate: An Italian case study*. Sustainable Cities and Society. 54:1-12. <https://doi.org/10.1016/j.scs.2019.101984>.
- Ferreira, C., Canhoto, L., Silva, A., Brito, J. (2019), *Stochastic Petri-net models to predict the degradation of ceramic claddings*. Building Research & Information. 47(6):697-715. <https://doi.org/10.1080/09613218.2018.1501873>.
- Flores-Colen, I. e Brito, J. (2010), *A systematic approach for maintenance budgeting of buildings façades based on predictive and preventive strategies*. Construction and Building Materials. 24(9):1718-1729. <https://doi.org/10.1016/j.conbuildmat.2010.02.017>.
- FREITAS, J. G. (2012), “*A influência das condições climáticas na durabilidade dos revestimentos de fachada: estudo de caso na cidade de Goiânia-GO*”, Dissertação (Mestrado em Engenharia Civil), Escola de Engenharia Civil, Universidade Federal de Goiás.
- Gaspar, P., Brito, J. (2005), *Mapping defect sensitivity in external mortar renders*. Construction and Building Materials. 19(8):571-578. <https://doi.org/10.1016/j.conbuildmat.2005.01.014>.

- Maciel, A. C. F., Carvalho, M. T. (2019), *Operational energy of opaque ventilated façades in Brazil*. Journal of Building Engineering. 25:1-10. <https://doi.org/10.1016/j.jobe.2019.100775>.
- Mazer, W., Silva, L. M. R., Lucas, E., Santos, F. M. C. (2016), *Evaluation of pathological manifestations in buildings in terms of geographical orientation*. Revista ALCONPAT. 6(2):145-156. <https://doi.org/10.21041/ra.v6i2.135>.
- Padaratz, I. J., Canova, J. A., de Mori, L. M., Botter, R. R. (2002), “*Incidências patológicas em fachadas e áreas comuns de edificações para ensino - caso do campus da Universidade Estadual de Maringá*”, Encontro Nacional de Tecnologia do Ambiente Construído, Foz do Iguaçu: PR(BR), pp. 1453–458.
- Postingher, C. M., Kremer, B. M., Rossatto, F. C., Pacheco, F., Christ, R. (2019), “*Avaliação das manifestações patológicas em revestimentos argamassados externos com VANT: estudo de caso em edificação multifamiliar do município de Garibaldi-RS*”, XV Congresso Latinoamericano de Patología de Construcción y XVII Congreso de Control de Calidad en la Construcción, CONPAT. 2:1-15. <https://doi.org/10.21041/CONPAT2019/V2PAT296>.
- Prefeitura de Fernandópolis (2012), “*Fernandópolis – nossa história nossa gente*”. Vol. II. Ed. Anglo. Santo Amaro.
- Rodrigues, J. D. (2014), *Defining, mapping and assessing deterioration patterns in stone conservation projects*. Journal of Cultural Heritage. 16(3):267-275. <https://doi.org/10.1016/j.culher.2014.06.007>.
- Saviz, M., Luc E, C., Saeed, M. M. (2020), *Design strategies using multi-criteria decision-making tools to enhance the performance of building façades*. Journal of Building Engineering. 30:1-28. <https://doi.org/10.1016/j.jobe.2020.101274>.
- Segat, G. T. (2005), *Manifestações patológicas observadas em revestimentos de argamassa: estudo de caso em conjunto habitacional popular na cidade de Caxias do Sul (RS)*, Dissertação (Mestrado Profissionalizante em Engenharia), Universidade Federal do Rio Grande do Sul.
- Sentena, J. A. A., Kazmierczak, C. de S., Krein, L. A. (2018), *Degradação de revestimentos de argamassa com finos de resíduos de concreto por ciclos térmicos*. Ambiente Construído. 18(1):211-224. <https://doi.org/10.1590/s1678-86212018000100217>.
- Silva, A. Dias, J. L., Gaspar, P. L., Brito, J. (2013), *Statistical models applied to service life prediction of rendered façades*. Automation in Construction. 30:151-160. <https://doi.org/10.1016/j.autcon.2012.11.028>.
- Silva, A., Brito, J. de, Gaspar, P. L. (2011), *Service life prediction model applied to natural stone wall claddings (directly adhered to the substrate)*. Construction and Building Materials. 25(9): 3674-3684. <https://doi.org/10.1016/j.conbuildmat.2011.03.064>.
- Silva, A., Brito, J., Gaspar, P. L. (2018), *A comparative multi-criteria decision analysis of service life prediction methodologies for rendered façades*. Journal of Building Engineering. 20:476-487. <https://doi.org/10.1016/j.jobe.2018.08.009>.
- Souza, J. Silva A., Brito, J. Bauer, E. *Service life prediction of ceramic tiling systems in Brasília-Brazil using the factor method*. Construction and Building Materials. 192:38-49. <https://doi.org/10.1016/j.conbuildmat.2018.10.084>.
- Souza, J. S., Piazzarollo, C. B., Bauer, E. (2019), “*Degradação nas diferentes zonas de fachadas em sistemas de revestimento*”, Simpósio Brasileiro de Tecnologia das Argamassas, XIII STBA, Goiania: GO(BR), pp. 136-144.
- Takeda, O. T., Mazer, W. (2018), *Potential of thermographic analysis to evaluate pathological manifestations in façade cladding systems*. Revista ALCONPAT. 8(1):38-50. <https://doi.org/10.21041/ra.v8i1.181>.
- Terra, R. C. (2001), “*Levantamento de manifestações patológicas em revestimentos de fachada de edificações da cidade de Pelotas*”, Dissertação (Mestrado em Engenharia), Universidade Federal do Rio Grande do Sul.

Thomaz, E. (2020), “*Trincas em edifícios: causas, prevenção e recuperação*”. 2. ed. 1ª reimp. São Paulo, Ed. Oficina de Textos.

Vieira, S. M., Silva, A., Sousa, J. M. C., Brito, J., Gaspar, P. L. (2015), *Modelling the service life of rendered facades using fuzzy systems*. Automation in Construction. 51:1-7. <https://doi.org/10.1016/j.autcon.2014.12.011>.

Documentation of the pathological manifestations of the Portico of the Cultural Baptism of Goiânia - *Art Déco* historical monument

T. L. Pio Santos^{1*}, P. F. Silva Júnior¹

*Contact author: taislara.19@gmail.com

DOI: <https://doi.org/10.21041/ra.v11i3.531>

Reception: 19/02/2021 | Acceptance: 03/08/2021 | Publication: 01/09/2021

ABSTRACT

This article aims to present the methodology for the inspection and mapping of pathological manifestations of the Portico of Cultural Baptism of Goiânia. It is a monument from the beginning of the 1940s, representative of the Art Deco architectural style. In 2003 this monument was listed by the National Historical and Artistic Heritage Institute, but despite its invaluable historical importance, the structure has several pathological manifestations. To achieve this objective, the following procedures were performed: (1) visual inspection; (2) photographic record; (3) anamnesis and (4) trials. The tests performed were sclerometer, cover meter, and strain measurement. The main pathological manifestations identified were cracking, mortar detachment, reinforcement corrosion and excessive deformation.

Keywords: pathological manifestations; diagnosis; historical monument; art déco.

Cite as: Pio Santos, T. L., Silva Júnior, P. F. (2021), "*Documentation of the pathological manifestations of the Portico of the Cultural Baptism of Goiânia - Art Déco historical monument*", Revista ALCONPAT, 11 (3), pp. 108 – 122, DOI: <https://doi.org/10.21041/ra.v11i3.531>

¹Instituto Federal de Goiás, R. São Bartolomeu, s/n - Vila Esperança, Luziânia - GO, 72811-580, Brasil

Contribution of each author

In this work, author Taís Lara Pio Santos contributed with the data collection, carrying out of the tests, analysis and discussions of the results and the writing of it. The author Paulo Francinete Silva Júnior contributed with the original idea, development of essays, general coordination and review of the essay.

Creative Commons License

Copyright 2021 by the authors. This work is an Open-Access article published under the terms and conditions of an International Creative Commons Attribution 4.0 International License ([CC BY 4.0](https://creativecommons.org/licenses/by/4.0/)).

Discussions and subsequent corrections to the publication

Any dispute, including the replies of the authors, will be published in the second issue of 2022 provided that the information is received before the closing of the first issue of 2022.

Documentação das manifestações patológicas do Pórtico do Batismo Cultural de Goiânia - monumento histórico *Art Déco*

RESUMO

Este artigo tem o objetivo de apresentar a metodologia para a inspeção e o mapeamento das manifestações patológicas no monumento Pórtico do Batismo Cultural de Goiânia. É um monumento do início dos anos 40 do século XX, representante do estilo arquitetônico art déco. No ano de 2003 esse monumento foi tombado pelo Instituto do Patrimônio Histórico e Artístico Nacional, porém apesar do seu inestimável valor histórico, a estrutura apresenta diversas manifestações patológicas. Para alcançar esse objetivo foram realizados os seguintes procedimentos: (1) inspeção visual; (2) registro fotográfico; (3) anamnese e (4) ensaios. Os ensaios realizados foram esclerometria, pacometria e medição de deformações. As principais manifestações patológicas identificadas foram fissuração, destacamento de argamassa, corrosão de armaduras e deformação.

Palavras-chave: manifestações patológicas; diagnóstico; monumento histórico; art déco.

Documentación de las manifestaciones patológicas del Pórtico del Bautismo Cultural de Goiânia - monumento histórico *Art Déco*

RESUMEN

Este artículo tiene como objetivo presentar la metodología para la inspección y el mapeo de las manifestaciones patológicas en el monumento del Pórtico del Bautismo Cultural de Goiânia. Es un monumento de principios de los años 40 del siglo XX, representativo del estilo arquitectónico art déco. En 2003 este monumento fue catalogado por el Instituto Nacional del Patrimonio Histórico y Artístico, pero a pesar de su invaluable valor histórico, la estructura tiene varias manifestaciones patológicas. Para lograr este objetivo, se realizaron los siguientes procedimientos: (1) inspección visual; (2) registro fotográfico; (3) anamnesis y (4) ensayos. Las pruebas realizadas fueron esclerometría, pacometría y medición de deformación. Las principales manifestaciones patológicas identificadas fueron agrietamiento, desprendimiento de mortero, corrosión de refuerzos y deformación excesiva.

Palabras clave: manifestaciones patológicas; diagnóstico; monumento histórico; art déco.

Legal Information

Revista ALCONPAT is a quarterly publication by the Asociación Latinoamericana de Control de Calidad, Patología y Recuperación de la Construcción, Internacional, A.C., Km. 6 antigua carretera a Progreso, Mérida, Yucatán, 97310, Tel.5219997385893, alconpat.int@gmail.com, Website: www.alconpat.org

Reservation of rights for exclusive use No.04-2013-011717330300-203, and ISSN 2007-6835, both granted by the Instituto Nacional de Derecho de Autor. Responsible editor: Pedro Castro Borges, Ph.D. Responsible for the last update of this issue, Informatics Unit ALCONPAT, Elizabeth Sabido Maldonado.

The views of the authors do not necessarily reflect the position of the editor.

The total or partial reproduction of the contents and images of the publication is carried out in accordance with the COPE code and the CC BY 4.0 license of the Revista ALCONPAT.

1. INTRODUCTION

The architectural heritage is one of the proofs of the presence of history in cities and of its importance to society. It is a social and cultural asset. Considering this, it is necessary that the assets are preserved, restored and that maintenance and intervention routines are planned when relevant. Given that new cities are defined by their quick transformation, ensuring that historical and/or artistic values are preserved is unquestionable. The memory and cultural identity of a community are only constituted through these values, so the Cultural Heritage expresses the testimony of the constitution of community, which are the products and brands of different cultures, finally providing the transmission of identity and meanings for future generations (Barbosa et al., 2011; Tavares, 2011).

The concept of performance is important in this matter, since it concerns the building's capacity to remain in full conditions of use for as long as it lasts, making it possible to establish an intimate connection between performance and preventive measures. Over time, the structure loses its initial capacity, so the failure to carry out periodic maintenance leads to a reduction in its duration (Medeiros et. al., 2011).

In historic buildings, making a correct diagnosis of their pathological manifestations is a challenge due to the lack of maintenance, preventive measures, or because they have had inefficient restorations over the years. Thus, these historic buildings are subject to several different problems. The study of damage with onsite or laboratory tests is essential (Tavares, 2011).

The historical monument of the present study is a portico built for the Cultural Baptism of the city of Goiânia. According to Galli (2007), the Cultural Baptism took place on July 5, 1942 and corresponded to a set of events with the purpose of carrying out the inauguration of the new capital of the state of Goiás.

The Portico was built with the concept of *art deco* architecture. This style of decorative character emerged in France and spread in Brazil in the 1930s and 1940s (Correia, 2008). Due to its historical and architectural importance, the monument was listed by the National Institute of Historical and Artistic Heritage (IPHAN) through Ordinance No. 507 from November 18, 2003.

The Portico has become a representative and symbolic work of the art deco style and this is demonstrated by its presence on fridge magnets, in the Art Deco Tourist Guide in Goiânia and in a brochure for the dissemination of events about art deco, as illustrated in figures 1, 2 and 3.

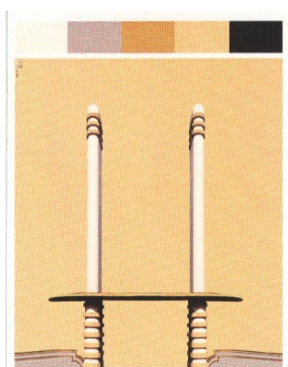


Figure 1. Illustrated portico on a fridge magnet

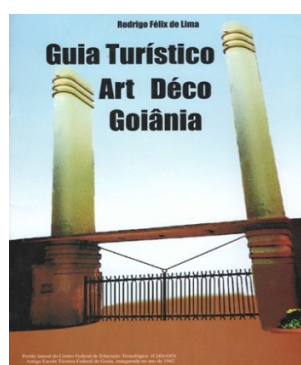


Figure 2. Portico featured in the *art deco* tourist guide of Goiânia



Figure 3 Portico in the flier of an event about *art deco* in Goiânia.

In the structure mentioned, two important questions lead the study, which are the importance of noticing and diagnosing the existing pathological manifestations for its safety and the restoration of its architectural visibility, restoring the aesthetic importance of the property.

2. PROCEDURE

The method proposed for the inspection of the object of study was based on the methodology of Lichtenstein (1986), starting with the search of the characteristics so that the diagnosis can be made afterwards. Visual inspection, anamnesis and tests were carried out. The method was chosen considering that it is available and widespread in the country, allowing segmentation of the analysis.

2.1 Object of the study

The object of study is the Portico depicting the Cultural Baptism of Goiânia located on the Goiânia Campus of the Federal Institute of Goiás (IFG).

The Portico is a reinforced concrete structure coated with mortar. The structure is made of two pillars of approximately 12 meters high and a slender slab with an ellipsoidal shape with a thickness of around 8 centimeters. The pillars are similar, each pillar has at its top and its base, respectively, three and seven friezes equidistant from each other, as can be seen in Figure 4.



Figure 4. View of the Portico of the Cultural Baptism of Goiânia in 1942, on the left (Galli, 2007) and in 2002 (IFG Collection)

A typical feature of the Art Deco style observed in the Portico architecture is the use of aerodynamics and sinuosity. In the pillars of the Portico there are similarities with the geometry of the chimneys of the 20th century ocean liners, a typical characteristic of the Art Deco style. Another feature observed is the use of reinforced concrete as a prominent object, bringing volume to the structure, conveying a sensation of grandeur and modernity.

The Santos Dumont airport in Rio de Janeiro and the Congonhas Airport in São Paulo are outstanding examples of art deco buildings.

2.2 Survey of characteristics

The purpose of the survey was to collect documents relating to the Portico, verify the pathological manifestations present as well as carrying out tests on the structure.

2.2.1 Visual Inspection

An on-site inspection was carried out for a visual analysis when pictures of the Portico were also taken with the aim of surveying pathological manifestation and the dimensions of the structure were also measured.

To carry out the inspection, the Portico pillars were named North and South (based on the compass) as shown in Figure 5. Each pillar also had its faces identified as North, South, East and West as it is indicated by Figure 6.

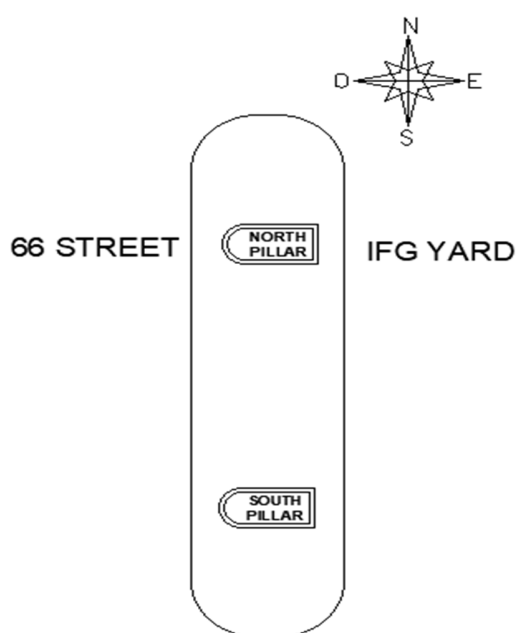


Figure 5. Portico floor plan

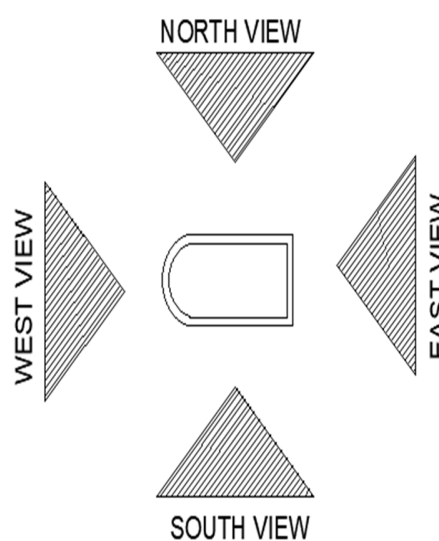


Figure 6. View of the facades of the pillars

2.2.2 Anamnesis

The purpose of the anamnesis was to collect as much information as possible in order to understand the history of the structure and then obtain a more accurate diagnosis of the pathological manifestations found in the Portico.

Technical documents such as projects, maintenance plans and reports on the already carried out maintenance were requested to the IFG (Federal Institute of Goiás).

2.2.3 Additional tests

The tests were performed to collect data and carry out a more detailed analysis complementary to the visual inspection. As it is a historic and listed structure, there has been an attempt to carry out the analysis through non-destructive tests so as not to damage the structure. Sclerometer, cover meter and slab deflection tests were carried out.

The sclerometer test was carried out on the upper part of the slab due to the fact that the lower part was difficult to access with the presence of props that made the test unfeasible.

The test execution followed the guidelines of the NBR 7584 (ABNT, 2012).

The sclerometer test was performed in four regions of the slab. Locations where there was no segregation of concrete and with homogeneous and regular surfaces were sought. Figure 7 shows the test execution and Figure 8 illustrates the location of the tested areas along with their dimensions.



Figure 7. Carrying out the sclerometer test

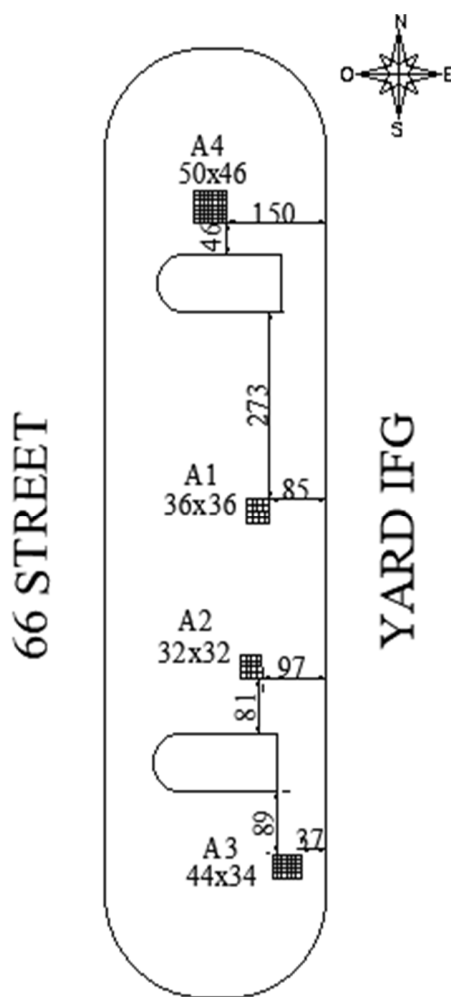


Figure 8. Location of the tested areas for the sclerometer test

The cover meter was also carried out aiming to obtain information about the location of the slab reinforcement as well as verifying the coverage of the reinforced concrete. The areas chosen for the test were those that presented the best conditions for the device to work which are the areas that were free of mold and dirt. In Figure 9 the test being carried out is shown.

Figure 9. Carrying out the cover meter test.



Figure 9. Carrying out the cover meter test

Finally, the deflections in the slab were verified. Measurements were collected from a reference level and using a water level and a measuring tape, points were collected in the overhanging part and between the pillars.

3. RESULTS AND DISCUSSIONS

3.1 Analysis of the visual inspection

From the visual inspection, it was possible to see that the slab at its bottom presents detachment of the concrete in some places (Figure 10) as a result of the corrosion of the reinforcement.



Figure 10. Detachment of concrete at the bottom of the slab

As shown in Figure 11, a considerable presence of mold and dirt was observed on the slab. Mold proliferates in humid, hot and dimly lit environments. This environment may have happened due to the presence of trees near the structure. It was also observed the presence of dirt or black crust, which were caused by the accumulation of dust, soot and pollution particles, originated from the burning of fossil fuels in the combustion engines of vehicles, brought by rainwater or by the action of the wind.



Figure 11. Mold and dirt on the slab

Part of the edge of the slab was detached and this was due to the carbonation and corrosion process of the reinforcements that took place in its reinforced region. As the carbonation process evolved over time, the cracking of the structure caused its movement, culminating in the detachment of the mortar at its ends (Figure 12).



Figure 12. Detachment of the edge of the slab

The painting on the slab was quite damaged, showing regions with detachment probably due to the application of paint over an existing layer (another layer of paint of a color different from the visible color that was applied previously was observed), impairing the adhesion between. In the process of lack of adherence, the incidence of rain and humidity are aggravating (Figure 13).



Figure 13. Detachment of the slab paint.

On the pillars, pathological manifestations related to the finishing were verified. Structural manifestations were not detected which made unnecessary running tests to measure the strength of the concrete and location of reinforcements such as sclerometer and cover meter test.

In addition, the pillars do not have exposed concrete and to carry out the tests it would be necessary to remove the coating layers from the surface, causing the deterioration of the historic monument, which diverges from the focus of the survey.

Another manifestation noticed in the pillars was the presence of dirt, as shown in Figure 14. This factor is mainly due to the lack of waterproofing and drainage mechanisms at the top of the pillar, which accumulated soot and dust brought by the wind. As noticed on the slab, there was also the detachment of the painting on the pillars and the visible color is also another previously applied coat of paint (a green one), compromising adherence.



Figure 14. Dirt and detachment of the paint on top of the pillar

The discoloration of the paint was verified and could have been caused mainly by its natural aging. Other factors such as the use of yellow colored paint, which is more susceptible to ultraviolet rays, since the pillar suffers a high incidence of sunlight, may also have aggravated the discoloration process. Cracks were noticed at the base of the pillars, possibly caused by the shrinkage of cementitious materials caused by the loss of water by evaporation in a fresh or hardened state and by the variation in temperature due to the high incidence of sunlight (Figure 15). Bubbles were

noticed in the painting of the pillars caused by the presence of humidity (which may have been absorbed by the cracks in the plaster and the hydrostatic pressure caused when its evaporation through the pores of the mortar happened, breaking and pushing the paint film), lack of adhesion and possible application failures such as running a thick layer under extreme heat conditions on a dirty and unprepared surface.



Figure 15: Incidence of cracks and paint discoloration

3.2 Analysis of the anamnesis

The following were provided by the IFG Projects and Infrastructure Directorate and by the IFG Administration and Maintenance Management Campus Goiânia: slab shoring project dated 2013; reinforcement project dated 2014; sclerometer test result dated 2013; and technical evaluation report of the Portico slab dated 2019.

Regarding the maintenance plans and maintenance monitoring reports, it was reported that these did not exist, as well as the original Portico project. Near the Portico, a plaque was found (Figure 16) indicating that it was restored on its 60th anniversary, in 2002, but there are no records detailing how this intervention took place.



Figure 16. Portico identification sign

The shoring project was carried out on the slab due to the deteriorated conditions in which it found itself in 2013. The reinforcement project carried out in 2014 proposes interventions in the area of steel and concrete reinforcement with grouting and increased thickness of the slab. However, the project was never executed.

The result of the sclerometer test, carried out in 2013 by the Carlos Campos Consultoria e Construções Ltda Laboratory, in only one region obtained an average sclerometric rebound index equal to 29, indicating 22 MPa as the compressive strength of concrete. Cascudo (2019), for the production of the technical report, carried out two inspections on the Portico slab called preliminary and detailed. While the preliminary one designated the visual analysis, the detailed one corresponded to the performance of sclerometer, ultrasound, electrical resistivity, corrosion potential and concrete carbonation tests.

As observed in the visual inspection, Cascudo (2019) also found corrosion of the reinforcements in some parts of the slab, presence of mold, dirt and degradation of the painting system. The author also identified visible deformations in the slab and attributed these to corrosion of part of the flexion reinforcement, which occurred due to the slenderness of the slab and the low inertia that, associated with the corrosion of the reinforcement, provide strong and immediate impacts on the slab.

In the sclerometer test, Cascudo (2019) evaluated 10 regions of the slab, called E1 to E10 and obtained IE values between 21 and 30 and values for concrete strength between 14 MPa and 24 MPa. Regarding the ultrasound test, Cascudo (2019) performed eight ultrasonic velocity measurements, four of which reached values below 2500 m/s. Such values classify, according to the British standard BS 1881 (BSI, 2001), concrete as bad. One of these measurements obtained a value lower than 2000 m/s, which according to BS 1881 (BSI, 2001) configures a very bad concrete. Finally, it was concluded that these low values correlate with a high void index, which is compatible for a concrete with an estimated strength of 14 MPa to 24 MPa. The low ultrasonic speed is still justified by the presence of cracks, since these cause an increase in the wave propagation time. It is observed that the estimated values are low compared to the values required by current standards, but for the time of the construction of the structure it falls within acceptable values. Cascudo (2019) also states that there are probably microcracks in the internal structure of the slab.

In the concrete carbonation test carried out by Cascudo (2019) on two specimens, both extracted from the central region of the slab, it was possible to visually observe the effects of a carbonation that was observed in an advanced degree.

3.3 Analysis of the sclerometer test

Through the sclerometer test, indices were obtained from the two equipment used, which ranged from 23.7 to 28.7, generating a strength variation in MPa from 17.0 to 23.4.

Figure 17 shows the graph with the compressive strength values obtained from the sclerometer test performed on the structure during the anamnesis process and those carried out in this research. The values shown are an average of the compressive strengths of areas tested by test event. It can be seen from the graph that the results found converge to an average value of estimated strength of 20 MPa, despite the tests having been carried out on different dates and by different operators.

About the normative standards for the minimum strength of concrete structures, since there is no information about the structural design of the frame, knowing that the NB-1 standard- Calculation and Execution of Reinforced Concrete (ABNT, 1940)- which was used at the time when the structure was built recommends a minimum strength for concrete structures of 125 kgf/cm², that is, 12.5 MPa. The current standard NBR 6118 – Design of concrete structures – Procedure (ABNT, 2014) provides a minimum strength of 20 MPa for concrete structures. Thus, the graph in Figure 17 also presents a comparison between the estimated results of compressive strength of concrete, obtained in different sclerometer tests, with the minimum values of characteristic strength of concrete under compression (f_{ck}) recommended by the standard of concrete structure that was used at the time of the construction of the Portico and today.

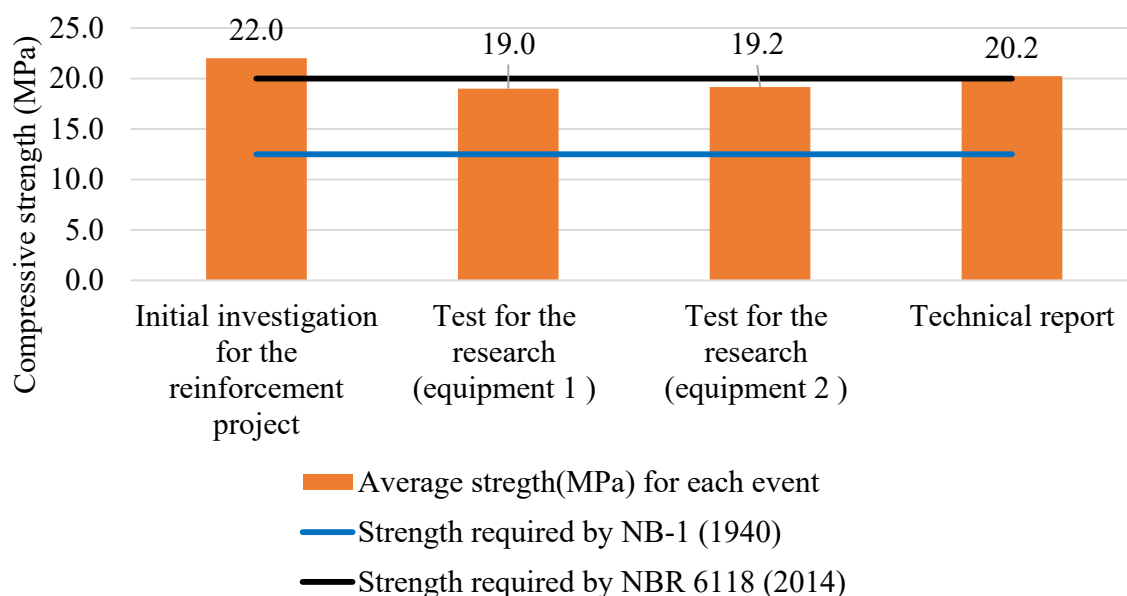


Figure 17. Comparative graph of strength obtained with normative requirements

From the cover meter test, it was possible to map and identify places where there is reinforcement and at what depths they are. From these values, it was identified that most reinforcements had an inefficiency in covering the slab in relation to the requirement of the NBR 6118 standard (ABNT, 2014). According to the class of environmental aggressiveness in which the structure fits, the covering should be at least 2.5 cm, which does not occur in some regions of the slab that reached 1.1 cm.

The standard used at the time of the construction of the NB-1 frame (ABNT, 1940) provides that outdoor slabs must have at least 1.5 cm of coverage, which also demonstrates that for some regions of the slab the coverage is insufficient.

It was observed in some places the value of “0” which, according to the equipment, means lack of depth would indicate that the reinforcement is superficial and without covering. However, the same was not observed visually.

3.4 Analysis of slab deflection verification

The slab deflection measurement was performed by collecting the dimensions from a reference level of 2.0 meters at the points present in Table 1.

Table 1. Values referring to the values found in the points

SPOT	VALUE (cm)
A	193,7
B	200,7
C	198,8
D	196,1
E	199,0
F	199,2
G	193,8

The slab deflections verified in the slab were obtained through the difference in dimensions being in the balance on the left side, the difference between the dimensions A and B, in the central region, the arithmetic mean between the difference of points C and D and the difference of points D and E, while the balance on the right side is due to the difference between points F and G. Table 2 shows the values obtained and their representation (exaggerated) in Figure 18.

Table 2. Values of the slab deflections obtained

PLACE	VALUE (cm)
Overhang slab deflection on the left side	7,0
Central region slab deflection	2,8
Right side slab deflection	5,4

The verification of the permitted slab deflection was performed taking into account the free span, as recommended by NBR 6118 (ABNT, 2014) for sensory acceptability and visual limitation. Equation (1) designates the equation provided by the standard.

$$D = \frac{l}{250} \quad (1)$$

Considering l to be the span and D to be the limit displacement. When it comes to overhanging slabs, the equivalent span to be considered must be twice the overhang length (distance between the support and the end of the slab), obtaining equation (2).

$$D = \frac{l}{125} \quad (2)$$

Through Equations (1) and (2) the limit displacement of 2.74 cm is obtained for the overhang region and the limit displacement of 2.80 cm for the central span region.

It is then observed that both overhanging regions whose maximum slab deflections are 7.0 cm at point “A” and 5.4 cm at point “B” are much higher than allowed by the NBR 6118 (ABNT, 2014). For the central region, the slab deflection found at point “D” has a value of 2.80 cm, which is equivalent to that allowed by the standard requirement.

Due to the lack of preventive and corrective maintenance over time, the structure suffered excessive deformations so that the values of the slab deflections verified in the overhang regions demonstrate that it is outside its service limits.

It is worth saying that because it is an old structure, over 70 years old, the creep of the concrete may have been one of the reasons that contributed to the total deformation of the slab. However, this was not considered in the present survey.

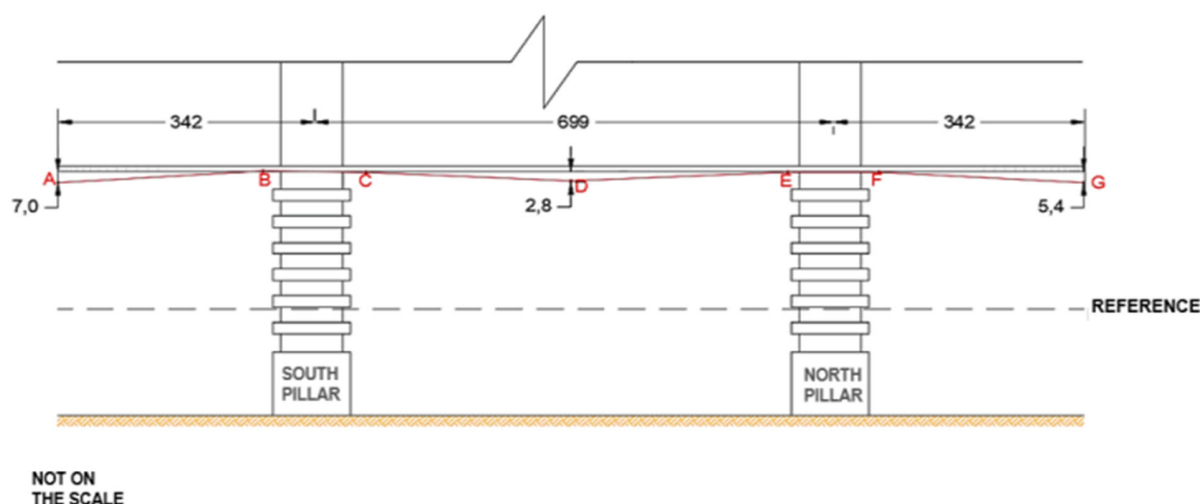


Figure 18. Representation of the biggest slab deflections verified

4. CONCLUSIONS

The historic monument is quite degraded and this is mainly due to the absence of a preventive maintenance plan. Through visual inspection, it can be seen how compromised the architectural representation of the portico is. The structure is surrounded by trees that prevent its full visibility and by safety devices (used due to the advanced level of deterioration) that prevent people from seeing the aesthetics such as props and fences. As for the pathological manifestations, the determining factors for the appearance of these are:

- Presence of humidity intensified by the proximity of the surrounding trees;
- Insufficient coverage on the slab;
- No preventive maintenance;
- Lack of waterproofing system;

The analysis of the anamnesis revealed that there is little information about the structure and this made it difficult to accurately analyze the causes and origins of pathological manifestations. The sclerometer tests pointed to the low strength of the concrete, while the cover meter test showed covering problems. Both results reinforce the structural damage that affects the structure already noticeable on visual inspection.

Finally, it is essential that the Portico depicting the Cultural Baptism of Goiânia maintains its functions, both as a structure and as a historical and architectural monument. For this, it is necessary to prepare maintenance plans, so that it is possible to guarantee the useful life of the structure.

5. ACKNOWLEDGEMENTS

The authors acknowledge and thank the support of the Federal Institute of Goiás (IFG).

6. REFERENCES

- Associação Brasileira de Normas Técnicas (1940). *ABNT NB-1: Cálculo e execução de obras de concreto armado – Procedimentos*. Rio de Janeiro.
- Associação Brasileira de Normas Técnicas (2014). *ABNT NBR 6118: Projeto de estruturas de concreto – Procedimento*. Rio de Janeiro.
- Associação Brasileira de Normas Técnicas (7584). *ABNT NBR 6118: Concreto endurecido –*

- Avaliação da dureza superficial pelo esclerômetro de reflexão — Método de ensaio*. Rio de Janeiro. Barbosa, P. P. et al. (2011). *Patrimônio Histórico em cidades novas: o caso de Maringá, PR. Maringá* in: XIV Seminário de arquitetura latino-americana. Campinas, São Paulo (BR). pp. 16 - 31.
- Brasil. Ministério do estado da cultura (2003). *Portaria nº 507, de 18 de novembro de 2003*. Diário Oficial da União: seção 1, Brasília, DF, ano 228, p.30, 18 nov.
- British Standards Institution (2001). *BS 1881: Testing concrete*. London.
- Cascudo, O. (2019). *Avaliação de laje em concreto armado constituinte do pórtico de entrada lateral do IFG - Câmpus Goiânia*. Goiânia: UFG, 2019. 38 p.
- Correia T. B. (2008), *Art déco e indústria: Brasil décadas de 1930 e 1940*. Na An. mus. paul.vol.16 no.2 São Paulo July/Dec. <https://doi.org/10.1590/S0101-47142008000200003>
- Galli, U. (2007). *A história do batismo cultural de Goiânia*. Goiânia: Ed. UCG/ Contato Comunicações, p. 98.
- Medeiros, M. H. F.; Andrade, J. J. O.; Helene P. (2011). *Cápítulo 22: Durabilidade e Vida Útil das Estruturas de Concreto* in: Geraldo Isaia (Org.). *Concreto: Ciência e Tecnologia*. 1 ed. São Paulo: IBRACON. p. 37.
- Tavares, F. M. (2011). *Metodologia de diagnóstico para restauração de edifícios dos séculos XVIII e XIX nas primeiras zonas de mineração em Minas Gerais*. Faculdade de Engenharia, Universidade Federal de Juiz de Fora, Juiz de Fora, 98 p.